AALBORG UNIVERSITY

DENMARK

Air Interface of Beyond 3G Systems with User Equipment Hardware Imperfections: Performance & Requirements Aspects

A case study on UTRA Long Term Evolution Uplink

Priyanto, Basuki Endah

[Link to publication from Aalborg University](#)

Air Interfaces of Beyond 3G systems with User Equipment Hardware Imperfections: Performance & Requirements Aspects

A case study on UTRA Long Term Evolution Uplink

Basuki Endah Priyanto
Aalborg University
Denmark

To my wife Dina and my parents.

" Whoever treads a path seeking knowledge therein, Allah directs him to a path leading to paradise."

-Sahih Muslim Hadith-

Summary

Orthogonal Frequency Division Multiple Access (OFDMA) and Single-Carrier FDMA (SC-FDMA) are the key air interfaces to achieve high spectral efficiency for UTRA Long Term Evolution (LTE) system, which is also known as the beyond 3rd generation (B3G) system. The selection of air interface techniques is influenced by the RF transmitter constraints, i.e. the hardware imperfections. The RF transmitter imperfections create in-band performance degradation and increase the out-of-band emissions. The latter can lead to violate Spectral Emission Mask (SEM) and Adjacent Channel Leakage Ratio (ACLR) requirements. This thesis deals with the air interface design of beyond 3G systems to achieve high spectral efficiency, and the impact of the imperfections on both performance and the transmitter requirements.

Baseline performance results without the imperfections show that OFDMA is generally better than SC-FDMA with a Minimum Mean Square Error (MMSE) receiver. Depending on the modulation and coding schemes, the performance of SC-FDMA with turbo equalizer becomes better or equal to OFDMA. The effects of well-known RF transmitter imperfections on LTE link level performance are investigated by simulation. The results show that the Error Vector Magnitude (EVM) is a good measure to estimate the performance loss for numerous imperfections in the anticipated EVM range. Furthermore, in simulations these imperfections can be replaced by a white noise source as an equivalent model. As shown, the nonlinear power amplifier is the crucial imperfection affecting the transmitter design. The hardware imperfections impact on the out of band spectrum is also investigated. A spectrum shaping technique to control spectrum emission of the LTE User Equipment (UE) is proposed. The proposed technique is capable of controlling the spectrum emission for various bandwidth

settings, and provides good trade-off between spectrum emission control, performance loss, and implementation complexity. While all these investigations were done for the most common transmitter architecture - the cartesian type - an investigation was similarly done for the impact of the polar transmitter imperfections on LTE performance. The polar transmitter is a candidate for the future RF transmitter architecture to realize highly efficient power amplification. Similarly here, the results show that the EVM measurement results can be used to estimate the performance loss. As a final topic, the in-band interference effects on LTE resource block allocation are investigated. The UE's transmit signal leakage within the in-band channel cannot be controlled by the transmitter shaping filter and therefore create interference. The results show that the Radio Resource Management (RRM) functionality should take care to place the UE resource block allocation to avoid a significant performance loss due to the leakage generated by the RF imperfections and different Power Spectral Density (PSD) level among UEs.

In general, it is important that the out-of-band emission meet the SEM and ACLR requirements. Therefore, the in-band performance degradation can be kept in the acceptable level. The results confirm that SC-FDMA for the uplink of B3G system is a good selection as it achieves a high spectral efficiency whilst gaining higher power amplifier efficiency, thereby increasing the cell coverage.

Dansk Resumé

(Abstract in Danish)[1]

Orthogonal Frequency Division Multiple Access (OFDMA) og Single-Carrier FDMA (SC-FDMA) er nøgle transmissionsteknologier i UTRA Long Term Evolution (LTE) systemet, også kendt under navnet beyond 3rd generation (B3G) systemet. SC-FDMA er foretrukket til uplink transmission på grund af dedet lavere Peak-to-Average Power Ratio (PAPR). Valget af transmissionsteknologier er afhængigt af begrænsninger i RF-trinnet, dvs. ikke-idealiteter i hardwaren. Ikke-idealiteter i RF-trinnet reducerer systemets ydeevne og øger spektralemissionen uden for systembåndbredden. Sidstnævnte kan føre til overskridelse af de fastsatte værdier for spektralemission (Spectral Emission Mask - SEM) og nabokanalemission (Adjacent Channel Leakage Ratio - ACLR). Afvejningen mellem implementeringsomkostninger, ikke-idealiteternes indvirkning på ydeevnen og overholdelse af SEM og ACLR er vigtige elementer i designet af senderen.

Betragtes ydeevnen uden ikke-idealiteter viser denne afhandling at OFDMA generelt set er bedre end SC-FDMA for en Minimum Mean Square Error (MMSE) modtager. Afhængig af modulation og kodning, vil ydeevnen af SC-FDMA med turbo equalizer blive bedre end eller lig med OFDMA. Studier inkluderende kendte RF ikke-idealiteters indvirkning på LTE link performance viser at Error Vector Magnitude (EVM), indenfor det praktisk anvendelige område, er et godt mål for estimering af tabet i ydeevne for de fleste ikke-idealiteter. Ydermere viser det sig, at disse ikke-idealiteter kan modelleres ved en hvidstøjs kilde som ækvivalent model. Den ulineære effektforstærker er den væsentligste ikke-idealitet med indvirkning på designet af senderen. Afhandlingen undersøger

---

[1] Translation by Christian Rom, Troels B. Sørensen & Ole K. Jensen, Department of Electronic Systems, Aalborg University Denmark

vi

også indvirkningen af ikke-idealiteter på spektralemission, og introducerer en filtreringsteknik for implementering i LTE terminaler til at kontrollere denne. Med denne teknik er det muligt at kontrollere spektralemissionen ved forskellige transmissionsbåndbredder, med en god afvejning mellem spektralemission, tab i ydeevne og implementeringskompleksitet. Tilsvarende undersøger afhandlingen også den nyere polære senderarkitektur med hensyn til ikke-idealiteters indvirkning på LTE performance. Den polære senderarkitektur kandiderer til fremtidige RF-arkitekturer pga. dens meget effektive effektforstærkning. Resultaterne viser at EVM også i denne sammenhæng er et velegnet mål til estimering af performance tab. Emissioner inden for transmissionsbåndbredden kan ikke kontrolleres ved filtrering hvorfor der vil opstå interferens indenfor systemet. Afhandlingen undersøger derfor de resulterende interferenseffekter med henblik på LTE radioressourceallokering. Resultaterne viser at ressourceallokeringen, for at undgå tab i ydeevne, skal tage hensyn til denne interferens der følger af ikke-idealiteter og forskellig spektraleffekttæthed mellem terminaler.

Overordnet set er det vigtigt at overholde de fastsatte værdier for SEM og ACLR. Det er vist at dette er muligt samtidig med at tabet i ydeevne kan holdes indenfor et acceptabelt niveau. Resultaterne viser at SC-FDMA er et godt valg for B3G uplink idet der opnås en høj spektraleffektivitet sammen med effektiv effektforstærkning og deraf forbedret radiodækning.

Preface & Acknowledgments

This dissertation is the result of a three years research project carried out at Radio Access Technology Section (RATE) and Technology Platforms Section (TPS), Department of Electronic Systems, Aalborg University. The dissertation has been completed in parallel with the mandatory courses and teaching/ working obligations required in order to obtain PhD degree. The project has been conducted under the supervision of Associate Professor Troels B. Sørensen and Associate Professor Ole K. Jensen and the co-supervision of Professor Preben E. Mogensen and Professor Torben Larsen. This PhD research project has been sponsored by Aalborg University (Tek NAT) and Center for TeleInfrastruktur (CTIF), Denmark.

My deepest gratitude to my supervisors for their guidance, encouragement and wise advices during the completion of this PhD work. Also, I would like to thank my co-supervisors for their insightful suggestions towards my study. This PhD study has significant impact to my life from both personal and professional point of view. Further, I would like to thank the members of the assessment committee who through their detailed reading and constructive feedback have helped in the correction and clarification of the text throughout this dissertation.

I would like to express my gratitude to my colleagues and former PhD students in both RATE and TPS section. Thanks to Lisbeth S. Larsen and Jytte Larsen for the constant support, assistance, and the proofreading. Many appreciations are paid to Christian Rom, Akhilesh Pokhariyal, Wei Na, Carles Navarro, and Gilberto Berardinelli for their fruitful discussions and help in the link level studies. Further, I want to thank my RISC colleagues Tian Tong, Nastaran Behjou, Yong Hui, and Jorge Martires. A special thanks goes to my former

diligent students Humbert Codina, Sergi Rene, and Danish Khan.

My sincere appreciation goes to the members of Radio System Technology, Nokia Siemens Networks A/S for their contribution to my personal and professional growth. In particular, thanks to Troels Kolding, Frank Frederiksen, Claudio Rosa, Klaus I. Pedersen, and Istvan Kovacs. It has been a pleasure to work together with you and providing me an excellent working environment.

I would like to thank my parents for their encouragement. They deserve the dedication of this dissertation. Foremost, I would like to thank my dearest wife Dina for the patient, persistent supports and endless love.

Aalborg, March 2008

Basuki Endah Priyanto

Contents

List of Figures

List of Tables

List of Abbreviations

3GPP	Third Generation Partnership Project
ACLR	Adjacent Channel Leakage Ratio
ADC	Analog to Digital Converter
AGC	Automatic Gain Control
AM/AM	Amplitude Modulation/Amplitude Modulation
AM/PM	Amplitude Modulation/Phase Modulation
AMC	Adaptive Modulation and Coding
ARQ	Automated Repeat reQuest
AWGN	Additive White Gaussian Noise
B3G	Beyond the 3rd Generation
BB	Baseband
BER	Bit Error Rate
BLER	Block Error Rate
BPF	Bandpass Filter
CDMA	Code Division Multiple Access
CCDF	Cumulative Complementary Distribution Function
CP	Ciclic Prefix
CRC	Cyclic Redundancy Check
DAC	Digital to Analog Converter
DFT-s-OFDM	DFT-Spread OFDM
DL	Downlink
EER	Envelope Elimination and Restoration
EDGE	Enhanced Data rates for Global Evolution
EUTRA	Evolved UMTS Terrestrial Radio Access
EvDO	Evolution Data Only
EVM	Error Vector Magnitude

FDD	Frequency Division Duplexing
FDMA	Frequency Division Multiple Access
FFT	Fast Fourier Transform
GPRS	Global Packet Radio Service
GSM	Global System for Mobile Communications
H-ARQ	Hybrid-ARQ
HSPA	High Speed Packet data Access
ICI	Inter Carrier Interference
IDFT	Inverse Discrete Fourier Transform
IFDM	Interleaved Frequency-Division Multiplexing
IFDMA	Interleaved Frequency-Division Multiplexing
IFFT	Inverse Fast Fourier Transform
ISI	Inter-Symbol Interference
LPF	Lowpass Filter
LO	Local Oscillator
MC	Multi-Carrier
MIMO	Multiple Input Multiple Output
ML	Maximum Likelihodd
MMSE	Minimum Mean-Square-Error
MRC	Maximal Ratio Combining
NLA	Non-Linear Amplifier
LA	Link Adaptation
LTE	Long Term Evolution
OFDM	Orthogonal Frequency-Division Multiplexing
OFDMA	Orthogonal Frequency-Division Multiple Access
PA	Power Amplifier
PAE	Power Added Efficiency
PAPR	Peak-to-Average Power Ratio
PER	Packet Error Rate
PSK	Phase Shift Keying
QAM	Quadrature Amplitude Modulation
RF	Radio Frequency
RC	Raised Cosine

RRM	Radio Resource Management
SAW	Surface Acoustic Wave
SC	Single-Carrier
SDR	Software Defined Radio
SCFDM	Single-Carrier Frequency-Division Multiplexing
SCFDMA	Single-Carrier Frequency-Division Multiple Access
SIMO	Single-Input Multiple-Output
SISO	Single-Input Single-Output
SNR	Signal-to-Noise Ratio
TDD	Time Division Duplexing
UE	User Equipment
UL	Uplink
UMTS	Universal Mobile Telecommunications System
UTRAN	Universal Terrestrial Radio Access Network
VHF	Very High Frequency
VGA	Variable Gain Amplifier
WCDMA	Wideband CDMA
WLAN	Wireless Local Area Network
Wimax	Wireless Interoperability for Microwave Access
ZF	Zero-Forcing

*" A journey of a thousand miles must
begin with a single step."*

Lao Tze

Introduction

The research and development of wireless communication systems has been
rapidly growing for the last decades. Multi-carrier technology in the form of Or-
thogonal Frequency Division Multiplexing (OFDM), adaptive modulation and
coding, Multiple Input Multiple Output (MIMO) antenna techniques, packet
scheduling, link adaptation are the new paradigms in the upcoming wireless
communication system to achieve high spectral efficiency and high data rate
transmission. In parallel, The micro-electronic and semiconductor technologies
development is fastly growing and often refers to Moore's Law:

"The number of components on a chip will double every eighteen months."

The synergy between the rapid development of the micro-electronic and semi-
conductor technologies and wireless communication research makes the wireless
communication algorithms become reality and implemented in the hardware. It
can easily be observed from the trend of the mobile terminal in a small size with
many features.

The necessity of high data rates wireless communication becomes important
for the end-user, especially to support high mobility lifestyle "always get con-
nected", and demand for the multimedia communication, such as the video
phone, live streaming, online gaming, and the Internet. For a high data rate

communication, a high performance mobile terminal or user equipment with minimal RF imperfections is required. It is also essential to maintain low power consumption, small physical hardware size, and long duration battery life. The mobile terminal requirement is getting challenging since the price must be kept low to reach the market. Therefore, the main challenge is to achieve the optimum solution.

Wireless cellular evolution in the last decade is illustrated in Figure 1.1 [1]. The second generation of the cellular system, GSM evolution started with GPRS, EDGE, and WCDMA. WCDMA in the form of High Speed Downlink Packet Access (HSDPA) is now widely deployed, and it will still be evolved to the LTE system. The CDMA, or mostly known as the second generation for the north America system evolution, started with CDMA2000 1xRTT (Radio Transmission Technology) and then evolved to CDMA EV-DO (EVolution-Data Only) Revision A and finally the EV-DO Revision C. The new standard, Wimax, started from the fixed wireless access before it evolved into the mobile wireless access. Finally, the long term goals of each wireless cellular system are similar, which are aiming at all internet protocol (IP) networks [1]with 100 Mbps peak downlink data-rate and 50 Mbps uplink data-rate [1].

1.1   UTRA Long Term Evolution System (LTE)

The evolution of 3G system towards 4G system is shown in Figure 1.2. The first generation, release 99, offers both circuit and packet switched data services. The next, release 4, offers full packet switched data service. Subsequently, each 3GPP release offers a better peak-data rate.

UTRA Long Term Evolution (LTE) is the next generation of wireless cellular communication systems to ensure the competitiveness of UMTS system in the upcoming years. Moreover, LTE is also known as Beyond 3G system and designed as a step towards the 4G system. It is expected that the main functionality of the 4G system is based on the LTE system while the 4G system uses 100 MHz frequency spectrum or 5 times wider than the LTE. The first phase of the LTE framework started in the study item [5] targeting release 8 of the UTRA specifications. The objective of this study item is to develop a framework for the evolution of the 3GPP radio access technology towards a high data rate, low-latency, and packet optimized radio access technology [7]. When writing this thesis, the 3GPP is in the work item phase and expected to be finalized by March 2008 [8].

---

[1]a packet data network, where the voice and data are encapsulated in a data format.
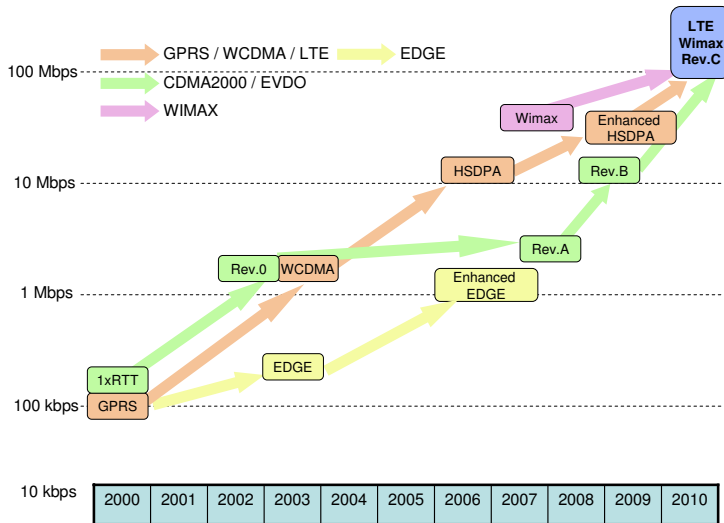
Figure 1.1: The Evolution of Wireless Cellular System [1].
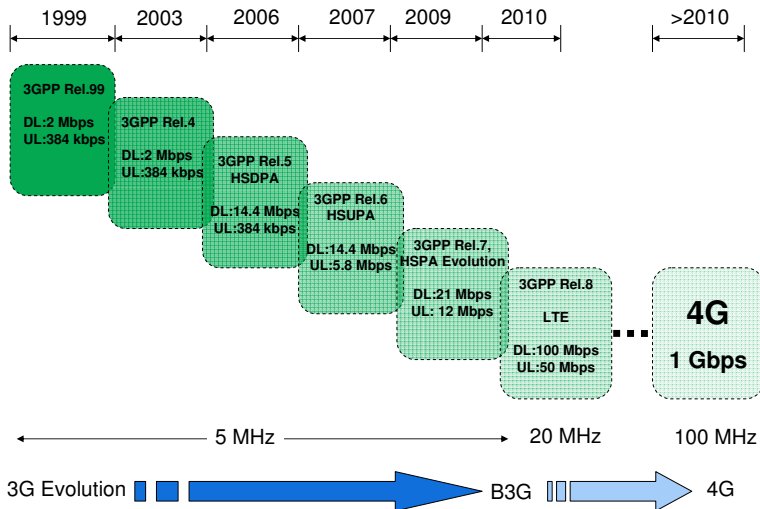
Figure 1.2: 3GPP release specifications towards 4G system.

The targets for the evolution of the radio-interface and radio-access network architecture are [7]:

- Significantly increased peak data rate, e.g. 100 Mbps (downlink) and 50 Mbps (uplink).

- Increases "cell edge bit-rate" whilst maintaining the same site locations as deployed today.

- Significantly improved spectral efficiency over release 6 HSPA e.g. 3-4 times for the downlink and 2-3 times for the uplink direction.

- Possibility for a Radio-access network latency below 10 ms.

- Scalable bandwidth:

    - 5, 10, 20 and possibly 15 MHz.
    - 1.25, 1.6, 2.5 MHz: to allow flexibility in narrow spectral allocations where the system may be deployed.

- Support for inter-working with existing 3G systems and non-3GPP specified systems.

- Reasonable system and terminal complexity, cost, and power consumption.

- Efficient support of the various types of services, especially from the PS domain (e.g. Voice over IP, Presence).

- Support for inter-working with existing 3G systems and non-3GPP specified systems.

- The system should be optimized for low mobile speed, but also support high mobile speed.

Orthogonal Frequency Division Multiple-Access (OFDMA) has been selected as the multiple access techniques for the LTE downlink and Single-Carrier Frequency Division Multiple-Access (SC-FDMA) for uplink. OFDM is recognized as an attractive modulation technique in a cellular environment because of its capability to enable low-complexity multipath channel mitigation. Nevertheless, OFDM requires an expensive and inefficient power amplifier in the transmitter due to the high Peak-to-Average Power Ratio (PAPR) of the multi-carrier signal.

Single Carrier transmission with Cyclic Prefix (SC-CP) is a closely related transmission scheme with the same attractive multipath interference mitigation property as OFDM [9],[10],[11]. Therefore, SC-CP can achieve a performance comparable to OFDM for the same complexity, but at reduced PAPR. Moreover,

the choice of single carrier transmission in a DFT-Spread OFDM form allows for a relatively high degree of commonality with the downlink OFDM scheme and the possibility to use the same system parameters [5].

1.2 State of the Arts on Achieving High Spectral Efficiency

High spectral efficiency for achieving high data rate is expected for the LTE. High spectral efficiency can be achieved from the following Layer-1 features. In general the following Layer-1 features aim at efficiently managing the frequency and time-slot resource. These are the essential aspects for the Beyond 3G system on account of the usage of a wideband channel of 20 MHz.

Air Interfaces
Both OFDMA and SC-FDMA are fundamentally based on the OFDM radio transmission. The OFDM time-frequency representation is shown in Figure 1.3. OFDM technique transmits the information onto several parallel narrow-band channels / sub-carriers. Typically, each sub-carrier carries an M-PSK/M-QAM symbol. The sub-carriers are orthogonal to each other, and a guard interval is added to each symbol to mitigate inter-symbol interference in frequency selective fading channel. The guard interval length is designed in such a way so that it is longer than the maximum excess delay of the channel. Therefore, all of the multipath components fall within guard interval, and the guard interval will be removed at the receiver. High spectral efficiency is achieved by allowing the sub-carriers overlap and properly arranged so that the sub-carriers orthogonality can still be maintained.

High User Orthogonality.
SC-FDMA transmission allows a high orthogonality among users within a cell. Each user in a cell is allocated in different frequency allocation in the Frequency Domain Multiplexing (FDM) mode. Therefore, the intra-cell interference which typically exists in the 3G system can be avoided.

Short Transmission Time Interval (TTI)
In LTE, user transmission is assigned in a 1 ms period. It is much shorter than the HSUPA system in a 2 ms period or even significantly shorter than the release 99 system in the order of 10 - 20 ms. The short transmission time interval allows high dynamic user allocations.

Fast Variable Transmission Bandwidth
The uplink transmission bandwidth can be scaled depending on various con-
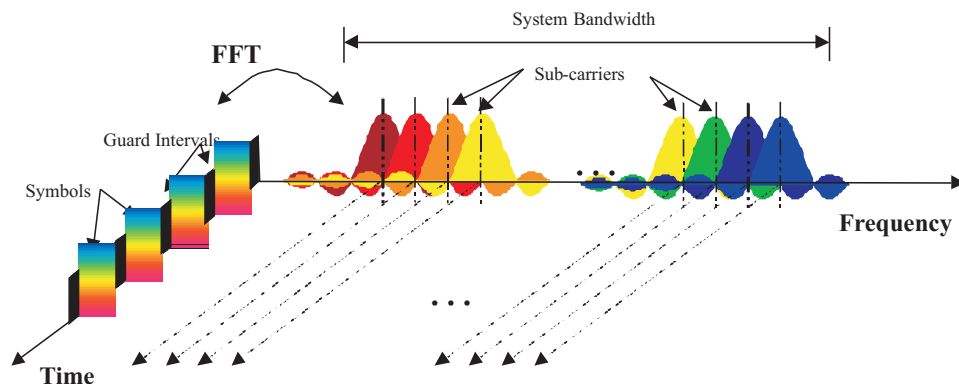
Figure 1.3: Frequency-Time representation of an OFDM signal [2].

ditions on a TTI basis (1 ms), such as buffer status, QoS requirements, and instantaneous channel conditions. The minimum transmission bandwidth is one resource block (RB) or 180 kHz, and the maximum one can be the whole transmission bandwidth in a 20 MHz.

Fast Variable Modulation and Coding Schemes
LTE supports various modulation schemes, from QPSK, 16QAM and 64QAM. 64QAM is optional for most of the UE classes in LTE uplink [8]. Different modulation and coding rates can be used depending on the channel condition and updated every TTI. This situation will enable fast link adaptation to achieve the highest possible spectral efficiency on each channel condition.

Fast L1 Hybrid ARQ
H-ARQ is an automatic repeat request process that has combined the received data block with the previous one in order to increase the likelihood of successful decoding [12]. There are two well known H-ARQ with soft combining processes, namely H-ARQ Chase Combining and H-ARQ Incremental Redundancy. The fast H-ARQ is realized by implementing the medium access mechanism control in the node-B. The fast H-ARQ can maximize data throughputs, capacity and minimize the delay.

Frequency Domain Channel Aware Scheduling
Frequency domain channel aware scheduling is defined with the target of increasing user and sector throughput. The frequency allocation is scheduled by the node-B so that the user frequency allocation is assigned to the frequency allocation where the user experiences a better channel condition. This situation is also known as multi-user diversity. In LTE uplink the frequency domain channel aware scheduling requires channel sounding from the UE. Each UE

transmits the sounding reference signal in a wider bandwidth, and the node-B measures the channel statistic indication for each UE. Having the knowledge of the channel condition, the UE data transmission can be allocated by the node-B.

Antenna Configuration
In LTE the target peak data rates are specified in terms of a reference UE configuration comprising:

- Downlink Capability - 2 receive antennas at UE.

- Uplink Capability - 1 transmit antenna at UE.

The above reference is mainly in consequence of the physical size constraint and limited power at the UE. For the uplink direction, 1x1 SISO and 1x2 SIMO antenna configurations have been considered for the working assumptions. The downlink direction has more degree of freedom of the antenna variations in comparison to the uplink direction.

1.3 Hardware Imperfections: The Limiting Factor

A generic radio transmitter consists of the baseband and Radio Frequency (RF) part, and both interactions are shown in Figure 1.4. The high spectral efficiency requirement can be achieved by performing a proper design of both advanced wireless techniques at the baseband level and the RF system architecture. The LTE system level features, including advanced modulation and coding, MIMO antenna schemes and the interaction with higher layer protocol for link adaptation and packet scheduling, are implemented in the baseband. The RF system design covers the investigation of the suitable RF architectures, detailed requirements for each RF components, and the RF imperfections in the selected RF architectures.

Typically, each entity has its own evaluation metrics. The system level uses spectral efficiency performance, Block Error Rate (BLER), and cell-level capacity. In the RF design it is common to use moduation accuracy represented in the Error Vector Magnitude (EVM), and the spectral regrowth aspects. It is also very important to provide a link between these two entities. The evaluation metric in the RF design can be further extended to analyze the impact of the hardware imperfections in the system level. Moreover, the RF requirements can be determined from the system level requirement on the acceptable performance
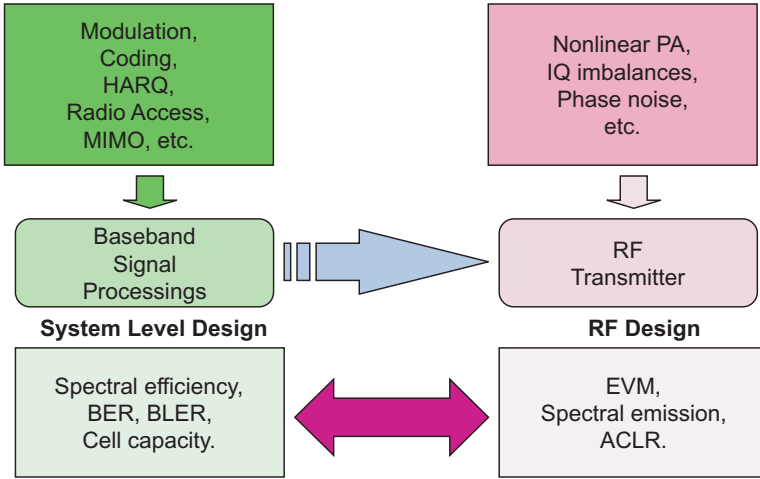
Figure 1.4: Hardware imperfections in the RF part limit the system level performance.

loss. In some cases, the RF requirement can be the main bottleneck of a wireless communication system. Although the performance loss is still acceptable.

The RF imperfections occur in both transmitter and receiver. The RF imperfections can lead to the performance degradation, and therefore it can limit the actual performance. In this work the RF imperfections are limited to the RF imperfections generated at the transmitter. Typically, the RF parts at the UE dominate the UE bill of material (BOM) cost. A low cost RF part will reduce the cost, and on the other hand the low performance component should also be expected. Besides, the power amplifier is always the main consideration in the design of the RF transmitter. The main reason is that the good selection of a power amplifier results in an efficient power amplifier. The selection of the radio access scheme can also be decided due to the power amplifier characteristics. A radio transmission with low peak-to-average power ratio is always preferred for the uplink direction to obtain a better power amplifier efficiency.

Prior to the hardware implementation, the RF imperfections modelling and computer simulation offer some benefits in providing the results in term of link level performance degradation due to the hardware imperfections. Moreover, the result can be used as the reference for the actual hardware measurement results in the latter stage.

Some work has been done in the RF imperfection modelling studies. Costa [13] analyzed the M-QAM-OFDM system performance in the presence of nonlinear

power amplifier and phase noise. Georgiadis [14] provides analytical study on the impact of gain, phase imbalance, and phase noise on EVM. These works provide the analysis in a limited scope and do not provide the relation between the RF and system level requirements.

A consistent RF imperfection model is required for the wireless system standardisation work (e.g: 3GPP) which cannot be based on a specific RF architecture. Nevertheless, it is also difficult to make the study completely independent of the RF architecture because some imperfections are specific to some RF architectures. For example, the gain and phase imbalance are produced in the Cartesian transmitter architecture, and the envelope and phase timing alignment problem are in the Polar transmitter architecture.

The popular and commonly used RF architecture is the superheterodyne architecture and direct conversion architecture recently gained more popularity [15]. Each RF architecture has common components, such as local oscillator, mixer, filter, and amplifier. Those components have specific RF imperfections [16]. Furthermore, certain RF imperfections may occur in particular RF architecture [16]. In this work the study of the impact of hardware imperfections is facilitated by defining a behavioral model of each component. The behavioral model is obtained from the hardware measurement characteristics.

The relation between modulation format and power amplifier imperfection (nonlinearity) plays an important role in the physical layer design stage, especially for uplink transmission. The modulation format generally provides trade-off between bandwidth efficiency, power efficiency, and detectability [Raz99]. These three parameters determine the capacity, the talk time, and the maximum range [raz99]. The uplink direction prefers a modulation format which has low PAPR and leads to a better talk time duration. It becomes critical for wide cell coverage in the cellular system.

An investigation on nonlinear power amplifier (PA) for the OFDM transmission has been carried out, and the non-linearity introduced a performance degradation [17]. This is due to the high PAPR of the OFDM signals. The PAPR can be reduced using several PAPR mitigation techniques [18]. However, there is a design trade off between hardware complexity and system performance. Phase noise in the local oscillator may degrade the performance, and it is known that a multi-carrier based system is more sensitive to the phase noise [13]. The effect of phase noise in the LTE with channel estimation has also been investigated [19]. The channel estimation is based on the pilot aided channel estimation (PACE) scheme.

Polar transmitter is considered as an alternative RF transmitter architecture aiming at a better power amplifier efficiency. Recently, it has been investigated

for various wireless systems, such as EDGE, WCDMA, and OFDM wireless LAN [20], [21], [22]. The main benefit is a high power amplifier efficiency at varying power levels [23], and therefore it is suitable for a transmitter with varying envelope signals. 3GPP LTE is one of the new wireless systems, which has a varying envelope signal since it uses DFT-spread OFDM modulation with various modulation schemes (BPSK, QPSK, and 16QAM). A polar transmitter has numerous practical imperfections leading to spectral regrowth, increased EVM, and link performance loss. One of the main challenges is that a polar transmitter requires high precision timing alignment between the envelope and phase path [24].

1.4 Objectives

The motivation of this PhD project is to design the uplink physical multiple-access for the upcoming B3G mobile communication system taking into account the combined constraints from system requirements and RF hardware imperfections. The selection between single carrier and multi-carrier transmission schemes are the bottom line in the design consideration since the multiple-access schemes mainly depend on the radio transmission techniques. According to the best knowledge of the authors, no work has been done which provide a comprehensive result in relating the system level performance and RF requirements.

The PhD research work is expected to result in the preferred multiple access technique for the B3G system considering RF hardware imperfections and the RF transmitter requirements for the uplink direction. The work-scope can be illustrated in Figure 1.5. Physical layer parameter design, such as trade-off analysis, methodology and guidelines for RF architecture including RF impairments model will be given. It is essential to consider both system requirements and RF hardware constraints to determine a feasible and realistic air interface for LTE uplink. The approach/methodology gathered in this project can also be applied as the baseline in the design of uplink 4G system.

The PhD project has the following objectives:

1. Investigate the suitable air interfaces for the uplink transmission in Beyond 3G (B3G) system.

2. Investigate the beyond 3G system performance using advanced modulation & coding, multiple-antennas, link adaptation, and H-ARQ techniques on spectral efficiency, cell coverage, and link quality of the uplink direction.
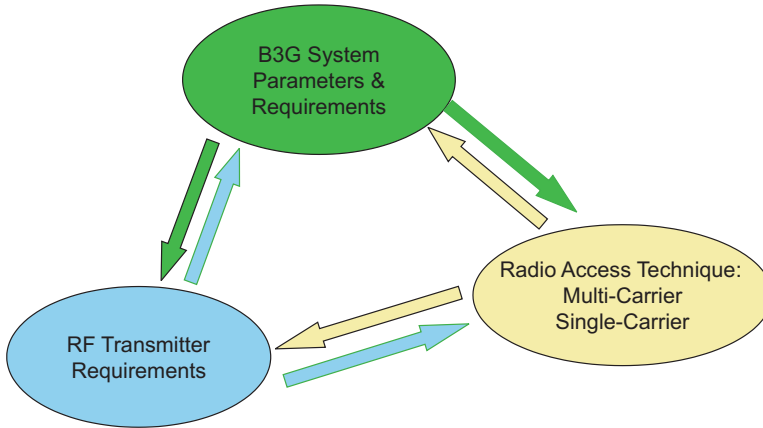
Figure 1.5: Work-scopes of the research project.

3. Identify and model the RF transmitter imperfections for the uplink direction.

4. Identify the RF transceiver requirements suitable for the uplink in B3G system.

5. Investigate the impact of the RF imperfections on the B3G uplink multi-user scenario that has a flexible transmission bandwidth.

6. Investigate the impact of the RF imperfections of the polar transmitter as the candidate for the future RF Transmitter Architecture which offers a high efficient power amplifier.

7. Investigate the impact of inband inter-user interference on the uplink multiple access of B3G system.

1.5 Scientific Methodology

This project considers the UTRA Long Term Evolution (LTE) system as a suitable system beyond 3G context to make the project results concrete and specific. Design of multiple-access for LTE has the objective to achieve high spectral efficiency. However, some of the multiple access schemes are vulnerable to RF imperfections. The uplink includes handset transmitter and base-station receiver. Therefore, in the uplink direction that has limitations related to handset cost, size and power consumption, these limitations in combination with RF imperfections will most likely necessitate a different, or at least modified,

physical access. Moreover, the many-to-one situation in the uplink require considerations on interference and power control related issues which are different than in the downlink direction.

Due to the complexity of the problem at hand the project makes extensive use of link simulations to observe the performance impact of different design choices in the presence of RF and baseband hardware imperfections. For this purpose, detailed link simulation software has been developed with specific contributions from this project on the RF hardware imperfections modelling. Analytical treatment is considered and is expected mainly to support the model development and confirm selected reference simulation results. The RF hardware architecture for the uplink transmitter and receiver chain, and the corresponding RF hardware imperfection models, are analyzed separately and summarized in computer simulation models to be used in the detailed link layer simulations.

The results have been obtained through link level simulation and analytical studies. A Monte Carlo link level simulation consists of a transmitter and receiver chain including a time dispersive channel model. The link level simulation consists of numerous advances techniques in wireless system to achieve high spectral efficiency [7]. The RF imperfection models have also been included to construct a practical simulator. The research methodology and obtained results are verified through the theoretical analysis and the comparison with the other existing simulation or measurement results.

The work of this project is divided in to two phases:

- The first phase provides the baseline results for the LTE uplink performance. A detailed study on the specific LTE uplink physical layer parameter settings in both transmitter and receiver is performed to find out the optimized settings. Most of the physical layer features, including various antenna schemes, adaptive modulation and coding schemes, Hybrid-ARQ, link adaptation, are considered. The performance for both multiple access schemes, OFDMA and SC-FDMA, are analyzed.

- The second phase is focused on the impact of RF transmitter hardware imperfections and results in the RF transmitter requirement for LTE uplink. RF transmitter design will define the minimum requirement using the parameters and test cases specified in the standardization. B3G system has stringent requirement in order to achieve high spectral efficiency. Thus, it is a big challenge to design the RF transmitter part, such as defining the RF architectures and RF component specifications. The key RF measurement parameters for the transmitter are the modulation accuracy or the Error Vector Magnitude (EVM), Spectrum Emission Mask (SEM) requirements, and Adjacent Channel Leakage Ratio (ACLR). Based on

these key parameters, the RF transmitter requirements for the uplink in B3G system can be specified.

1.6 Thesis Structure and Contributions

This thesis consists of 8 chapters. The overview of each chapter is presented and the contributions are highlighted in the bullet points.

Chapter 2 provides the background for the RF transmitter architectures, such as cartesian and polar type architectures. The hardware imperfections on the RF transmitter architecture model and assumptions are also presented.

Chapter 3 presents the summary of LTE Uplink baseline performance results. A detailed description on the developed link level simulator for LTE Uplink is made and the link level simulator validation is given in Appendix. A. The results are firstly given on the two main multiple-access schemes for the beyond 3G system, SC-FDMA and OFDMA. The impact of the new techniques in the beyond 3G system, such as H-ARQ, antenna schemes, frequency allocation/diversity, to enhance the spectral efficiency is then given. The additional feature to increase the performance by means of turbo equalization implementation at the receiver is discussed.

- Develop the UTRA LTE uplink link level simulator with most of L1 main functionalities. Analysis of the LTE uplink performance in the ideal condition without the hardware imperfections. My major contributions are the interleaver and de-interleaver, structuring the LTE uplink from the baseline LTE downlink[2], RF hardware imperfection model, and the turbo equalization for the uplink[3].

Chapter 4 summarizes the effect of RF imperfections on LTE Uplink performance. The Cartesian type architecture is assumed and the typical RF imperfections for Cartesian architecture, such as nonlinear power amplifier, phase noise, gain imbalance, phase imbalance and DC offset are considered.

- Provide the relation between individual RF imperfection EVM characteristics to the link level performance, especially to obtain a clear insight

---

[2]The LTE downlink was jointly developed together with the other PhD students: Akhilesh Pokhariyal, Na Wei, and Christian Rom.

[3]This study was undertaken in collaboration with the following research assistant: Gilberto Berardinelli.

in the sensitivity on each RF impairment. The link level performance is evaluated for AWGN and frequency selective fading channels. Performance evaluation in an AWGN channel represents the conditions under which EVM measurements are obtained for type approval, whereas the performance evaluation in frequency selective fading is more representative of actual operating conditions.

- Provide the relation between different RF transmitter impairment models in LTE uplink and how accurately the effect of each RF impairment can be modelled by an equivalent white Gaussian noise source in the transmitter.

- Performance of SC-FDMA and OFDMA with the presence of nonlinear power amplifier is evaluated.

Chapter 5 summarizes the RF transmitter design analysis on the spectrum emission control aspect. The peak-to-average power ratio reduction is mainly the design strategy to increase the power amplifier efficiency, and the spectrum emission control is to comply the transmit signal with the specification requirements.

- Propose and evaluate a spectrum shaping technique for LTE UE using an Inverse Chebyshev Digital Infinite Impulse Response (IIR) filter. The filter selection is based on studies in [25] where this filter type achieves minimum capacity loss.

Chapter 6 discusses the alternative RF transmitter architecture solution based on polar transmitter to achieve a high-efficiency power amplifier for LTE Uplink. The focus is on the impact of the polar transmitter imperfections, such as timing delay alignment, non-linear amplifier and filter.

- Provide a link between individual RF imperfection EVM characteristics to the link level performance, especially to obtain a clear insight of the sensitivity of each RF imperfection.

Chapter 7 discusses the In-band Inter-User Interference aspect on LTE Uplink. The scalable transmission bandwidth and flexible frequency allocation of the user equipment, fractional power control, and RF imperfections leads the LTE uplink vulnerable to the inter-user interference.

- Propose and evaluate the power control parameters and the acceptable RF imperfections level to reduce the inter-user interference in the LTE uplink.

Finally, Chapter 8 presents the conclusions and the future work.

1.7 Publications

During the PhD studies, the following publications have been published:

1. B.E Priyanto, G. Berardinelli, T.B. Sørensen, "Single Carrier Transmission for UTRA LTE Uplink," Long Term Evolution : 3GPP LTE Radio and Cellular Technology Handbook. Editor: Borko Furht, Syed A. Ahson. Boca Raton, Florida : CRC Press, April 2009.

2. B.E. Priyanto, T.B Sørensen, O.K. Jensen, "In-Band Interference Effects on UTRA LTE Uplink Resource Block Allocation," IEEE 67th Vehicular Technology Conference, Singapore, Singapore, May 2008.

3. B.E. Priyanto, T.B Sørensen, O.K. Jensen, T.E. Kolding, T. Larsen, P. Mogensen, "A Spectrum Shaping Technique to Control Spectrum Emission of UTRA LTE User Equipment," IEEE Norchip 2007 Conf, Aalborg, Denmark, November. 2007.

4. B.E. Priyanto, T.B Sørensen, O.K. Jensen, T.E. Kolding, T. Larsen, P. Mogensen, "Impact of Polar Transmitter Imperfections on UTRA LTE Uplink Performance," IEEE Norchip 2007 Conference, Aalborg, Denmark, November. 2007.

5. B.E. Priyanto, T.B Sørensen, O.K. Jensen, T.E. Kolding, T. Larsen, P. Mogensen "Assessing and Modelling The Effect of RF Impairments on UTRA LTE Uplink Performance," IEEE 66th Vehicular Technology Conference, Baltimore, United States, September 2007.

6. B.E. Priyanto, H. Codina, S.R. Simo, T.B Sørensen, P. Mogensen "Initial Performance Evaluation of DFT-Spread OFDM Based SC-FDMA for UTRA LTE Uplink," IEEE 65th Vehicular Technology Conference, Dublin, Ireland, April 2007.

7. B.E. Priyanto, C. Rom, , C.N. Manchón, T.B. Sørensen, P. Mogensen, O.K. Jensen, "Effect of Phase Noise on Spectral Efficiency for UTRA Long Term Evolution," IEEE 17th International Symposium on PIMRC, Helsinki, Finland, September. 2006.

8. B.E. Priyanto, T.B Sørensen, O.K Jensen, "On Investigation of Nonlinear Amplifier Distortion in OFDM Transmission," IWS2005, International Wireless Summit 2005, Aalborg, Denmark, September 2005.

Co-authored publications:

1. G. Berardinelli, B.E Priyanto, T.B. Sørensen, P.E. Mogensen, "Improving SC-FDMA Performance by Turbo Equalizer in UTRA LTE Uplink," IEEE 67th Vehicular Technology Conference, Singapore, Singapore, May 2008.

2. N. Wei, A. Pokhariyal, C. Rom, B.E. Priyanto, F. Frederiksen, C. Rosa, T.B. Sørensen, T.E. Kolding, P. Mogensen, "Baseline E-UTRA Downlink Spectral Efficiency Evaluation," IEEE 64th Vehicular Technology Conference, Montreal, Canada, September 2006.

3. N. Behjou, B.E. Priyanto, O.K. Jensen, T. Larsen, "Interference Issues between UMTS & WLAN in a Multi-Standard RF Receiver," IST Mobile Summit Proceedings, Myconos, Greece, June 2006.

4. N. Behjou, B.E. Priyanto, O.K. Jensen, T. Larsen, "RF Sub-System Design for Multi-Standard Digital-IF," International Symposium on Wireless Personal Multimedia Communcations, San Diego, United States, September 2006.

" No one is perfect... that's why pencils have erasers."

Anonymous

RF Transmitter Architectures & Imperfections

2.1 Introduction

In a wireless communication system, a transmitter produces an RF signal for sending the information to the receiver over the air. The transmitter can transmit at a high power level to overcome path loss and maintain a high transmission quality. Nevertheless, transmitting at high power can interfere other users since the transmission medium is shared among users. A power efficient transmitter is also prefered, especially for a battery operated device to maintain long battery life. Hence, there is a design trade-off in designing a transmitter.

A transmitter can be divided into two major parts: baseband and RF. Typically, the baseband part is implemented digitally and the RF part is analog. A digital to analog converter (DAC) is placed in between and connecting the baseband and RF part. The RF part for LTE has high requirements since it has a specific target to deliver high speed transmission for both uplink and downlink. Moreover, the users have demand on a handy, stylish, and long battery life user equipment [16]. Therefore, it is expected that the user equipment has the following target: keep minimizing the physical hardware size, efficient power usage, and high performance transmitter with minimal RF imperfections.

An RF transmitter plays an important role in a transceiver and principally has three main functionalities: modulation, upconversion and power amplification. An RF transmitter consists of analog devices with high cost and with relatively high power consumption. The RF transmitter design deals with the above functionalities and aims to choose the proper block diagram/analog components.

The type of transmitted signal is also a main factor in an RF transmitter. It can be classified as the constant and non-constant envelope signals. An RF transmitter gains advantage by processing a constant envelope signal because the signal can be amplified by the power amplifier at high efficiency [26]. The non-constant envelope or variable envelope modulation has a large signal dynamic range which can cause either a nonlinear distortion by the power amplifier or a low efficiency signal amplification. The 2nd generation of cellular systems, GSM and GPRS use a constant envelope signal, while the most recent systems, including LTE, use non-constant envelope signals.

The RF transmitter design results in various types of RF transmitter architectures. The motivation is to adapt to the signal type from the baseband, increase the power efficiency, reduce the cost and possibly to support multimode operation. In general, the RF transmitter architectures can be divided into two major different types: Cartesian architectures and polar architectures. Each of those types can be divided in several transmitter architectures and have advantages/drawbacks which must be considered during the design phase.

The performance of the RF transmitter must be evaluated and follow the requirements defined by the relevant standard. The transmit signal should conform with the transmit emission mask to ensure it does not interfere significantly with other channels. The accuracy of the transmitted modulated signal should be maintained high for reliable detection at the receiver and maintain high performance transmission. This is usually evaluated by the Error Vector Magnitude (EVM) parameter. Finally, a low power consumption is always preferred.

In this chapter, the overview of RF transmitter architectures on both cartesian and polar types is briefly introduced. A summary on the advantages and the disadvantages of each architecture is given. The most common RF imperfections in both cartesian and polar types are also elaborated, including the RF imperfections models. These models are later used in the study of the impact of RF imperfections.
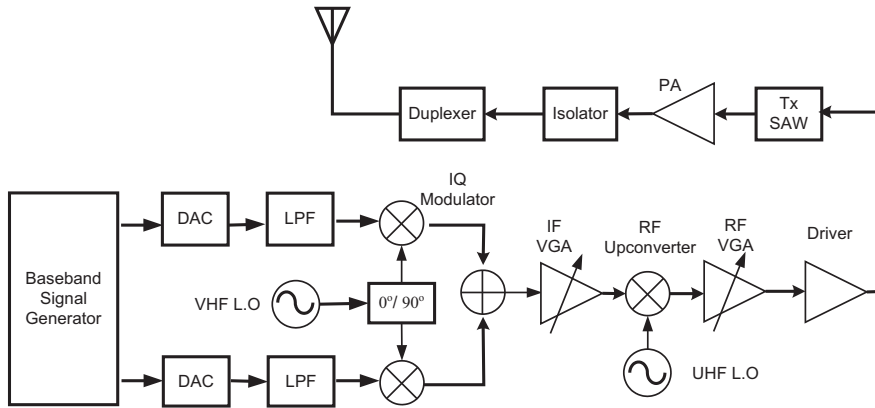
Figure 2.1: Cartesian superheterodyne RF transmitter architecture.

2.2 Cartesian Transmitter Architectures

Cartesian transmitter architectures fundamentally modulate the I&Q signals from the baseband generator separately and then add them together to form an IF or RF signal. There are many types of RF transmitter architectures based on the cartesian form, but one which is very popular is the superheterodyne architecture. This architecture was invented in 1918 and still widely used until now. A block diagram of the superheterodyne architecture is shown in Figure 2.1.

The I & Q baseband filtered analog input signals are mixed separately with an offset local oscillator (LO) in a non-linear device (mixer) to produce intermediate frequency (IF) signals. The LO signal for the Q channel is phase shifted by 90 degree to provide orthogonality with the I channel. The mixing and combining of I & Q channels are performed in the IQ modulator and produce a single IF signal. The IF signal is then amplified by a variable gain amplifier (VGA). The amplified IF signal is up-converted to the RF frequency. The RF signal is further amplified by an RF VGA and then by a driver amplifier to a level that is sufficient to drive the power amplifier (PA). Figure 2.1 shows that the variable gain control is located in both the IF and RF stage. The gain control in the IF is the crucial part since it dominates the overall gain control (around 75%) [15].

The commonly used PA is either a class AB or class C PA. Class AB is widely used in the TDMA, CDMA, and wideband CDMA mobile phones [15]. Class C is often employed in the GSM system [15]. An RF BPF filter is inserted between the driver amplifier and PA to select the desired frequency band and suppress

out of band noise and unwanted mixing products generated by the up-converter. The PA gain and linearity performance can be affected by the load impedance. Thus, an isolator may be required at the PA output to reduce the effect of antenna impedance variation [15]. This varying impedance problem is also very common in most other RF transmitter architectures. Finally, the duplexer has the primary task to reduce the transmitter signal leakage to the receiver and to suppress the noise and spurious emission.

Most of the cellular systems are operating in Frequency Division Multiplexing (FDD) mode, where the uplink and downlink channels are assigned to two differents frequency band. Each frequency band consists of multi-channels and typically each communication link occupies one channel. In this scenario, the frequency planning in the superheterodyne architecture is very important. The frequency planning task is to find and select the IF frequency, which should minimize the spurious response and should provide an excellent transceiver performance [15]. A superheterodyne transceiver may have the following fundamental signals:

- An RF local oscillator signal.

- A reference oscillator signal.

- Two or multiple RF signals.

- Two or multiple IF signals.

- A weak received RF signal.

- A high power transmitted signal.

The problem may occurs when there is a mixing products and harmonics in the superheterodyne architecture due to the nonlinear components (LNA, high power amplifier, and mixer). These potential issues are analyzed in the frequency planning stage[15]. In the frequency planning stage, potential problems related to mioxing products and harmonics due to nonlinear components (LNA, power amplifier, and mixer) are investigated.

The advantages and the disadvantages of the superheterodyne RF transmitter architecture are shown in Table 2.1

A solution to alleviate the superheterodyne RF transmitter is to employ a direct conversion RF transmitter architecture. The direct conversion is also known as the zero IF or homodyne architecture. The basic operation is a direct upconversion operation from the baseband to the RF signal without the IF stage. The

Table 2.1: The superheterodyne architecture.

The advantages:	The disadvantages:
• Widely used and a proven technology since 1918. • Implementation is quite straightforward. • Excellent performance in linearity.	• Requires a carefull design in the frequency plan, especially for a multi-mode user equipment. • High component counts. • High cost. • Large size.

configuration of a direct conversion architecture is shown in Figure 2.2. The direct conversion is less complex than the superheterodyne since the number of components is reduced. At least, it eliminates the need for IF components, such as filters, amplifiers, mixers, and local oscillator [27]. The benefit of the direct conversion transmitter is not so attractive as the direct conversion receiver since there is no expensive IF channel filter saving at the transmitter [15].

As for the heterodyne transmitter, the baseband IQ signals from the digital to analog converter (DAC) are filtered by low pass filters to suppress the adjacent channel and eliminate aliasing products. The low pass filter can be implemented by an active LPF. Therefore, the bandwidth can be adjusted with the benefit to support multi-mode transmission. The IQ signals are then up-converted to RF and combined together by an IQ modulator. The RF output signal is amplified by an RF VGA and a driver amplifier so that the output signal can drive the power amplifier. Most of the direct conversion transmitter gain (almost 90%) is generated in the RF stage [15]. An RF BPF is placed at the input of the PA to suppress the out-of-band emission, leakage at the receiver band, and the noise emission. An isolator and duplexer are also required for the direct conversion transmitter.

Beside the advantages, the direct conversion transmitter suffers from the implementation issues, such as the injection pulling [16]. In a direct conversion transmitter, the output signal and the local oscillator signal have the same frequency. The injection pulling occurs when the signal at the high power amplifier output is coupled back to the oscillator. The impact of the injection pulling can be reduced if the high power amplifier output spectrum is sufficiently higher
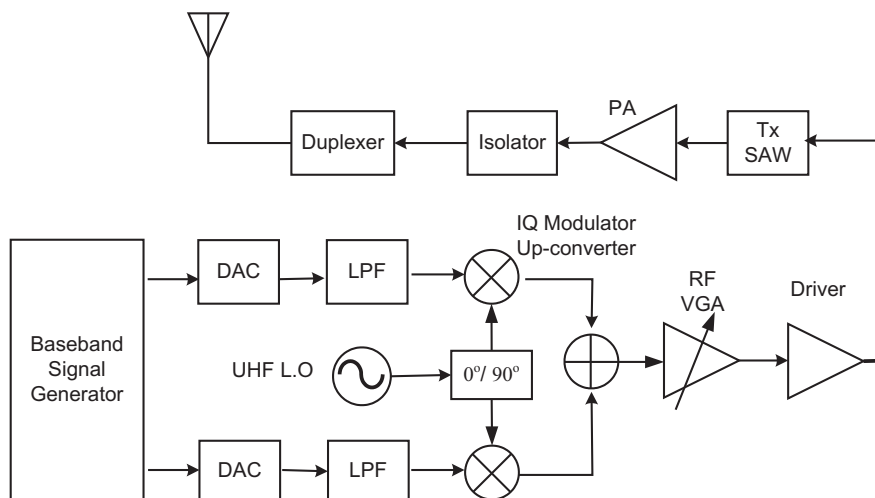
Figure 2.2: The direct conversion (homodyne) RF transmitter architecture.

or lower than the local oscillator frequency. It can be done by employing two local oscillators and the frequency input to the modulator is the addition or substraction of these two local oscillator frequencies. Alternatively, the local oscillator voltage controlled oscillator (VCO) may be operated at twice the RF frequency with subsequently frequency division by a factor of two. The direct conversion is also sensitive to the I&Q imbalance issues since the modulation is performed in RF stage. The dynamic range in RF stage is also difficult to obtain and requires high power consumption [28].

The advantages and the disadvantages of the direct conversion (homodyne) RF transmitter architecture is shown in Table 2.2.

Recently introduced is another alternative architecture with I&Q modulation in the digital domain. It can be achieved by recent developments in the digital semiconductor technology. The architecture is known as bandpass sampling RF transmitter and shown in Figure 2.3.

The baseband I&Q signals filtering and I&Q modulator are performed digitally. The I&Q modulator output is a digital low-IF signal. Prior to the analog conversion by a high performance DAC, the signal is oversampled to further shift the image product. When this architecture is used with a commercial cellular system (WCDMA), the DAC must have at least 14 bits to maintain a high sig-

Table 2.2: The direct conversion architecture.

The advantages:	The disadvantages:
• Cost reduction by reducing the number of components. • Size reduction. • Easy for multi-mode operation. • Does not need a frequency plan. • Much less spurious products than for the superheterodyne type [15].	• Problem with the injection pulling. • Problem with the I&Q imbalances issue. • Difficulty to maintain high dynamic range. • Current consumption relatively high. • Difficult for multi-band operation.

nal to noise ratio output [15]. The analog output is connected to the RF BPF filter with the task to select one of the spectral replicas of the signal centered at the carrier frequency and suppress the other replicas and the out-of band noise. The bandwidth of the RF BPF filter is usually the frequency range of the intended application. The filter output is then amplified by the driver amplifier and a power amplifier. The transmitter signal dynamic range is controlled by the PA gain control range, driver amplifier, and adjustable DAC voltage level output [15].

The bandpass sampling RF transmitter architecture has the advantages and the disadvantages as shown in Table 2.3.

From these three types of cartesian based architectures, it can be observed the filters have three functionalities. First, the baseband lowpass filter to limit the transmit signal in the channel bandwidth and shape the transmit signal spectrum. Second, the IF/RF bandpass filter to remove the unwanted output after the frequency conversion. Third, the bandpass filter in the duplexer is to prevent spurious and out of band emission [29].
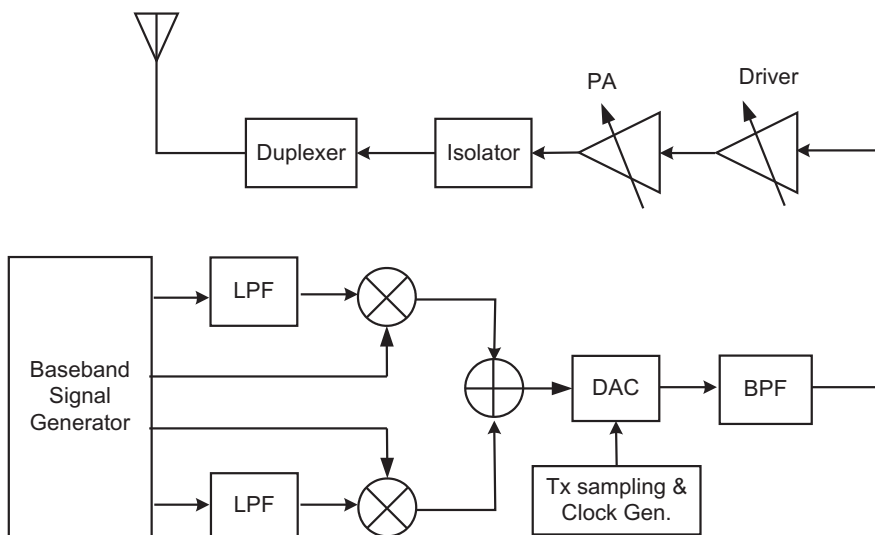
Figure 2.3: The bandpass sampling RF transmitter architecture.

Table 2.3: The bandpass sampling architecture.

The advantages:	**The disadvantages:**
• Most of of the blocks can be implemented in an integrated circuit. • Cost reduction. • Size reduction. • Some technical problems in the direct conversion architecture can be solved.	• Requires a DAC with high sampling rate and a high dynamic range. • High power consumption, especially at high sampling rate operation.

2.3 Cartesian Transmitter Imperfections

In practice, the RF cartesian transmitter described in the previous section is accompanied with the imperfections from the components. The basic components of an RF transmitter are analog filter, mixer, local oscillator and power amplifier. The imperfections become more severe for a transmitter with the low end (low cost) components. This section describes the most common RF transmitter imperfections, including nonlinear power amplifier, phase noise, gain and phase imbalances and DC offset. The generic imperfections models are also given. These well-known models are used to facilitate the study on the impact of imperfections. The models of the imperfections are not dependent on the choice of the architectures mentioned above.

2.3.1 Nonlinear Power Amplifier

The power amplifier amplifies the transmitted signal to ensure the received signal has sufficient signal to noise ratio by compensating the path-loss between transmitter and receiver. One factor which must be highly considered is that the power amplifier consumes a lot of power used in both handset and base-station transceivers. Therefore, achieving a highly efficient power amplifier is always desirable [30].

A power amplifier typically operates as a linear device for a small-signal. Increasing the input power signal makes the power amplifier operate as a nonlinear device and start to distort the transmitted signal. The distortion generates additional noise within the in-band channel and increase spectral regrowth in the adjacent channel. The linear and nonlinear operating region of a power amplifier is clearly defined by a saturation point of an amplifier. Within the linear region, a power amplifier provides a linear gain and at the saturation point the gain of output signal is reduced by 1 dB. From this characteristic, the saturation point is also known as 1 dB compression point. For simplicity, a power amplifier is assumed to be a time variant memoryless devices, and the nonlinearity effect of a power amplifier on the transmitted signal is modeled as a power series [16]:

$$y(t) \approx \alpha_1 x(t) + \alpha_2 x^2(t) + \alpha_3 x^3(t) \tag{2.1}$$

The higher-order terms is known as harmonic distortion products. In (2.1), the nonlinearity effect of input signal with the power higher than 3 is neglected.

If a sinusoid signal $x(t) = A\cos\omega t$ is the input signal, the output signal can be

written as:

$$y(t) \approx \frac{\alpha_2 A^2}{2} + \left(\alpha_1 A + \frac{3\alpha_3 A^3}{4} \right) \cos \omega t + \frac{2\alpha_2 A^2}{2} \cos 2\omega t + \frac{\alpha_3 A^3}{4} \cos 3\omega t \quad (2.2)$$

The nonlinearity is often described as the third order nonlinear effect. To form the saturation impact in which increasing the input power results in saturated output signal, α_3 parameter in (2.2) is defined as a negative coefficient. Therefore, the third order nonlinear effect reduces the gain of the fundamental frequency ($\alpha_3 < 0$):

$$y(t) \approx \left(\alpha_1 A + \frac{3\alpha_3 A^3}{4} \right) \cos \omega t \quad (2.3)$$

From (2.3), the 1-dB compression point can be derived as follow:

$$A_{1dB} = \sqrt{0.145 \left| \frac{\alpha_1}{\alpha_3} \right|} \quad (2.4)$$

Beside the harmonic distortion, the non-linearity of a power amplifier can create intermodulation distortion. It is typically measured when two signals at different frequencies are the input of a power amplifier and generates output signal with the new frequency components that are not harmonic to the input frequencies. The intermodulation distortion is often characterized by the third order intermodulation and the performance is measured as third order intercept point, IP_3. The third order intercept point is defined as the intersection between the linear gain curve of the input signal and the third order product curve of the input signal. From 2.1, the input IP_3 can be written as [16]:

$$A_{IP_3} = \sqrt{\frac{4}{3} \left| \frac{\alpha_1}{\alpha_3} \right|} \quad (2.5)$$

From. (2.4) and (2.5), the input IP_3 and 1dB compression point have the following relationship:

$$\frac{A_{1dB}}{A_{IP_3}} \approx 9.6 \text{ dB} \quad (2.6)$$

The power amplifier output signal characteristic is illustrated in Figure 2.4

The nonlinear power amplifier gain as explained in (2.3) is usually known as AM/AM characteristic (amplitude to amplitude distortion), where the relation of input and output signals in both linear and nonlinear regions can be observed. The phase component of a power amplifier output signal also poses a nonlinearity
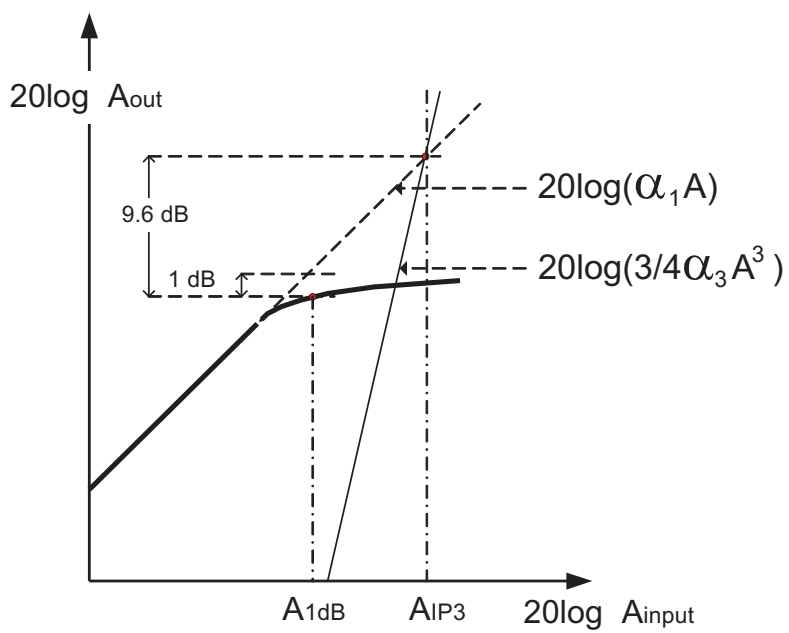
Figure 2.4: The power amplifier output signal characteristic.

effect and it is known as AM/PM characteristic (amplitude to phase distortion). The AM/PM has a similar behaviour as the AM/AM, when the input power signal is increased, the phase output start to deviates. In practice, both AM/AM and AM/PM are characterized from a hardware measurement.

The performance of a power amplifier also includes to the efficiency factor. The power amplifier efficiency is usually defined as DC supply efficiency and power added efficiency (PAE). The power amplifier DC supply efficiency is expressed as follow [31]:

$$\eta_{DC} = \frac{P_o}{P_{DC}} \tag{2.7}$$

where P_o is the power amplifier ouput delivered to the antenna and P_{DC} is the DC power in watts supplied to the power amplifier. PAE is a measure of the signal power added by the power amplifier and it is expressed as follows [31]:

$$\eta_{PAE} = \frac{P_o - P_i}{P_{DC}} \tag{2.8}$$

where P_i is the input signal power.

2.3.2   Gain & Phase Imbalances

An analog IQ modulator has a task to combine the I & Q channels to form the IF or RF signal. A perfect I&Q modulator provides equal gain in the I&Q channels and the Q channel is upconverted by a 90 degree phase shift relative to the I channel. The practical I&Q modulator usually has imperfections and results in imperfect match between the I & Q signals. The imperfections are known as gain and phase imbalances. A gain imbalance makes the I channel becomes slightly smaller than Q channel, or vice versa. The phase imbalance causes the Q channel not to be shifted by exactly 90 degree with respect to the I channel. In practice, the amplitude imbalance is in the order of 1 dB and phase imbalance below 5 degree [16].

The impact of gain and phase imbalance can be simply modeled using the baseband representation. The distorted modulator output signal is written as [32]:

$$y(t) = y_I(t) + jy_Q(t) \tag{2.9}$$

$$y_I(t) = \sqrt{\frac{2}{1+\alpha^2}} \left(x_I(t) - \alpha x_Q(t) sin(\theta) \right) \tag{2.10}$$

$$y_Q(t) = \sqrt{\frac{2}{1+\alpha^2}} \left(\alpha x_Q(t) cos(\theta) \right) \tag{2.11}$$

where α and θ are the gain imbalance and the phase imbalance parameters between the in-phase and quadrature channels, respectively. $x_I(t)$ and $x_Q(t)$ are the input signals to the I&Q modulator.

2.3.3 Phase Noise

The Phase noise can be described as the phase fluctuations due to the random frequency fluctuations of a local oscillator signal. A perfect local oscillator generates a discrete single carrier frequency. However, due to the instability of a local oscillator, it creates a random frequency around the center frequency of a local oscillator. The performance of local oscillator is usually characterized by measuring the sideband noise of the output signal center frequency. The single-side band (SSB) phase noise is specified in dBc/Hz at a specified frequency offset from the carrier frequency.

The phase noise can be modeled as a Wiener-Lévy process [33]. This model is quite accurate to model a free-running oscillator and appropriate for quantitative studies of system performance degradation due to phase noise [33]. The phase noise effects can be seen as a multiplication of the transmitted signal with a noisy carrier $e^{j\Phi(t)}$. The random phase of this carrier is modeled by a Wiener-Lévy process as follows [13]:

$$\Phi(t) = 2\pi \int_0^t \mu(\tau)\, d\tau \tag{2.12}$$

In (2.12), $\mu(t)$ is a zero-mean white Gaussian process with power spectral density N_0 . The resulting relative *single-sideband* (SSB) phase noise power spectral density follows a Lorentzian spectrum [13]:

$$L(f) = \frac{2}{\pi \Delta f_{3dB}} \cdot \frac{1}{1 + \left(\frac{2f}{\Delta f_{3dB}}\right)^2} \tag{2.13}$$

In (2.13), $\Delta f_{3dB} = 2\pi N_0$ is the two-sided 3 dB bandwidth of phase noise. The power spectrum in (2.13) is an approximation to practical oscillator spectra, which enables analytical treatment.

The impact of the phase noise on the output signal can be simply modeled in a baseband representation [34]:

$$y(t) = x(t) \cdot e^{\phi(t)} \tag{2.14}$$

where $x(t)$ is the input signal and $\phi(t)$ is time varying phase noise process generated by the local oscilator at the transmitter.

2.3.4   DC Offset

DC offset in the transmitter occurs because of the additional dc signal generated in the baseband gain stage. The DC offset distorts the signal by shifting the IQ origin center of the signal constellation diagram. Thus, it causes a signal saturation and bit error rate (BER) performance degradation [28]. The DC offset is also known as the major problem in a direct conversion receiver.

The DC offset effect can be modeled using a discrete baseband model representation and shown as [35]:

$$y(t) = y_I(t) + jy_Q(t) \tag{2.15}$$

$$y_I(t) = x_I(t) + DC_I \tag{2.16}$$

$$y_Q(n) = x_Q(t) + DC_Q \tag{2.17}$$

where $a_I(t)$ and $a_Q(t)$ are the inphase and quadrature input signals, respectively. DC_I and DC_Q are the DC offset values in voltage. A similar problem is the limited LO-RF leakage in the mixers in the modulator. The effect is the same and is also covered by the model described.

2.3.5   DAC resolution and sampling rate

The digital to analog Converter (DAC) is the interface between the baseband and RF part. The DAC has several key parameters of which the most common are the DAC number of bits and the sampling rate. A DAC with a higher number of bits is prefered for a better performance because it can increase the signal dynamic range and resolution. The usable dynamic range of a DAC is known as spurious free dynamic range (SFDR) and illustrated in Figure 2.5. SFDR is the measure of the difference in amplitude between the fundamental and largest harmonically or non-harmonically related spur from DC to the half
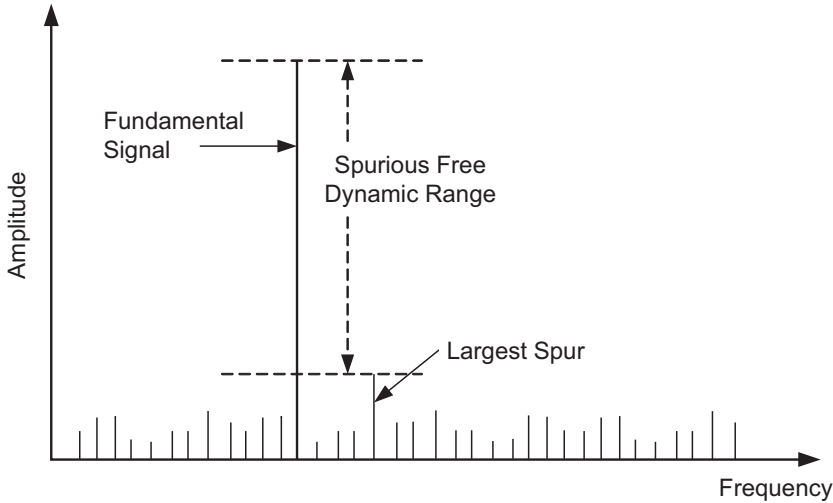
Figure 2.5: Measure of spurious free dynamic range [3].

the DAC sampling rate (the full Nyquist bandwidth) [3]. In an ideal DAC, the worst case Signal to Noise Ratio is given by [3]:

$$SNR_{ideal} = 6.02(N) + 1.76 \text{ (dB)} \tag{2.18}$$

where N is the DAC's number of bits. A DAC with 10 bits results in an SNR of 62 dB. This result is with an assumption that the quantization noise is uniformly distributed. The digital system does not have spurious noise which may affect the spectral performance. Therefore, the SFDR equals the worst case SNR [3]. The actual DAC can have the following factors: total harmonic distortion, non-linearity, power supply noise, which may affect the performance. Typically, an SFDR of -58 dBc is an average performance for a 10 bit DAC.

The sampling rate is usually defined by the input baseband signal sampling rate. A higher sampling rate for oversampled data input brings benefit to further shift the image product and results in more relaxed analog filter specifications. However, a high number of bits and large sampling rate has drawbacks in term of cost and high power consumption. For the latest application, such as Wimax, a 14 bits DAC with 80 MHz sampling rate (4x over sampling) provides a good transmitter performance[36].

In this work, the DAC is assumed to be ideal. The transmitter is assumed to use a sufficient DAC resolution. To limit the scope of the work, the DAC imperfections are not investigated.
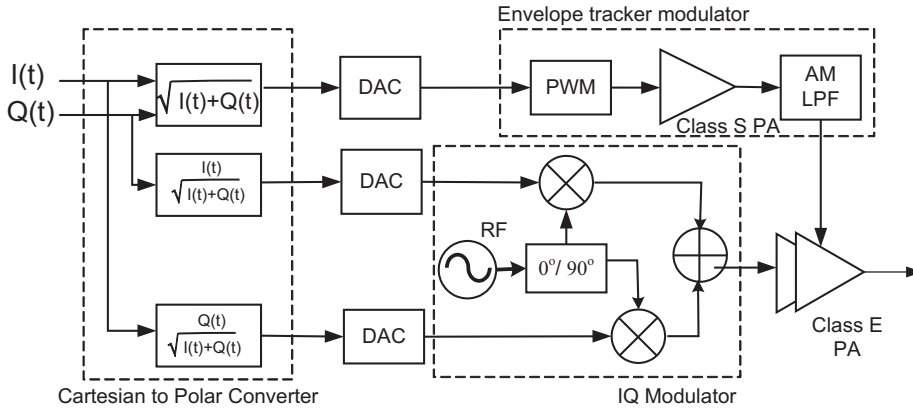
Figure 2.6: Polar EER transmitter architecture.

2.4   Polar Transmitter Architecture

The power amplifier efficiency is the main factor which may affect the wireless transceiver power consumption. There are many efforts in the RF transmitter architecture areas in order to increase the power amplifier efficiency [31], [26], [26]. Polar transmitter is one of RF transmitter architecture which offer a power amplifier with a high efficiency.

The polar transmitter was initially invented by Kahn and named as Envelope Elimination and Restoration (EER) transmitter [37]. Recently, it has been investigated for various wireless system, such as EDGE, WCDMA, and OFDM wireless LAN [20],[22],[21]. The main benefit is a high power amplifier efficiency at varying power levels [23] and therefore it is suitable for a transmitter with varying envelope signals. A polar transmitter has numerous practical imperfections leading to spectral regrowth, increase of Error Vector Magnitude (EVM) and link performance loss. One of the main challenges is that a polar transmitter requires a high precision timing alignment between the envelope and phase path [24].

The polar transmitter structure is shown in Figure 2.6. The baseband signal generator output is up-sampled and filtered to further shift the image product. The original EER polar transmitter separates the analog envelope and phase paths and processes them separately, and later restores the full signal at RF[37]. Here, the separation, or the envelope elimination process, is performed digitally. The purpose is to avoid analog RF coupler, envelope detector and limiter which typically are used in the original EER polar transmitter.

The envelope polar signal is defined as:

$$A(t) = \sqrt{I(t)^2 + Q(t)^2} \tag{2.19}$$

where $I(t)$ and $Q(t)$ are the Inphase and Quadrature signals, respectively. Similarly, the phase signal is defined via the two signals I_θ and Q_θ:

$$I_\theta(t) = \cos(\theta(t)) = \frac{I(t)}{A(t)} \tag{2.20}$$

$$Q_\theta(t) = \sin(\theta(t)) = \frac{Q(t)}{A(t)} \tag{2.21}$$

The nonlinear process results in a wider spectra of the output envelope signal compared to the input I&Q signals [24]. For the WCDMA application, Results in [38] shows that at least a filter with the bandwidth of three times baseband bandwidth is required to meet WCDMA spectrum emission mask. The envelope signal is amplified using a cascade of a pulse-width modulator (PWM), a switch mode class S amplifier, and a low pass filter (blocks inside the dashed box in Fig. 2.6). The wide bandwidth envelope signal requires a high switching frequency which can result in reduced class-S PA efficiency [39]. In this work, the envelope signal amplification is idealized. The phase path is up-converted to RF. It can be done by an IQ modulator as shown in Fig. 2.6 or by a two-point-modulation phase locked-loop (PLL) [22]. The RF phase signal is then driving the PA and the envelope is applied through the PA power supply.

2.5 Polar Transmitter Imperfections

A polar transmitter brings benefit for achieving a highly efficient power amplifier but also suffers from several imperfections. The most common imperfections in a polar transmitter are described in the following section.

2.5.1 Timing Delay Alignment

After the envelope elimination process, the envelope and phase paths are treated separately prior to the signal restoration in the class E power amplifier. The individual paths can generate a timing delay alignment problem in the signal restoration phase. The restored output signal phase, affected by the timing delay, Δt, in the phase path is defined as follows:

$$\theta'(t) = \theta(t + \Delta t) \tag{2.22}$$

2.5.2 Non-ideal PA

The AM/AM and AM/PM distortions always occur in the practical power amplifier, especially when operating the signal at the maximum output power. The output signal is also affected by a signal leakage from the phase path which shows up at low voltage levels [20]. The leakage is typically created due to capacitive parasitic components.

A simple non-ideal PA model is included in Figure 2.7. The envelope path is distorted by an AM/AM distortion. This distortion is modeled by a third order non-linearity which results in a signal amplitude given by:

$$A'(t) = A(t) + AM \cdot A(t)^3 \tag{2.23}$$

where AM is the power level factor of the harmonic product relative to the average signal input power. The AM parameter is basically the coefficient of the third order component. The AM/PM conversion also distorts the output signal.

Measurement results on a class E PA suggest a linear phase deviation as a function of input power level [20]. Here, the AM/PM is modeled by the linear slope PM to produce the signal phase:

$$\theta'(t) = \theta(t) + PM \cdot A(t) \tag{2.24}$$

The output signal is also affected by a signal leakage from the phase path which shows up at low envelope levels. The leakage is typically created due to capacitive parasitic components. Measurement results from [20] suggests that the leakage is modelled by the following additive phasor:

$$s_L(t) = L \cdot Re\left\{ e^{j\pi/2} \cdot e^{j\theta(t)} \cdot e^{j\omega_C t} \right\} \tag{2.25}$$

where L is the power level factor of the leakage signal relative to the average input signal power, and $e^{(j\pi/2)}$ is a constant phase offset of $\pi/2$.

Finally, the output signal affected by all of these imperfections is represented as:

$$s(t) = A'(t) \cdot Re\left\{ e^{j(\theta(t+\Delta t)+PM \cdot A(t))} \cdot e^{j\omega_C t} \right\} + s_L(t) \tag{2.26}$$

where ω_C is the RF carrier frequency.

The final model representing the timing delay alignment mismatch and the non-ideal PA is shown in Figure 2.7
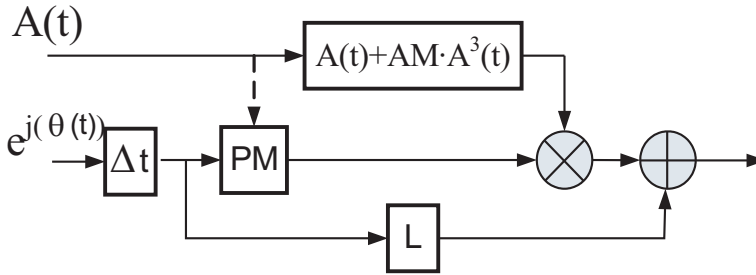
Figure 2.7: Imperfections model in a polar transmitter.

2.6 Summary

There are many RF transmitter architecture types and each of them has several advantages and disadvantages. Each architecture has its own RF imperfections consideration. The DC offset becomes a crucial factor in a direct conversion, but not for the other cartesian architecture family. The polar transmitter has a main issue in dealing with timing delay alignment mismatch. Therefore, it is very important to investigate the impact of those imperfections. The design challenge of the RF transmitter architecture is to supports a high transmission data rate, therefore it requires a high performance transmitter with small imperfections. The cartesian transmitter architecture still dominates and is widely used in the existing wireless systems. The polar transmitter which offer better power efficiency starts to be employed but comes along with many design challenges. It can be noticed that the power consumption still remains the main issue in the RF transmitter architecture design. High power consumption can be due to the high linearity power amplifier requirement or a high sampling rate of a DAC. The imperfections in each RF transmitter must be considered carefully so that the system can achieve a high performance and meet the requirement defined by the specification.

Baseline LTE Uplink Performance Analysis

3.1 Introduction

LTE uplink transmission has numerous recent physical layer considerations in comparison to the UTRA WCDMA system, mainly to achieve 2-3 times better spectral efficiency. These advances include a flexible channel bandwidth up to 20 MHz, flexible user resource blocks allocation in both time and frequency domain, and a shorter time transmission interval (TTI) of 1 ms. Specifically challenging for the uplink is that these enhancements are to be achieved, preferably, with reduced power consumption to extend the battery life and/or increase the cell coverage.

The radio access technique is one of the key issues in the LTE uplink air interface. In LTE, Orthogonal Frequency Division Multiple-Access (OFDMA) has been selected as the multiple access scheme for downlink and Single-Carrier Frequency Division Multiple-Access (SC-FDMA) for uplink. OFDM is an attractive modulation technique in a cellular environment to combat frequency selective fading channel with a relatively low-complexity receiver [40]. However, OFDM requires an expensive and inherently inefficient power amplifier in the transmitter due to the high Peak-to-Average Power Ratio (PAPR) of the

multi-carrier signal.

Single Carrier transmission with Cyclic Prefix (SC-CP) is an alternative transmission scheme with the same attractive multipath interference mitigation property as OFDM [9, 10, 11]. Therefore, SC-CP can achieve a link level performance comparable to OFDM for the same complexity, but at reduced PAPR [9]. In addition, the performance of SC-CP can be further improved by using a turbo equalization receiver [41]. The choice of single carrier transmission in a DFT-Spread OFDM form allows for a relatively high degree of commonality with the downlink OFDM scheme and the possibility to use the same system parameters [5]. Moreover, it enables a direct access to frequency domain to perform frequency domain equalization [9].

The aim of this work is to assess the LTE uplink performance and provide the baseline results in ideal condition without the RF imperfection. The impact and significance of the key techniques in LTE uplink are evaluated. The baseline performance evaluation is based on the two candidates for beyond 3G radio access technique which are OFDMA and SC-FDMA. OFDMA is evaluated because it is still a candidate for the other beyond 3G uplink system, such as Wimax and, later both performance can be assessed. The baseline results are used as the reference for the subsequent study in dealing with the RF transmitter imperfections.

This chapter is organized as follows. LTE uplink numerology is introduced in Section 3.2. The description of both radio access techniques is given in Section 3.3. LTE uplink transmitter & receiver model used in this study is given in Section 3.4. The peak-to-average power ratio (PAPR) evaluation for each radio access scheme is discussed in Section 3.5. Frequency domain equalization in LTE uplink receiver is discussed in Section 3.6, including both minimum mean-square error (MMSE) and zero forcing (ZF) techniques. Afterwards, the LTE uplink performance with various key techniques is presented, including fast H-ARQ in Section 3.8, link adaptation in Section 3.7, antenna configuration in Section 3.9, flexible frequency allocation in Section 3.10. Channel estimation with wiener filter is given in Section 3.11. Turbo equalizer, as a performance enhancement technique for SC-FDMA transmission, is presented in Section 3.12. Finally, a summary is given in Section 3.13.

3.2   LTE Uplink Numerology

The basic physical layer parameters that were originally designed for the uplink are shown in Table 3.1 [5]. The transmission scheme is SC-FDMA in a

DFT-spread OFDM form. Different transmission bandwidths have different parameter settings. The transmission is frame based with a radio frame duration of 10 ms and consists of 20 sub-frames of 0.5 ms. A sub-frame is equivalent to a transmission time interval (TTI). The sub-frame structure for uplink transmission is shown in Figure 3.1.
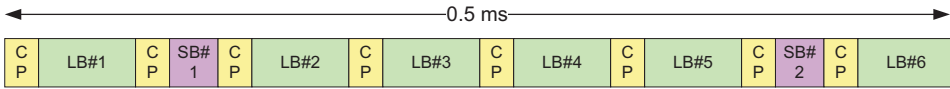
Figure 3.1: LTE uplink sub-frame structure with 2 short blocks.

Based on [5], a sub-frame consists of two short blocks and six long blocks. The short-block is a reference symbol and transmitted in a time-multiplex format with the long-block. It has the following purposes:

- Uplink channel estimation for uplink coherent demodulation/detection

- Possible uplink channel quality estimation for uplink frequency and/or time-domain channel dependent scheduling

The short block duration is half the long block duration. The long block is primarily used to transmit data.

In the work item phase, 3GPP has modified certain physical layer parameters, and hence has changed the assumptions that were initially applied for the evaluations. In particular, the sub-frame/TTI duration has changed to 1 ms to include two 0.5 ms slots, each with a structure as shown in Figure 3.2. The modified short blok duration is equal to the long block. At the writing of this dissertation, the position of the modified short block has not been finalized. In Figure 3.2, the modified short block is located in the middle of the slot. Initially, the supported modulation schemes are $\pi/2$ BPSK, QPSK, 8PSK, and 16QAM. In the work item phase, the supported modulation scheme for data transmission was changed in the work item phase to QPSK, 16QAM, and 64QAM (optional).
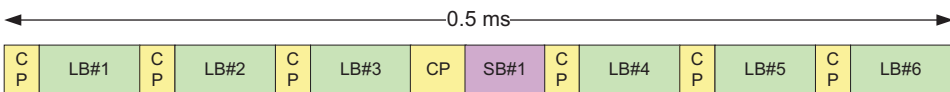
Figure 3.2: LTE uplink slot structure with 1 short block.

Transmission BW(MHz)	1.25	2.5	5	10	15	20
Sub-frame duration	0.5ms	0.5ms	0.5ms	0.5ms	0.5ms	0.5ms
Subcarrier spacing	15kHz	15kHz	15kHz	15kHz	15kHz	15kHz
Sampling frequency (MHz)	1.92	3.84	7.68	15.36	23.04	30.72
Long block FFT size	128	256	512	1024	1536	2048
Long block Number of occupied subcarriers	75	150	300	600	900	1200
Short block FFT size	64	128	256	512	768	1024
Short block Number of occupied subcarriers	38	75	150	300	450	600
CP length (μs /samples)	(3.65/7)x7, ((7.81/15)x1 ^{a}	(3.91/15)x7, (5.99/23)x1	(4.04/31)x7, (5.08/39)x1	(4.1/63)x7, (4.62/71)x1	(4.12/95)x7, (4.47/103)x1	(4.13/127)x7, (4.39/135)x1

Table 3.1: Parameters for LTE uplink [5]

---

^{a}$(x1/y1)$xn1,$(x2/y2)$xn2 means $(x1/y1)$ for $n1$ reference signal or data blocks and $(x2/y2)$ for $n2$ reference signal or data blocks

3.3 Modelling of Radio Access Techniques

The basic uplink transmission technique is single-carrier transmission with cyclic prefix to achieve uplink inter-user orthogonality and to enable efficient frequency-domain equalization at the receiver side. The transmitter and receiver structure for SC-FDMA transmission is shown in Figure 3.3. An SC-FDMA structure is identified by the insertion of a DFT spreading and an IDFT despreading at the transmitter and receiver, respectively. From this implementation structure, SC-FDMA is also known as DFT-spread-OFDM. DFT-Spread OFDM is a form of the single-carrier transmission technique where the signal is generated in frequency-domain. The DFT spreading combines parallel M-PSK/M-QAM symbols to form an SC-FDMA symbol.
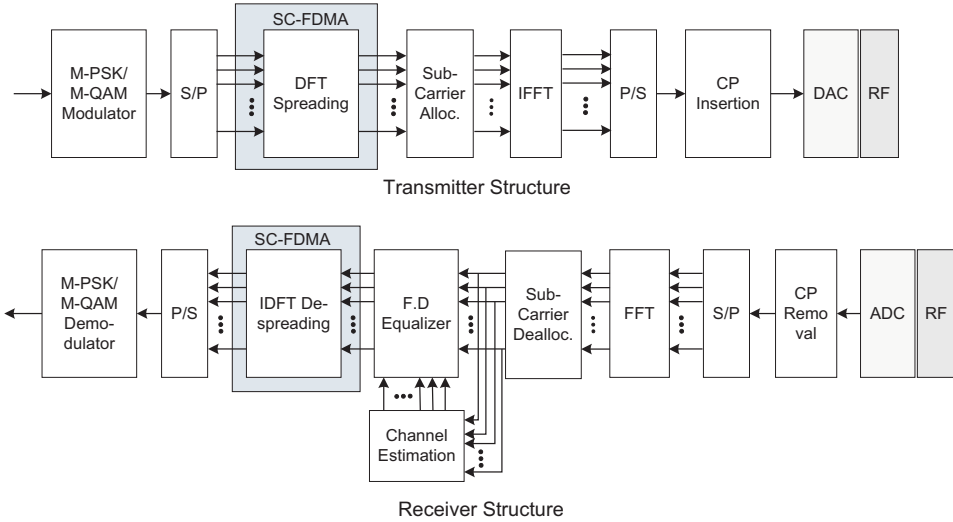
Figure 3.3: OFDMA & SC-FDMA basic transmitter & receiver structure.

To formulate the DFT-Spread system, we can start by defining s_m as the mth transmitted symbol at the output of an equivalent OFDM system. The modulator converts the random bit stream input to the M-QAM/M-PSK symbols and represented by the vector $\mathbf{x_m}$ of length N_d. The OFDM system then constructs s_m as:

$$\mathbf{s_m} = \mathbf{F_m} \cdot \mathbf{x_m} \tag{3.1}$$

where $\mathbf{F_m}$ is a matrix which performs an N_s point Inverse Fast Fourier Transform (IFFT) operation. N_s is the number of IFFT output samples. N_g is the length of the guard interval samples, and $N_{gs} = N_g + N_s$ is the length of the

$$\mathbf{D_m} = \begin{pmatrix} D_{m,0}[0] & & \cdots & & D_{m,N_d-1}[0] \\ & \ddots & & & \\ \vdots & & D_{m,k}[n] & & \vdots \\ & & & \ddots & \\ D_{m,0}[N_d-1] & & \cdots & & D_{m,N_d-1}[N_d-1] \end{pmatrix} \quad (3.3)$$

total time domain symbol.

The mth transmitted symbol in a DFT-S OFDM system can be expressed as a vector of length N_{gs} samples, defined by:

$$\mathbf{s_m} = \mathbf{F_m} \cdot \mathbf{T_m} \cdot \mathbf{D_m} \cdot \mathbf{x_m} \quad (3.2)$$

$\mathbf{D_m}$ is a matrix which performs an N_d points Discrete Fourier Transform (DFT) operation. The DFT spreading matrix element is expressed as:

$$D_{m,k}[n] = \frac{1}{\sqrt{N_d}} . e^{-j2\pi k\left(\frac{n}{N_d}\right)} \quad (3.4)$$

where k is the M-QAM/PSK symbol index. $\mathbf{T_m}$ is a $N_s \times N_d$ mapping matrix for the subcarrier allocation. The subcarrier allocation can be classified in two allocation modes, namely distributed and localized allocation [5] (See also Figure 3.18). In distributed mode, $N_s = S_f \cdot N_d$ with S_f defined as the spreading factor. The matrix of subcarrier allocation in localized mode is defined as:

$$\mathbf{T_m} = [\mathbf{0_{q \times S_f, 1}} \mathbf{J_{N_d, 1}} \mathbf{0_{N_s - N_d - q \times S_f}}; \mathbf{0_{N_s, N_d - 1}}] \quad (3.5)$$

Where q is the localized chunk index. $J_{a,b}$ is an $a \times b$ matrix of ones. For the distributed mode, the sub-carrier allocation matrix is defined as:

$$\mathbf{T_m} = [\mathbf{J_{1,1}} \mathbf{0_{S_f - 1, 1}} \cdots \mathbf{J_{N_d, 1}} \mathbf{0_{S_f - 1, 1}}; \mathbf{0_{N_s, N_d - 1}}] \quad (3.6)$$

Finally, F_m has matrix element given by:

$$F_{m,l}[n] = \frac{1}{\sqrt{N_s}} . e^{j2\pi l\left(\frac{n - N_g}{N_s}\right)} \quad (3.8)$$

where l is the subcarrier index.

$$
\mathbf{F_m} = \begin{pmatrix} F_{m,0}\left[0\right] & & \cdots & & F_{m,N_s-1}\left[0\right] \\ & \ddots & & & \\ \vdots & & F_{m,l}\left[n\right] & & \vdots \\ & & & \ddots & \\ F_{m,0}\left[N_{gs}-1\right] & & \cdots & & F_{m,N_s-1}\left[N_{gs}-1\right] \end{pmatrix} \tag{3.7}
$$

After the multipath channel and adding the additive white gaussian noise (AWGN), removing the cyclic prefix and going through the N points FFT, the received signal vector in the frequency domain can be expressed as:

$$
\mathbf{z_m} = \mathbf{H_m} \cdot \mathbf{T_m} \cdot \mathbf{D_m} \cdot \mathbf{x_m} + \mathbf{w_m} \tag{3.9}
$$

where $\mathbf{H_m}$ is the diagonal matrix of channel response, and $\mathbf{w_m}$ is the noise vector. In this system, the maximum excess delay of the channel is assumed to be shorter than the cyclic prefix duration and, therefore, the inter-symbol interference (ISI) can easily be eliminated by removing the cyclic prefix.

The linear amplitude and phase distortion in the received signal as a result of the multipath channel is compensated by a frequency domain equalizer (FDE). After FDE, the output signal is:

$$
\mathbf{V_m} = \mathbf{C_m} \cdot \mathbf{z_m} \tag{3.10}
$$

where C_m is the matrix diagonal of FDE coefficients:

$$
\mathbf{C_m} = \mathbf{diag}(\mathbf{C_{m,1}}, \mathbf{C_{m,2}}, \ldots, \mathbf{C_{m,N_d}}) \tag{3.11}
$$

The FDE coefficients generation is described in Section 3.6.

3.4 Modeling and Validation of LTE uplink Transmitter & Receiver

A model of the Layer-1 (L-1) LTE uplink transmitter and receiver structures is shown in Figure 3.4. The left side is the transmitter, corresponding to the user equipment (UE), and the right side is the receiver, corresponding to the node-B or base-station (BS). Several throughput enhancement mechanisms are implemented, including turbo coding, adaptive modulation coding (AMC) based on link adaptation (LA) and Hybrid ARQ (HARQ) based on fast L1 retransmissions. The detailed descriptions are provided in Appendix A.1. The validation of the transmitter and receiver chain is described in Appendix A.2.

3.5 Peak-to-Average Power Ratio Evaluation

The envelope variation of the transmitted signal can be represented in a peak-to-average power ratio parameter (PAPR). In this work, the PAPR of both SC-FDMA and OFDMA is evaluated. The PAPR is an essential parameter which can affect the RF part, since a transmitter signal with high PAPR is sensitive to the non-linear distortion at the power amplifier. The PAPR of the transmitted signal can be expressed as:

$$CCDF(P_{ins}) = Prob\left\{\frac{|v_i|^2}{P_{avg}} > P_T\right\} \tag{3.12}$$

where P_{ins} is the instantaneous power of the signal, v_i is the ith signal samples, P_{avg} is the long term average power, and P_T is the power threshold of the signal. For simplicity, P_{avg} has been normalized to one. In order to obtain accurate results, the transmitted signal has been oversampled 4 times according to the suggestion given in [18].

Figure 3.5 shows the PAPR results for SC-FDMA with various modulation schemes. The PAPR results vary depending on the modulation scheme so that higher order modulation schemes exhibits a higher PAPR compared to lower order modulation schemes. In SC-FDMA, as a single carrier transmission, the PAPR is mainly affected by the envelope variations in each modulation scheme, thus the higher order modulations lead to larger dynamic range and higher PAPR. The same results are also shown in [42].

In comparison, the PAPR results for OFDMA with various modulation schemes
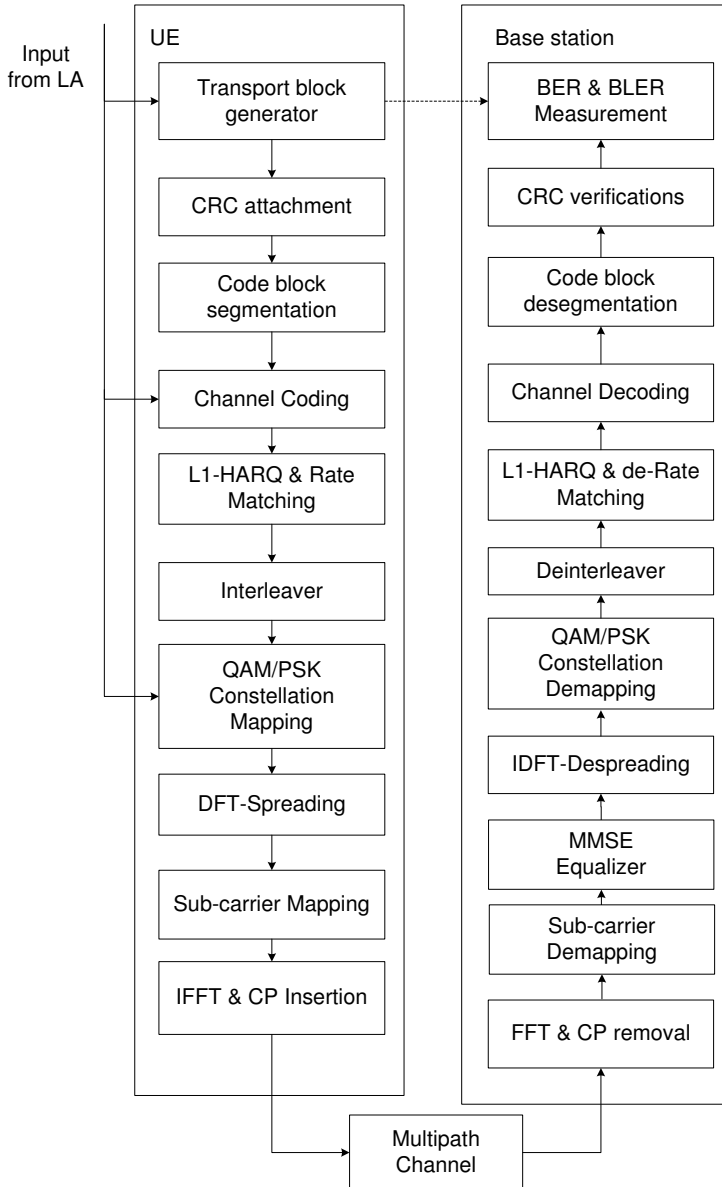
Figure 3.4: Layer-1 UTRA LTE uplink link level simulator
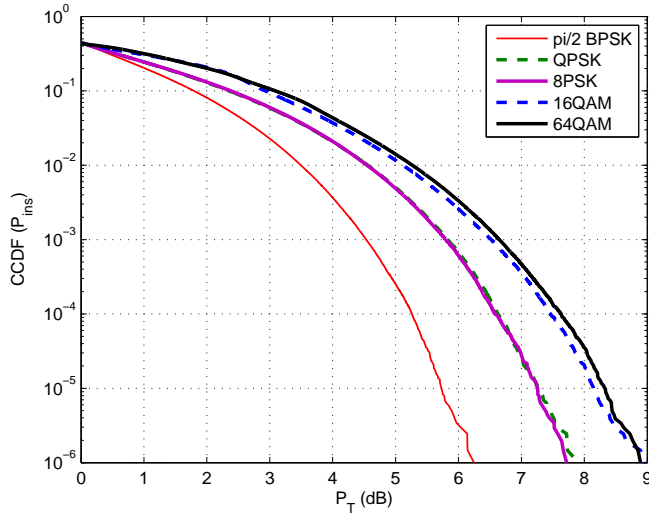
Figure 3.5: PAPR of SC-FDMA with various modulation schemes.
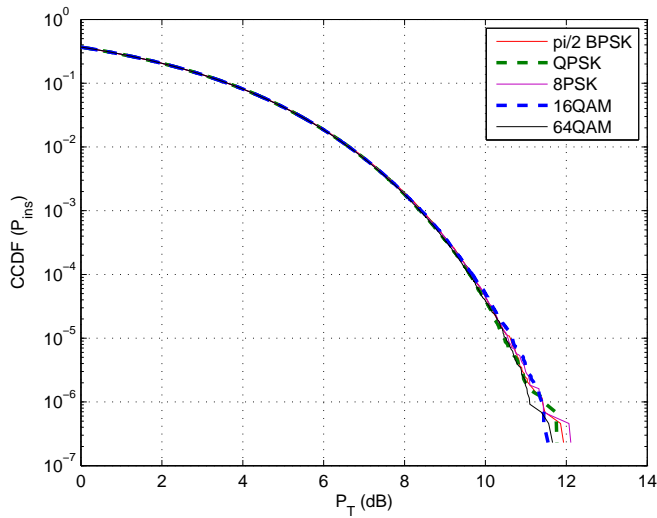
Figure 3.6: PAPR of OFDM for various modulation schemes.
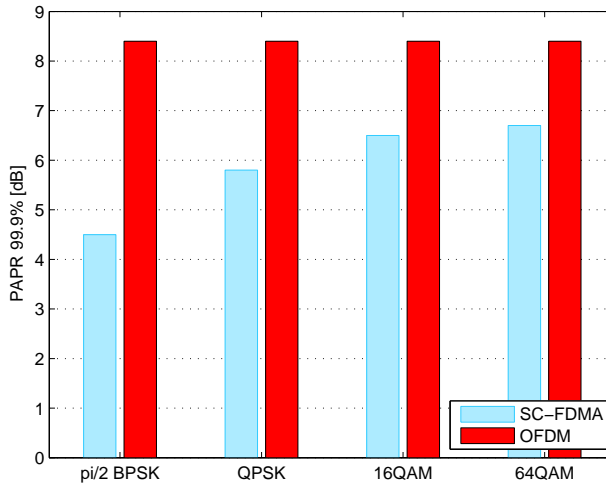
Figure 3.7: PAPR comparison of SC-FDMA and OFDMA.

are shown in Figure 3.6. It is observed that the PAPR is not affected by the type of modulation scheme, and all the modulation schemes have the same PAPR results. In [42], the same PAPR results are also indicated. After the IFFT modulation in an OFDM system, the modulated symbols are added together to form a multi-carrier signal. The addition increases the PAPR of the OFDM signal, but diminishes the impact of the modulation scheme.

The evaluation of SC-FDMA and OFDMA with regard to PAPR is summarized in Figure 3.7. SC-FDMA has an advantage in obtaining a small PAPR for the lower order modulation schemes. For pi/2 BPSK, the PAPR of SC-FDMA is around 4 dB lower than the same modulation format in OFDM. For 64QAM, the difference is smaller than 1.6 dB in comparison to OFDMA.

Figure 3.8 shows the impact of the number of subcarriers on the PAPR results in the SC-FDMA system. The subcarrier allocation of (72/128) [1] represents the smallest bandwidth allocation in LTE uplink. Increasing the number of sub-carriers does not affect the PAPR of the SC-FDMA signal. The same results are obtained for OFDMA system. The smallest sub-carriers allocation setting has a considerably high number of multi-carriers, therefore, a higher PAPR is not possessed for larger sub-carrier settings (1200/2048).

---

[1](N/M), where N is the active sub-carriers and M is the IFFT size.
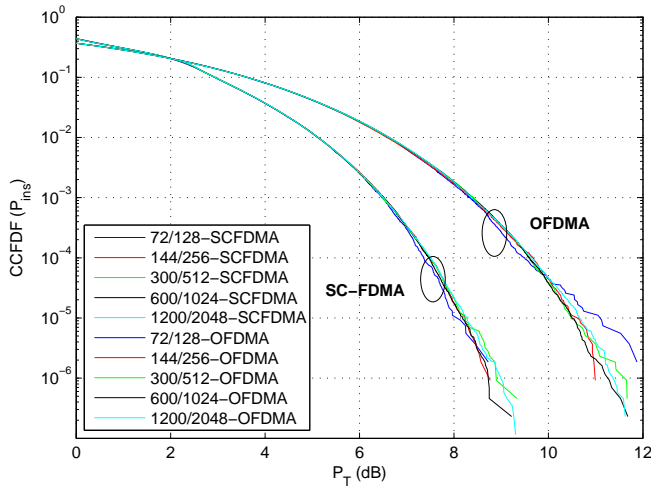
Figure 3.8: PAPR of SC-FDMA & OFDMA for different numbers of subcarriers.

3.6   Frequency Domain Equalization

The zero Forcing (ZF) and Minimum Mean Square Error (MMSE) are considered in the study. The detailed operation of the frequency domain equalization is presented in Appendix A.1. The performance of ZF and MMSE in LTE scenario is investigated in both the SC-FDMA and OFDMA case. The simulation parameters are shown in Table 3.2.

Figure 3.9 shows the performance of a lower order modulation and coding scheme, BPSK with coding rate 1/6. This result is to represent the impact to the low MCS. For such a low MCS, the operation is typically at the lower SNR region. SC-FDMA with ZF suffers from high BLER, and the MMSE significantly improves the performance over ZF. OFDM with MMSE is slightly better than OFDM with ZF. SC-FDMA and OFDMA achieve the same performance when MMSE is used.

The results for the higher modulation scheme, 16QAM rate 4/5 is shown in Figure 3.10, valid in the case where the system is operated at the higher SNR region. The reason is to analyze the impact to the higher order MCS. It is shown that the performance gap between SC-FDMA ZF and MMSE is getting smaller.

From the results shown in Figure 3.9 and Figure 3.10, it is noticed that dif-

Table 3.2: UTRA LTE uplink simulation parameters.

Parameter	Value
Carrier Frequency	2 GHz
Transmission BW	10 MHz
Sub-frame duration	0.5 ms
Sub-carrier spacing	15 kHz
SC-FDM symbols/TTI	6 LBs, 2 SBs
CP duration	4.1 μs
FFT size/Useful subcarriers	1024/600
MCS settings	pi/2 BPSK: 1/6, 1/3
	QPSK: 1/2, 2/3, 3/4
	8PSK: 1/3, 1/2, 2/3, 3/4
	16QAM: 1/2, 2/3, 3/4, 4/5
Channel code	3GPP Rel. 6 compliant Turbo code
	with basic rate 1/3
Rate Matching, Interleaver	3GPP Rel. 6 compliant
Channel Estimation	Ideal
Antenna schemes	SISO
Channel model	Typical Urban 6 paths [5]
Speed	3 kmph
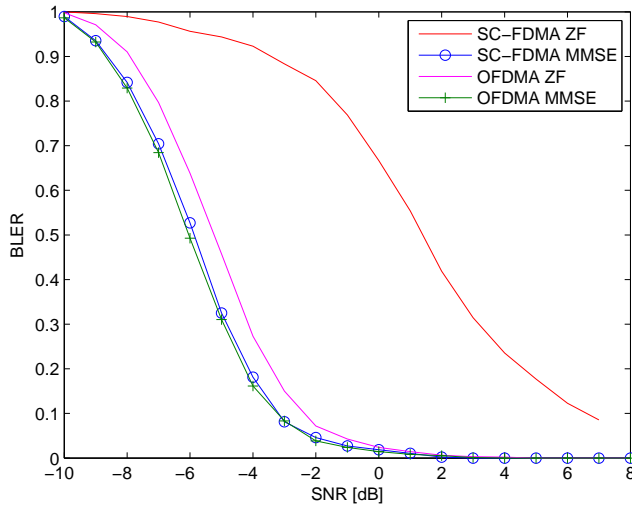
Figure 3.9: BLER performance of BPSK 1/6 SC-FDMA & OFDMA with different equalization.
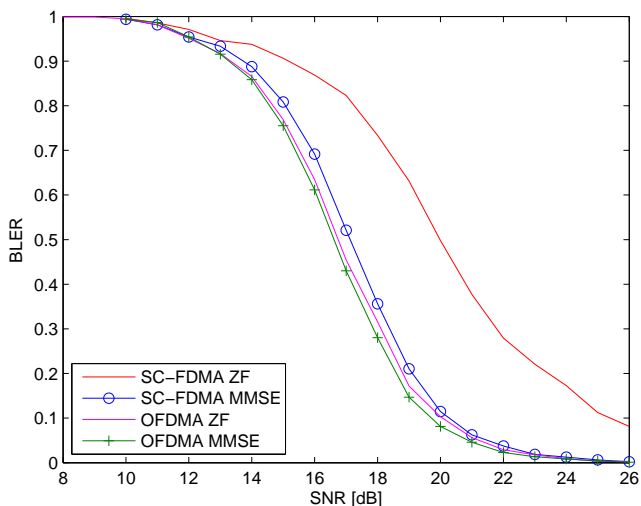
Figure 3.10: BLER performance of 16QAM 4/5 SC-FDMA & OFDMA with different equalization.

ferent equalization technique does not affect significantly the OFDM system. However, it becomes a critical issue for SC-FDMA. Forward Error Correction code used in this analyzes is the turbo code [12]. In OFDM transmission, the FEC provides an important role to provide additional diversity, especially for the transmission over frequency selective fading. While in SC-FDMA, the FEC is also still important, but it does not provide additional diversity since it has the DFT-spreading.

Figure 3.11 and Figure 3.12 show the SC-FDMA spectral efficiency results in both MMSE and ZF. The spectral efficiency which can also be called the throughput is calculated using:

$$TP = \frac{(1 - BLER) * P}{T * B} \tag{3.13}$$

Where BLER is the Block Error Rate, P is the subframe (block) size, T is the subframe duration, and B is the bandwidth. The results are also presented for all modulation schemes suitable for LTE uplink. MMSE is significantly better than ZF, especially in low SNR range. SC-FDMA with ZF suffers from noise enhancement. It is clearly shown that the SC-FDMA MMSE is always preferred to ZF in all simulated conditions.
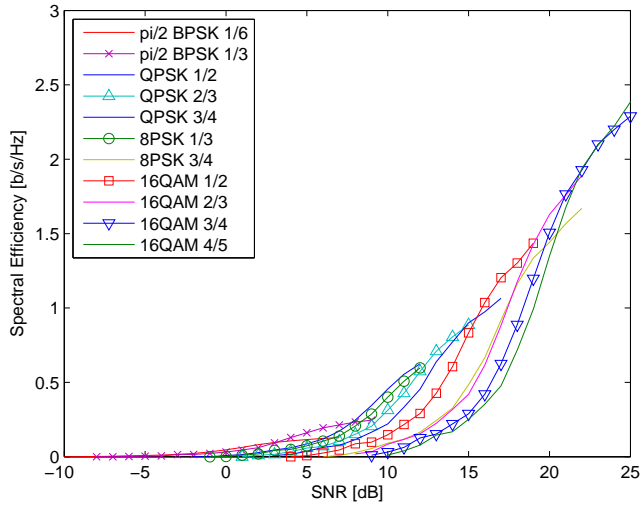
Figure 3.11: Spectral efficiency of SC-FDMA with Zero Forcing equalization.
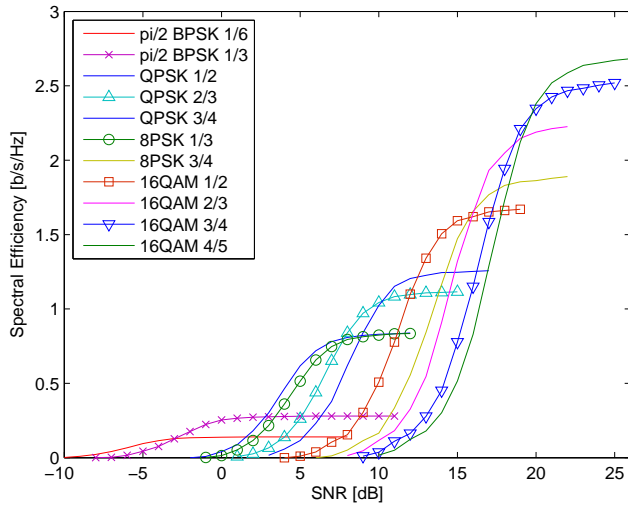
Figure 3.12: Spectral efficiency of SC-FDMA with MMSE equalization.

3.7   Impact of Link Adaptation

In this study, a simple link adaptation technique is adopted in which the link adaptation is defined as a maximum achievable throughput/spectral efficiency for various modulations and coding schemes. The selection of modulation and coding scheme is based on average signal to noise ratio (SNR). The measured SNR at the base station, represented as Channel State Information (CSI), varies depending on the channel condition. Here the CSI measurement is assumed ideal, whereas in practise it will be influence by measurement inaccuracy and quantization noise.

The spectral efficiency of different MCS in SISO case without HARQ is plotted versus the average SNR in Figure 3.13. Variable rate turbo encoding and modulation from pi/2 BPSK to 16QAM provide peak data rates from 1.2 Mbps up to 23 Mbps for the system with 10 MHz bandwidth. In these peak data rates, the 14% pilot overhead described in Section 3.2 has been taken into account. The used MCS formats and corresponding data rate values are summarized in Table 3.3. It can be observed that 8PSK does not contribute to the link adaptation curve.
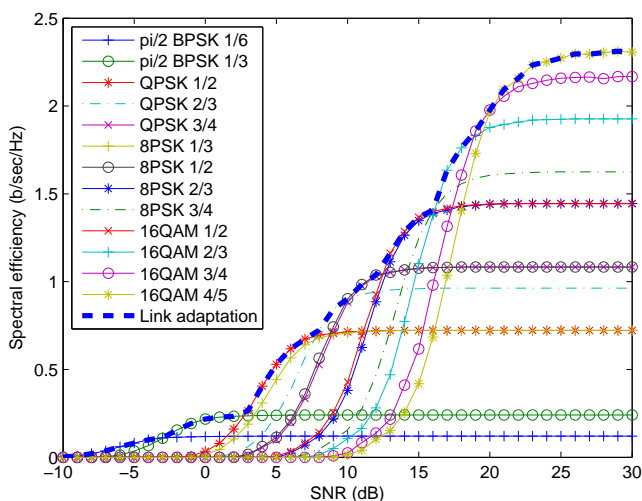
Figure 3.13: Spectral efficiency of SISO SC-FDMA with various MCS schemes.

Table 3.3: Peak Data Rate For 10 MHz System

MCS	Data Rate
pi/2 BPSK 1/6	1.2 Mbps
pi/2 BPSK 1/3	2.4 Mbps
QPSK 1/2 8PSK 1/3	7.2 Mbps
QPSK 2/3,	9.6 Mbps
QPSK 3/4, 8PSK 1/2	10.8 Mbps
16QAM 1/2, 8PSK 2/3	14.4 Mbps
8PSK 3/4	16.2 Mbps
16QAM 2/3	19.2 Mbps
16QAM 3/4	21.6 Mbps
16QAM 4/5	23 Mbps

3.8   Impact of Fast HARQ

A fast L1 Hybrid ARQ (HARQ) retransmission concept is used with the aim of facilitating a more aggresive and spectrally efficient packet scheduling [43]. Two soft combining HARQ retransmission mechanisms are considered, namely chase combining and incremental redundancy. Both retransmission mechanisms ensure that the past retransmission is fully utilized. The major difference between these two retransmission mechanisms is that chase combining requires the same transmitted signal in each retransmission, whereas incremental redundancy transmits different parity bits in each retransmission.

The HARQ within the MAC sublayer has the following characteristics:

- N-process Stop-And-Wait (SAW) HARQ is used; The HARQ processes are transmitted over N parallel time channels in order to ensure the continuous transmission to the UE.

- The HARQ is based on ACK/NACKs; The received data packets are acknowledged after each transmission. A negative ACK (NACK) implies a retransmission request either for an additional redundancy for HARQ incremental redundancy or an identical packet for HARQ chase combining case.

- For the uplink, the HARQ is based on synchronous retransmissions.
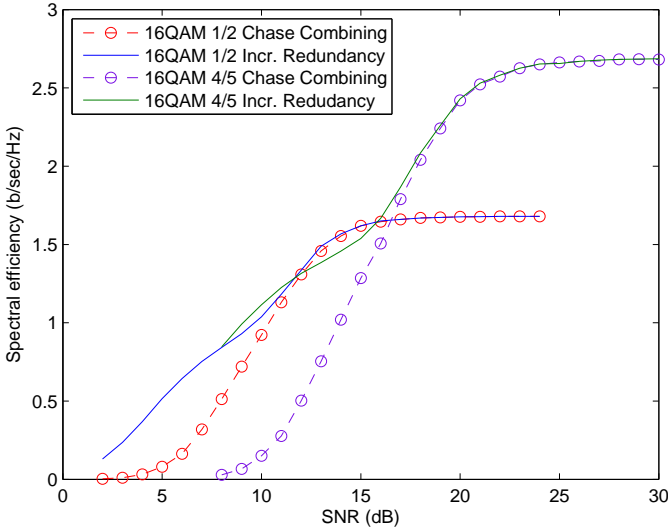
Figure 3.14: Spectral efficiency of SC-FDMA SISO case for chase combining (CC) and incremental redundancy (IR).

In the following simulations, we have assumed no error in the transmission of ACK/NACK from the BS to the UE, 6 SAW parallel channels, and maximum 4 retransmissions. In practice, 4-6 SAW parralel channels are used [44].

The effective throughput after retransmissions:

$$
\begin{aligned}
TP_{eff} = \frac{P}{T \cdot B} \left(1 - BLER_1\right) &+ \frac{P}{2 \cdot T \cdot B} \cdot BLER_1 \left(1 - BLER_2\right) \\
&+ \frac{P}{3 \cdot T \cdot B} \cdot BLER_1 \cdot BLER_2 \left(1 - BLER_3\right) \quad (3.14) \\
+ \frac{P}{4 \cdot T \cdot B} \cdot BLER_1 \cdot BLER_2 &\cdot BLER_3 \left(1 - BLER_4\right)
\end{aligned}
$$

Figure 3.14 shows the performance results of 16QAM for lower coding rate (1/2) and higher coding rate (4/5). The HARQ can improve the performance as it can be observed in the low SNR region for each coding rate. The benefit of incremental redundancy over chase combining can also be seen, especially for the higher coding rate. As a consequence, the general assumption for this study is to use incremental redundancy for coding rates exceeding 1/2 and chase combining for coding rates equal to or less than 1/2.
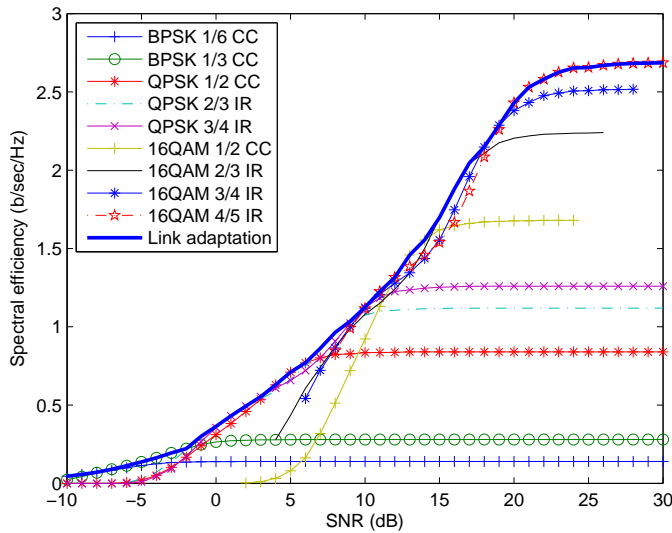
Figure 3.15: Spectral efficiency of SC-FDMA SISO case with HARQ.

The spectral efficiency with LA including all of the MCS is shown in Figure 3.15. The combining gain of HARQ can be observed in the smoothening out of the maximum achievable spectral efficiency results, when compared to Figure 3.13. It can also be observed that at low SNR most of the spectral efficiency curves are overlapped. This condition brings benefit when there is an error in the link adaptation mechanism. Although, the UE transmits with a sub-optimal MCS, it can still obtain the same spectral efficiency due to HARQ.

3.9   Antenna Configuration

Multiple antennas are essential for UTRA LTE in order to reach the targeted peak data rates, in particular, with the aim of improving the performance at the lower SNR operating range. In this work the combination of SC-FDMA with single-input single-output (SISO) and the single-input multiple-output (SIMO) antenna configurations was studied. In LTE, the baseline for uplink is to use one transmit antenna at the UE and two receive antennas with Maximal Ratio Combining (MRC) at the base station [7].

After MRC combining, the output signal is represented as follows:

$$V_{m,k} = \frac{z1_{m,k}H1^*_{m,k} + z2_{m,k}H2^*_{m,k}}{H1_{m,k}H1^*_{m,k} + H2_{m,k}H2^*_{m,k}} \tag{3.15}$$

where $z1$ and $z1$ are the received signals in the frequency domain representation of each antenna branch.

In Figure 3.16, the spectral efficiency for both SISO and SIMO antenna schemes is presented. The spectral efficiency of OFDMA is also presented for comparison. In the SISO case, OFDMA outperforms SC-FDMA with an MMSE receiver. The demodulation for OFDMA is performed in frequency domain, whereas for SC-FDMA, demodulation is performed in time domain. A deep fading may affect the whole data symbol in SC-FDMA, thus the performance of SC-FDMA is worse for frequency-selective fading channel. For the SIMO case, the SC-FDMA and OFDMA performance is improved due to the diversity gain and the spectral efficiency gap between OFDMA and SC-FDMA become unnoticeable. The MMSE receiver in SIMO with maximum ratio combining (MRC) further reduces the noise in comparison to the SISO case, beside greatly increasing the spectral efficiency of SC-FDMA.

Figure 3.17 shows the CDF of the measured instantaneous SNR for both SISO and SIMO at different average input SNR values: 0 dB, 10 dB, and 20 dB. The instantaneous SNR is measured after the equalization and IDFT despreading processes. It can be seen that for all cases, the dynamic range of instantaneous SNR is very limited due to a large bandwidth transmission. It implies that the selection of modulation and coding is almost constant for a given average SNR, and the simple LA model used here is valid. The dynamic range for low SNR is further reduced by reason of the advantage of using MMSE receiver. At high SNR, the instantaneous SNR dynamic range increases because the MMSE receiver becomes identical to the zero forcing (ZF) receiver. The results are also shown that the noise enhancement loss increases with the average input SNR, especially for the SISO case[9].

3.10 Impact of Frequency Allocation

LTE uplink transmission allows a flexible frequency allocation within the channel bandwidth. In the study item phase [5], The 3GPP has defined the localized and distributed frequency/subcarriers allocation as shown in Figure 3.18. The distributed case is used to gain frequency diversity, whereas the localized
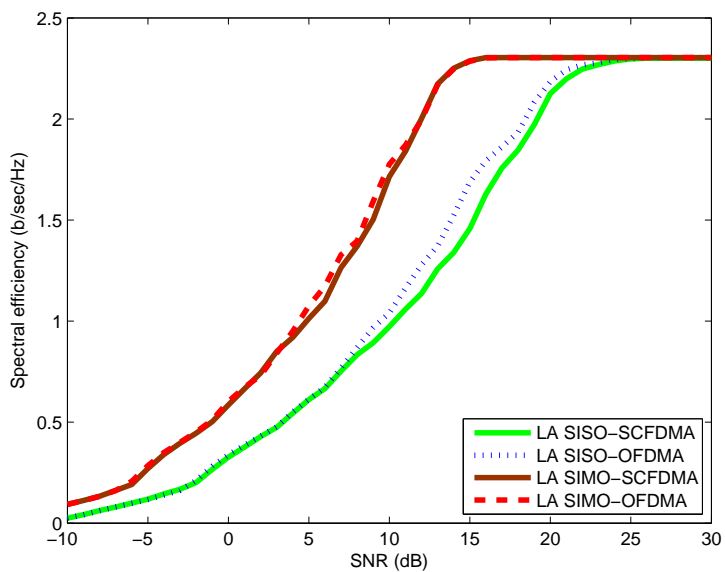
Figure 3.16: Spectral efficiency for SC-FDMA and OFDMA with two antenna configurations (SISO and SIMO).
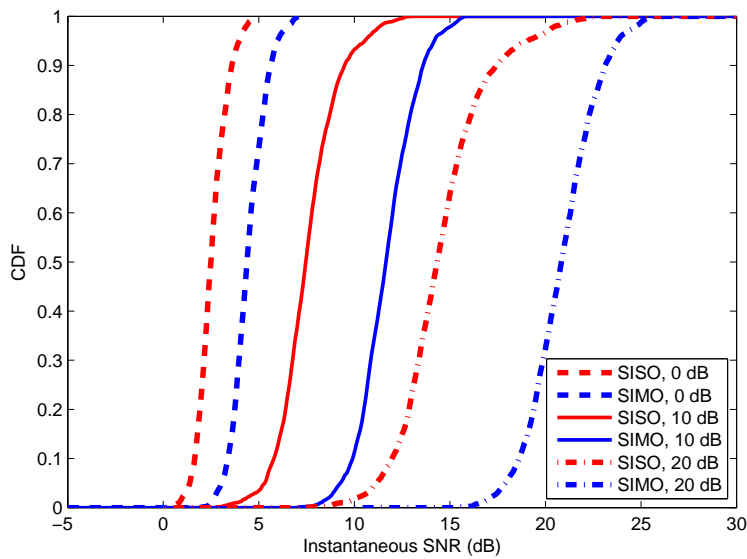
Figure 3.17: CDF of measured instantaneous SNR of SC-FDMA.
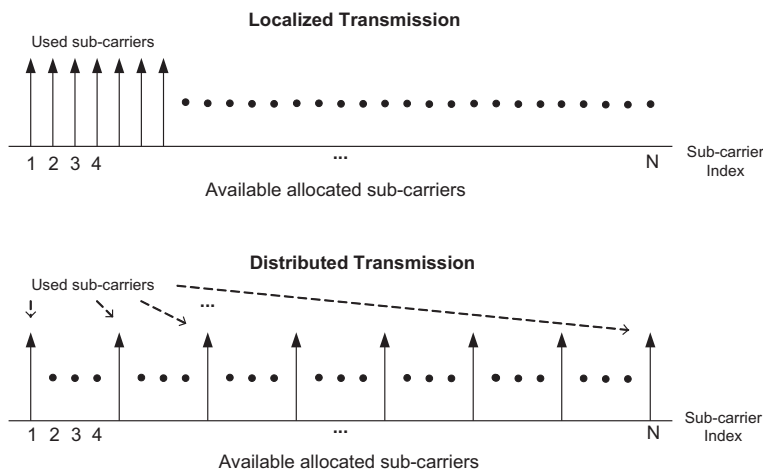
Figure 3.18: Localized and distributed frequency allocation in LTE uplink.

SC-FDMA can be used to simplify subcarrier allocation and benefit from opportunistic scheduling. Lately, the 3GPP only considered the localized case and not the distributed case since the localized case with frequency hopping can also gain the frequency diversity. Moreover, the distributed case is sensitive to the frequency error.

The BLER performance of the distributed and localized case in SC-FDMA with HARQ is presented in Figure 3.19. The SIMO case is assumed, and the channel bandwidth is 10 MHz. A 2.5 MHz bandwidth is allocated for the transmission. For the distributed case, this configuration will allow a repetition factor of 4 since all the subcarriers carrying data are spread over the full 10 MHz bandwidth.

It is shown that the distributed cases perform better than the localized one in most cases. For BLER 1%, it is clear that the distributed case is superior to the localized. It has around 1 dB gain over localized in 16QAM rate 4/5. The distributed case can maximize the frequency diversity by distributing the data in the whole bandwidth. In the real situation, when real channel estimation is taken into account, the localized is expected to perform better than the distributed. The reason is that considering the limited amount of pilot signals, the distributed has to estimate the channel transfer function in the full bandwidth, whereas the localized estimates the channel transfer function only in the allocated channel bandwidth. Thus, the distributed case is more sensitive to the error introduced by channel estimation.
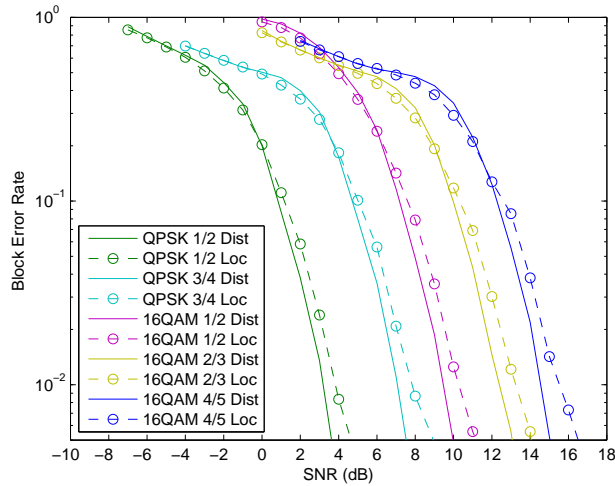
Figure 3.19: BLER performance of Distributed versus Localized in SC-FDMA.

3.11 Impact of Vehicle Speed

The impact of the UE speed on SC-FDMA and OFDMA is discussed. For the transmission over time varying and frequency selective fading channel, the receiver requires to estimate the channel transfer function in both time and frequency domain. The receiver utilizes the received pilot signals as described in Section 3.2 to perform channel estimation. In this work, the frequency domain channel estimation is based on Wiener filter as described in [45]. For the time domain, a linear interpolation is assumed. The detailed description on the channel estimation is presented in Appendix A.1.

LTE uplink must be operable at the high speed scenario. Figure 3.20 shows the results for the speed of 120 km/h. It is shown that OFDMA performance is more affected by the UE speed than SC-FDMA, especially at higher modulation and coding schemes (16QAM rate 4/5). The UE at high speed has a higher doppler frequency and creates Inter-Carrier Interference (ICI). In OFDM, each subcarrier carries different symbols, and therefore OFDM is more sensitive to the ICI.

Figure 3.21 illustrates the results for the speed of 200 km/h. It is shown that 16QAM rate 3/4 and above does not contribute to the link adaptation curves and operates at low spectral efficiency. At high speed, the subcarrier orthogonality is destroyed by the ICI.
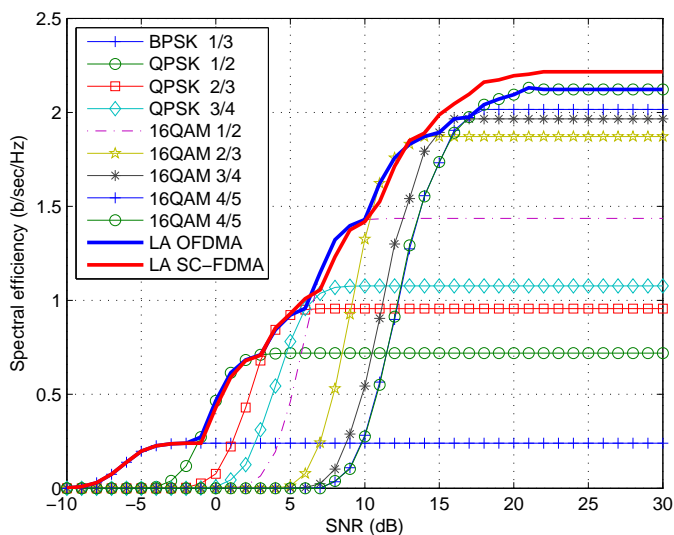
Figure 3.20: SC-FDMA and OFDMA with real channel estimation at speed of 120 km/h.
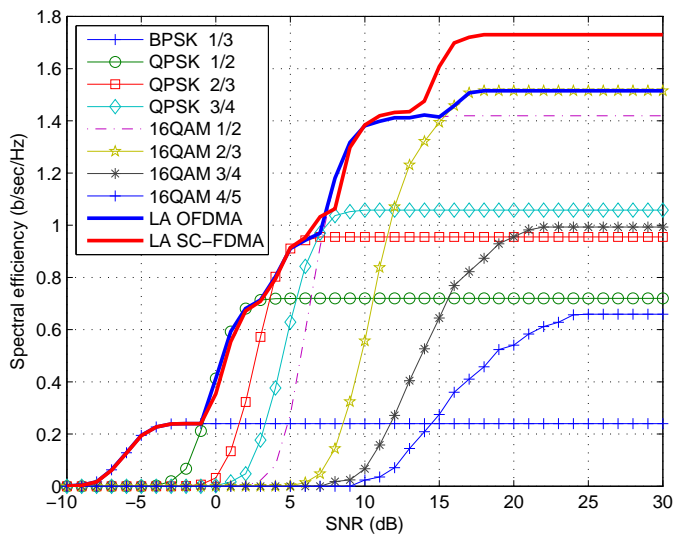
Figure 3.21: SC-FDMA and OFDMA with real channel estimation at speed of 200 km/h.

3.12 Turbo Equalization for Performance Improvement

In this work a turbo equalizer to improve Single Carrier Frequency Division Multiple Access (SC-FDMA) performance in the context of LTE uplink is proposed. Turbo equalization is an advanced iterative equalization and decoding techniques that allows enhancement of the performance for the transmission over a frequency selective fading channel. The turbo equalizer increases the receiver complexity. Nevertheless, the implementation is performed in the node-B, which does not have so stringent physical constraints and power consumption as the user equipment.

The proposed turbo equalization is based on a new adaptive coefficients solution for the frequency domain equalization. The detailed description of the proposed turbo equalizer is presented in Appendix. C.

The simulation results are obtained through Monte Carlo simulations, using a 10 MHz system bandwidth in the usage of 600 useful subcarriers. The COST 259 Typical Urban with power delay profile 6 paths is assumed [46]. A 1x2 SIMO antenna scheme has been considered. All the simulation parameters are shown in Table 3.2.

Figure 3.22 shows the BLER (Block Error Rate) performances of the SC-FDMA 16 QAM system with three different coding rates. The results of TEQ with different iterations and SC-FDMA with simple MMSE are given. Two different results for turbo equalization are plotted with 2 and 4 iterations of the algorithm, respectively. Compared with the MMSE receiver, the turbo equalizer shows a gain of around 1 dB. In our assumptions, the cyclic prefix allows complete removal of the ISI, hence the gain is exclusively due to the reduction of the noise component. The significant gain is already obtained from 2 iterations of the algorithm.

In Figure 3.23 the performance of OFDMA has also been included, and the results are shown for both QPSK and 16 QAM modulations. The purpose is to compare with the SC-FDMA TEQ receiver performance for 2 iterations of the algorithm. Note that for QPSK 2/3 and QPSK 3/4 the SC-FDMA with MMSE system performs better than OFDMA. This is due to the fact that low order modulation schemes are robust to the noise enhancement of SC-FDMA transmission. Moreover, OFDM transmission is more sensitive to the coding rate than SC-FDMA [12]. SC-FDMA takes advantage of spreading the data symbols over the transmission bandwidth, where the effect of a deep fade affecting few subcarriers will be diminished in the receiver combining all the
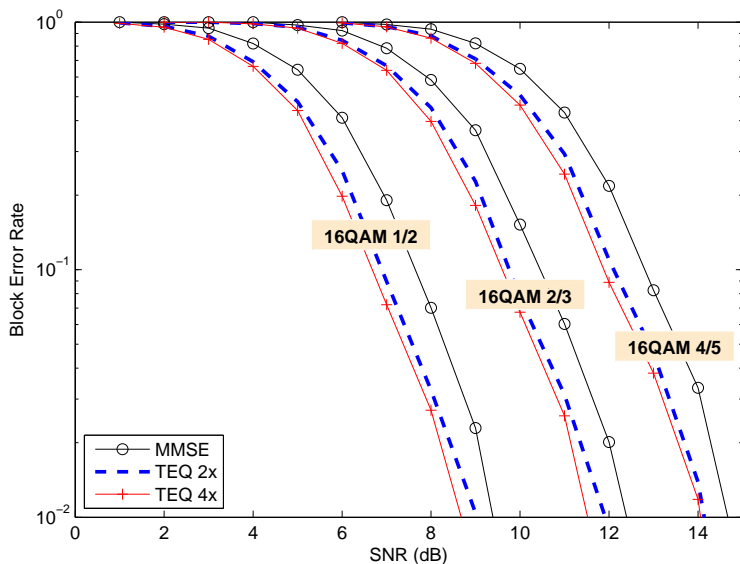
Figure 3.22: BLER performance for SC-FDMA 1x2 MRC with and without Turbo Equalizer in TU 06 channel.
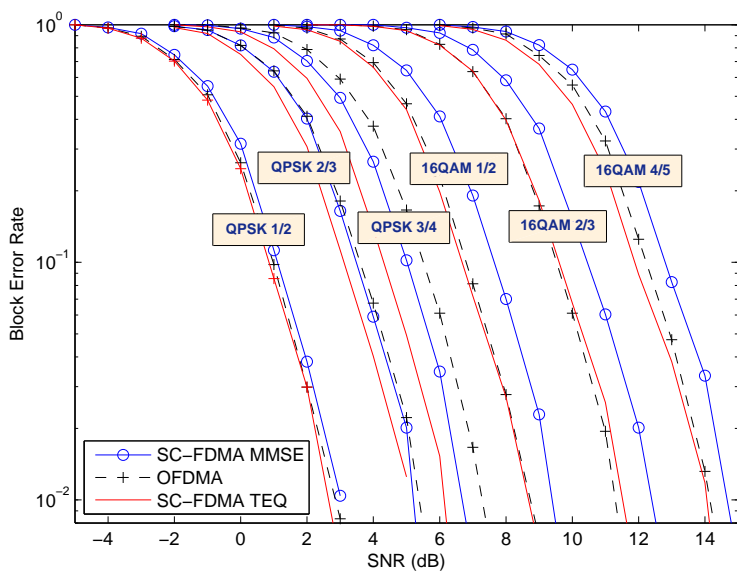
Figure 3.23: BLER performance for SC-FDMA versus OFDMA in TU 06 channel.
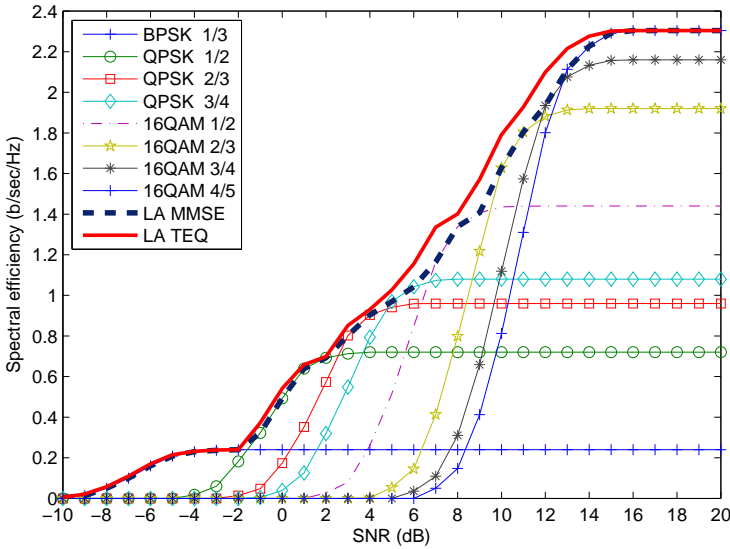
Figure 3.24: Spectral efficiency for SC-FDMA in TU 06 channel.

subcarriers information.

The receiver with turbo equalizer gives better performance in most cases, and in the worst case it shows the same performance as OFDMA. Therefore, turbo equalizer makes it possible to reduce the noise enhancement due to the time domain transmission in the SC-FDMA system, and makes performance the same or better than OFDMA. The gain depends mostly on the usage of equalization with adaptive coefficients.

The performance results for several modulation and coding schemes in terms of spectral efficiency are shown in Figure 3.24. The figure shows the link adaptation curve for both the MMSE and the TEQ receiver. It is shown that the turbo equalization is effective for higher order MCS, whereas for BPSK it does not show any performance improvement. Therefore, in order to exploit its performance gain, the turbo equalizer receiver could be used for high order modulation schemes, whereas the simple MMSE receiver can still be used for BPSK. In this way, the computational load for low order modulations can be reduced.

3.13 Summary

In this work, we have presented the key techniques for LTE uplink as well as presented the baseline performance. Radio access technology is the key aspect in LTE uplink and two radio access schemes, SC-FDMA and OFDMA, are studied. The performance results are obtained from a detailed UTRA LTE uplink link level simulator. The simulation results show that both SC-FDMA and OFDMA can achieve a high spectral efficiency, however SC-FDMA benefits in obtaining lower PAPR than OFDMA, especially for low order modulation schemes. 1x2 SIMO antenna configuration highly increases the spectral efficiency of SC-FDMA making the performance of SC-FDMA with MMSE receiver comparable to OFDMA, especially at high coding rate. The peak spectral efficiency results for SC-FDMA confirm that it meets with the requirement to achieve a spectral efficiency improvement of 2 or 3 times that of 3GPP rel.6. In high speed scenarios, the results indicate that SC-FDMA is more robust than OFDMA.

Despite of an increase of the receiver complexity in the base-station, the turbo equalizer can reduce the noise enhancement in the SC-FDMA system. Results show that a turbo equalizer receiver for SIMO system can improve the BLER performance by almost 1 dB compared to a traditional MMSE receiver. Most of the performance gain is obtained with 2 iterations of the algorithm. The gain is mostly obtained from the usage of an equalizer with adaptive coefficients. In our case, both forward and feedback coefficients are updated at each iteration. Furthermore, the simulation results show that the SC-FDMA turbo equalizer performance is better or equal to OFDMA for all the modulation and coding schemes. Link adaptation curves show that the turbo equalizer gain becomes effective for high order modulation schemes, and at high coding rates. Therefore, the turbo equalizer brings advantage in a high SNR scenario.

CHAPTER 4

RF Hardware Imperfections Effect on Inband Channel

4.1 Introduction

The performance of a radio link is also affected by the quality of the RF transmitter architecture. Each RF transmitter architecture has the advantage and disadvantage, including different RF imperfections, as explained in Chapter 2. The imperfections in each RF architecture can be modeled for further investigation in a link level or system level study. A consistent RF imperfections model is required for the 3GPP work item phase which cannot be based on a specific RF architecture. Nevertheless, it is also difficult to make the study completely independent from the RF architecture because some imperfections are specific to some architectures. For example, the gain and phase imbalance are produced in the Cartesian transmitter architecture and the envelope and phase timing alignment problem are in the Polar transmitter architecture.

Here, the validity of a simplified RF imperfection model is investigated in order to understand what scope of applicability it may have in a practical context, especially for the LTE 3GPP work. The investigation is focused on the impact of the imperfections on the in-band channel. The impact on the out-of band channel is also important and addressed in Chapter 5. The aim of this work is to link the individual RF imperfections Error Vector Magnitude (EVM) char-

acteristics to the link level performance, especially to obtain clear insight in the sensitivity on each RF imperfection. The link level performance is evaluated for AWGN and frequency selective fading channels. Performance evaluation in an AWGN channel represents the conditions under which EVM measurements are obtained for type approval, whereas the performance evaluation in frequency selective fading is more representative of actual operating conditions. The relation between different RF transmitter imperfection models in LTE uplink and how accurately the effect of each RF imperfection can be modelled by an equivalent white Gaussian noise source in the transmitter are also investigated.

The impact of each imperfection in a Cartesian transmitter on LTE uplink link performance is investigated. The most common imperfections, such as nonlinear power amplifier, gain imbalance, phase imbalance, DC offset, and phase noise are considered. The imperfection model is taken from an established imperfection model. Each imperfection is characterized by means of error vector magnitude (EVM) and equivalent link performance loss [47],[48],[14]. To simplify the modelling of RF imperfections on link and system performance, a simple AWGN generator in the transmitter is often used with a variance set according to a specific EVM level; e.g. as reported in [47] for the High Speed Downlink Packet Access (HSDPA) system. In this study, the applicability of the simple AWGN generator in the transmitter on beyond 3G system is carried out. For the case study, LTE uplink is considered.

This chapter is organized as follows. First, the EVM measurement definition in the LTE uplink is given in Section 4.2. Section 4.3 describes the used simulation models for the considered RF transmitter imperfections. Performance evaluation of EVM and the impact on link level performance are discussed in Section 4.4. Finally, the summary is given in Section 4.5.

4.2   LTE EVM Measurement

EVM is commonly used as a direct measure of the transmitter signal quality, in particular when related to any RF hardware imperfections in the system. EVM does not cover the aspect of disturbance to other users where Adjacent Channel Leakage Ratio (ACLR) must be used [15]. The EVM is a measure of the difference between the measured and the reference signals. In LTE, the EVM is measured in the constellation domain [49, 50, 51] rather than in time domain as for the previous UTRA specifications [52]. This approach allows pre-/post FFT time/frequency synchronization and amplitude/phase correction to be included in the frequency domain equalization block at the receiver as shown in Figure 4.1. Therefore, the filter group delay and amplitude/phase errors can

be compensated before the EVM calculation. The implication is that the filter does not have to be specified in the standard as it was previously specified FOR UTRA WCDMA system.

The EVM is measured at the symbol detection input as shown in Fig. 4.1, and can be calculated as [49]:

$$EVM_m = \sqrt{\frac{\sum_{l=0}^{L} \sum_{k=0}^{K-1} |Z_l(k) - R_l(k)|^2}{\sum_{l=0}^{L} \sum_{k=0}^{K-1} |R_l(k)|^2}} * 100\% \tag{4.1}$$

Where $Z_l(k)$ and $R_l(k)$ are the k-th complex baseband constellation point of the l-th measured SC-FDMA symbol and reference SC-FDMA symbols, respectively. L is the number of SC-FDMA symbols in one sub-frame, and K is the size of the resource block in one SC-FDMA symbol.

In our work, the final EVM measurement is achieved as an average over time [49]:

$$EVM = \frac{1}{M} \sum_{m=1}^{M} EVM_m \tag{4.2}$$

where M is the number of sub-frames, used for averaging.

4.3   RF Imperfections Model

The RF imperfection is located in the transmitter as depicted in Figure 4.1. In this section, a modelling of the most common RF transmitter imperfections used is described, including nonlinear power amplifier, phase noise, gain and phase imbalances, DC offset, and the equivalent white noise source.

4.3.1   Nonlinear Power Amplifier

The nonlinear power amplifier is usually characterized by AM/AM and AM/PM distortion curves. This nonlinearity phenomena lead to performance degradation and spectral regrowth. The AM/AM and AM/PM characteristics used in this study represented as $|S_{21}|$ and $\angle S_{21}$, are shown in Figure 4.2. These characteristics are based on the measurement result of a UE wideband CDMA power amplifier (PA) module [4]. This PA has a good compromise between linearity and power efficiency for varying envelope input signal. From Figure 4.2, the
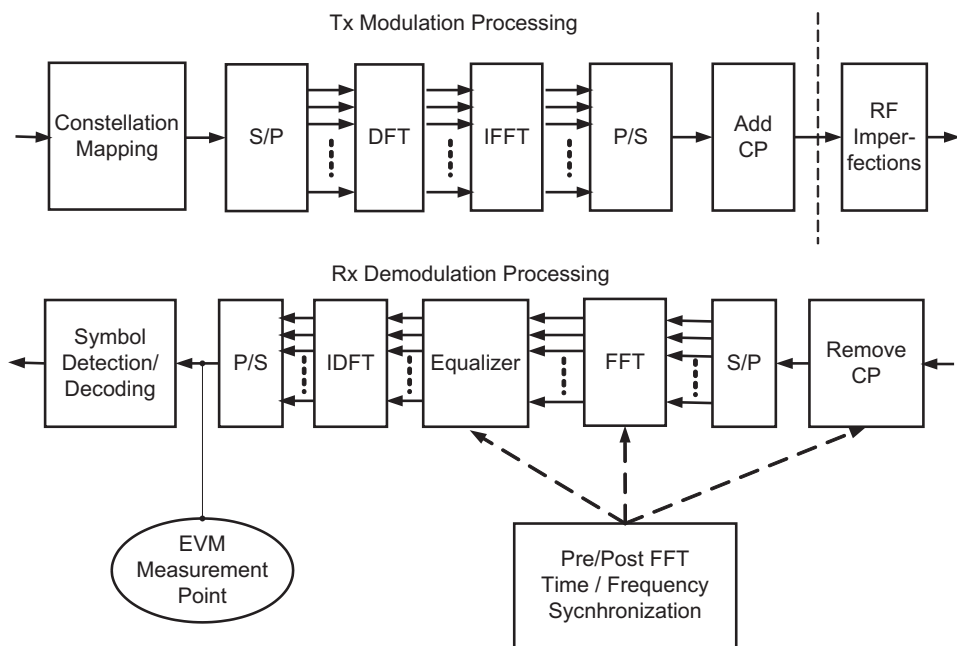
Figure 4.1: SC-FDMA modulation/demodulation and EVM measurement point.
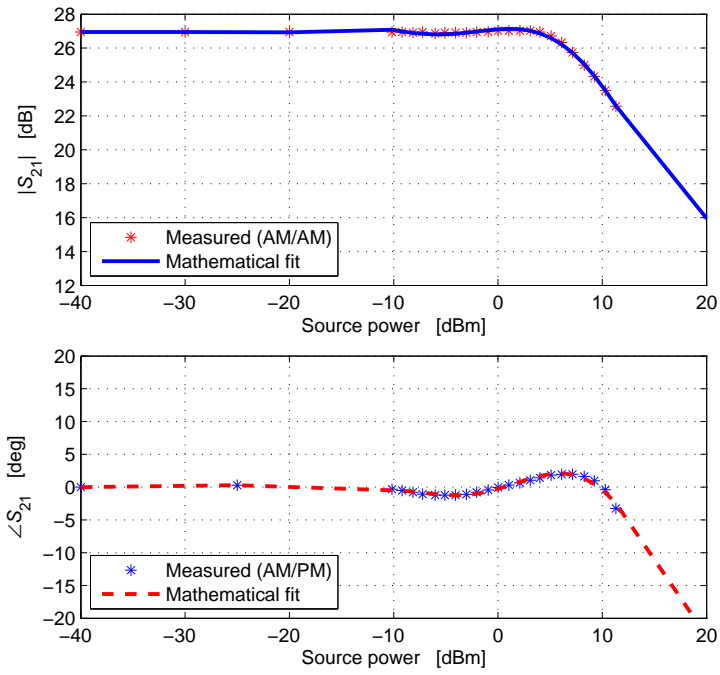
Figure 4.2: Measured AM/AM, AM/PM (asteriks) and model fit (solid) versus source power (dBm) [4].

power amplifier has 27 dB linear gain and 1 dB compression point at +6.1 dBm input power.

The results shown in Figure 4.2 is the S_{21} parameter or the voltage gain as a function of the input power level P_i. S_{21} can be expressed as [53]:

$$S_{21} \rightarrow S_{21}(P_i) = \alpha(P_i) \cdot \exp[j\theta(P_i)] \tag{4.3}$$

Where P_i is the time-varying input envelope power. The general expression of the input signal is given by:

$$x(t) = a(t) \cdot \cos(2\pi f_0 t + \phi(t)) \tag{4.4}$$

Where $a(t), \phi(t), f_0$ are the envelope of the input signal, the time varying phase of the input signal, and the carrier frequency, respectively. Applying the nonlinear model, the output signal can be expressed as follows:

$$y(t) = f_a(a(t) \cdot \cos(2\pi f_0 t + f_\phi(a(t), \phi(t)))) \tag{4.5}$$

Where f_a and f_Φ are nonlinear distortion functions of input power and phase given by:

$$f_a(a(t)) = a(t) \cdot \alpha(P_i(T)) \tag{4.6}$$

$$f_\Phi(a(t), \Phi(t)) = \Phi(t) + \Phi(P_i(T)) \tag{4.7}$$

The instantaneous input power $P_i(t)$ can be expressed as:

$$P_i(t) = \frac{a^2(t)}{2Z_0} \tag{4.8}$$

In most practical cases, the load impedance Z_0 is equal to the input and output impedance with a value of 50 ohm.

For the nonlinear modelling purpose, it is necessary to know the α and θ functions. Following the approach in [53], a power series function can be used to model the $|S_{21}|$ and $\angle S_{21}$ which represent the AM/AM and AM/PM distortion functions.

$$\alpha(P_i(t)) = \sum_{m=0}^{M} \alpha_m \cdot P_i^m(t) \tag{4.9}$$

$$\Phi(P_i(t)) = \sum_{m=0}^{M} \Phi_m \cdot P_i^m(t) \tag{4.10}$$

In (4.9) and (4.9), M is the order of the power series model. Applying this approach, the power amplifier measurement can be approximated as shown in

Figure 4.2. The results show that an 8th order power series fit well with the measurement results when suitable extrapolation is made towards lower and higher source power, respectively.

The power amplifier efficiency is shown in [53]. For this type of power amplifier, an efficiency of 38% is achieved at the output power of 30 dBm.

4.3.2   Gain & Phase Imbalances

The impact of gain and phase imbalances on the transmitted output signal is described in Section 2.3. The mathematical modelling is given in (2.9)-(2.11), with the gain imbalance α and phase imbalance θ:

$$\alpha = 10^{(\alpha/20)} \text{ , } \alpha \text{ in dB} \tag{4.11}$$

$$\theta = (\theta/180)\,\pi \text{ , } \theta \text{ in degree} \tag{4.12}$$

4.3.3   Phase Noise

Phase noise causes inter-carrier interference (ICI) and common phase error (CPE) [13]. The common phase error creates a fixed phase rotation in each SC-FDMA symbol and as discussed previously, it is assumed that the receiver fully compensates the CPE to minimize EVM and link performance degradation. The phase noise is modeled by a Wiener-Lévy process as described in Section 2.3. In a discrete time model, the phase noise can be modeled as a Markov process. The random phase value of the affected subcarrier at the nth sample of the mth SC-FDMA symbol can be written as:

$$\Phi_m\,[n] = \Phi_{m-1}\,[N_{gs} - 1] + \sum_{i=0}^{n} u\,[mN_{gs} + i] \tag{4.13}$$

where $u\,[i]$ is a white Gaussian random process with zero mean and variance $\sigma_u = 2\pi\Delta f_{3dB}\frac{T}{N_s}$, and T denotes the SC-FDMA symbol period. N_s is the FFT size.

The power spectral density of (4.13) is the phase noise SSB as the function of the 3dB phase noise bandwidth Δf_{3dB} parameter and is shown in Fig. 4.3. The phase noise power spectral density is following the Lorentzian spectrum with a
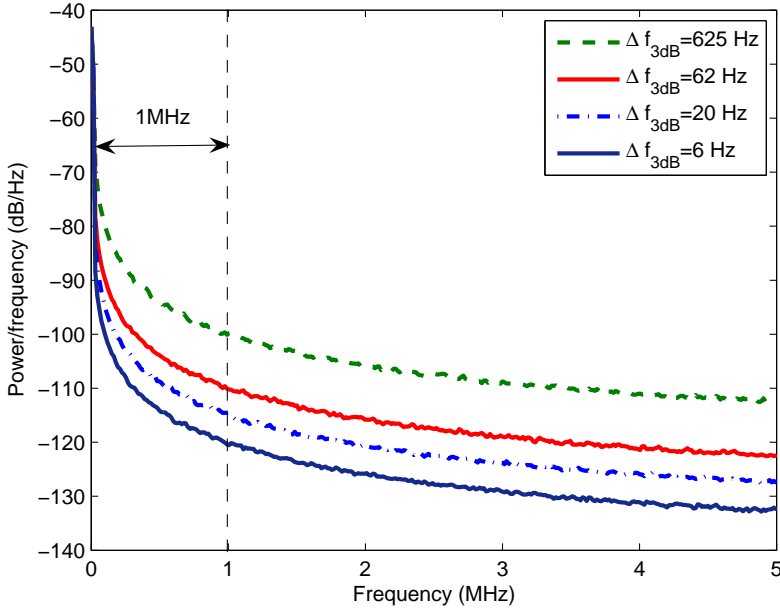
Figure 4.3: Phase noise power spectral density

power spectral density decrease by 20 dB per decade roll-off. It is also shown that the phase noise power at the frequency offset of 1 MHz is confirmed with the numerical calculation results by (2.13). A phase noise with $\Delta f_{3dB}=$ 625 Hz creates an SSB power of -100 dBc/Hz at the frequency offset of 1 MHz.

4.3.4   DC Offset

DC Offset on the transmitted signal is given by (2.16) and (2.17). The DC offsets in both I and Q channels are assumed identical and given by:

$$DC_I = 10^{(DC_I/20)} \tag{4.14}$$

Assuming the output power is maintained constant, increasing the DC offset saturates the transmitted signal.

4.3.5   White Noise Source

An approach to simplify the RF imperfection modelling effort is proposed. The model is based on a white noise source in the RF transmitter. This model has the restriction that can only be used to investigate the link level performance degradation due to the RF transmitter imperfection. The effect on the out-of band spectrum cannot be investigated based on this model.

The white noise source introduces the noise in the transmitted signal. The transmitted output signal affected by the white noise source imperfection is written as:

$$y\left(t\right) = a\left(t\right) + 10^{\frac{\sigma_S^2}{\sigma_M^2}/20} \tag{4.15}$$

The noise variance of this white noise source model σ_M^2 at the transmitter is set by a desired ratio compared to the variance of the transmitted signal σ_S^2. Hence, the signal to noise ratio at the transmitter is given by:

$$\frac{S}{M} = \frac{\sigma_S^2}{\sigma_M^2} \tag{4.16}$$

The transmitter noise generates EVM and the relation between the EVM and signal to noise ratio at the transmitter is given by:

$$\frac{S}{M} = -20\log(EVM) \tag{4.17}$$

4.4   Evaluation of Inband Performance

The performance evaluation of LTE uplink performance with the presence of hardware imperfections is carried out in a computer-based Monte Carlo simulation. The simulation is performed in accordance with the LTE uplink main parameters given in Table 4.1 unless otherwise specified. The details on the link level processing can be found in Appendix. A. During the simulation, the following assumptions are made:

- Both transmitter and receiver are perfectly synchronized in time and frequency.

- The maximum excess delay of the frequency selective fading channel is shorter than the cyclic prefix duration.

Table 4.1: UTRA LTE uplink simulation parameters.

Parameter	Value
Carrier Frequency	2 GHz
Transmission BW	10 MHz
Sub-frame duration	0.5 ms
Sub-carrier spacing	15 kHz
SC-FDM symbols/TTI	6 LBs, 2 SBs
CP duration	4.1 μs
FFT size/Useful subcarriers	1024/600
MCS settings	QPSK: 1/2 , 2/3, 3/4,
	16QAM: 1/2 , 2/3, 3/4
Channel code	3GPP Rel. 6 compliant Turbo code
	with basic rate 1/3
Receiver	MMSE Receiver
Channel Estimation	Ideal
Antenna schemes	SISO
Channel model	AWGN, Typical Urban 6 paths [5]
Speed	3 kmph
HARQ	No
RF imperfections	Nonlinear PA, Phase Noise,
	Gain and Phase Imbalances, DC offset
	White noise source

- The receiver performs ideal channel estimation. So that, it will not introduce additional performance degradation.

- One sub-frame consists of 6 Long Blocks (LBs) for data and 2 Short Blocks (SBs) for reference signals (14% overhead).

The power amplifier has an important role in the LTE uplink due to the high signal envelope variation, and resulting distortion which can affect the LTE performance. Figure 4.4 shows the EVM results for both SC-FDMA and OFDMA air interfaces. The results for both modulations, QPSK and 16QAM are presented. SC-FDMA has better EVM performance compared to OFDMA. A Change to lower modulation, QPSK, further improve the SC-FDMA performance, while this is not the case for OFDMA. These results are due to the fact that SC-FDMA has lower PAPR than OFDMA as shown in Figure 3.5 and Figure 3.6. OFDMA which has higher PAPR suffers from the nonlinear power amplifier.
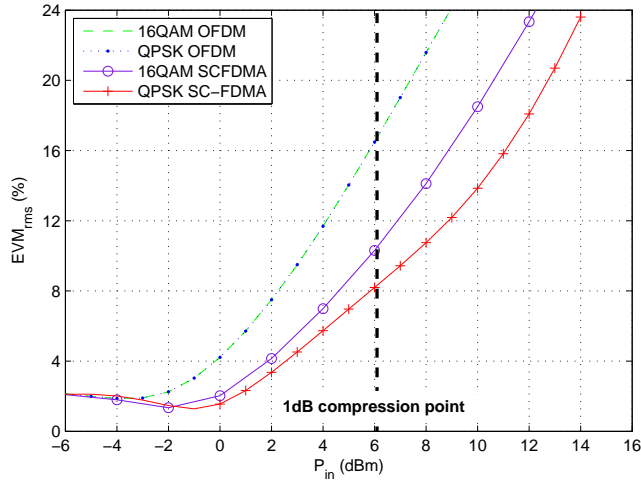
Figure 4.4: EVM results for Nonlinear PA

Figure 4.5 shows the EVM results for SC-FDMA with various number of sub-carriers. The number of sub-carriers is represented by the number of resource blocks (RB)s in which one resoure block consists of 12 sub-carriers. These results show that the number of sub-carriers/RBs does not affect much on the EVM results. The EVM variation is within 1%. This result is also in good agreement with the result shown in Figure 3.8 in which increasing the number of sub-carriers doe not affect the PAPR.

The impact of the non-linear power amplifier to the SC-FDMA and OFDMA spectral efficiency is shown in Figure 4.6. These results are obtained when an input back off (IBO) of 4 dB is assumed to maintain high efficiency. The result in the ideal case when there is no nonlinear PA is also given and represented in the link adaptation curve. It is shown that the nonlinear PA slightly reduce the SC-FDMA performance at higher modulation and coding scheme. In general, the nonlinear PA is also mainly affecting the higher order modulation and coding scheme for both SC-FDMA and OFDMA. A performance loss of 1.2 dB is observed for OFDMA with 16QAM 4/5.

Figure 4.7 summarizes the performance loss due the nonlinear PA at a BLER target of 10%. For 16QAM rate 4/5, SC-FDMA has a gain of 0.7 dB over OFDMA. A small gain of 0.2 dB can still be obtained at the lower coding rate. These results confirm that SC-FDMA radio access technique is the preferred solution over OFDMA in the presence of nonlinear power amplifier.
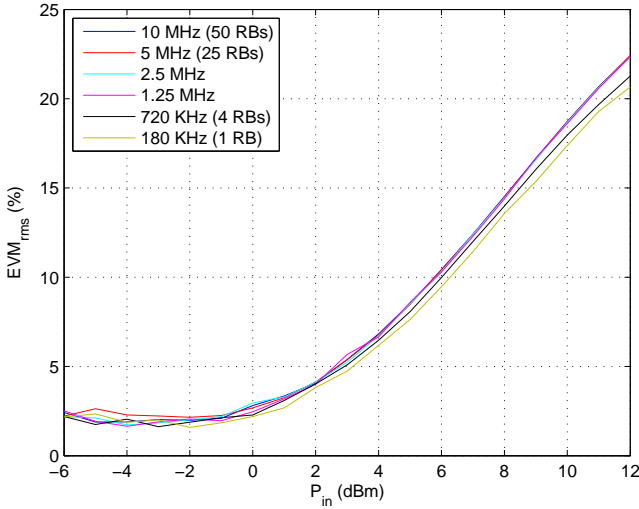
Figure 4.5: EVM results for different RB size in SC-FDMA (16QAM) with nonlinear PA

The individual EVM simulation results in LTE uplink for the different transmitter imperfections, including nonlinear amplifier, gain imbalance, phase imbalance, phase noise, DC offset, and white noise source 16QAM modulation are shown in Figure 4.8 Other modulation schemes obtain the same results, except for the impact of nonlinear amplifier. As previously explained, the modulation scheme affect the SC-FDMA PAPR and lead to different EVM results. The effect of the imperfections is analyzed in an EVM range up to 20%.

From Figure 4.8, it can be observed that the relation of each imperfection to the EVM is different. Gain and phase imbalance provide a linear relation, whereas it is not the case for the other imperfections. For the nonlinear amplifier, a high EVM level is mainly due to the soft clipping of the nonlinear power amplifier at the saturation point which can lead to additional in-band and out-of band distortion products. Knowing the relation between the imperfection and the EVM measurement, an investigation on the corresponding link level performance degradation can be proceed.

In [14], the analytical EVM expression of gain and phase imbalance is written as follows:

$$EVM_{rms} = \sqrt{\frac{1}{SNR} + 2 - \sqrt{1 + \frac{2\alpha}{1 + \alpha^2} + \cos(\theta) + \frac{2\alpha}{1 + \alpha^2}\cos(\theta)}} \quad (4.18)$$
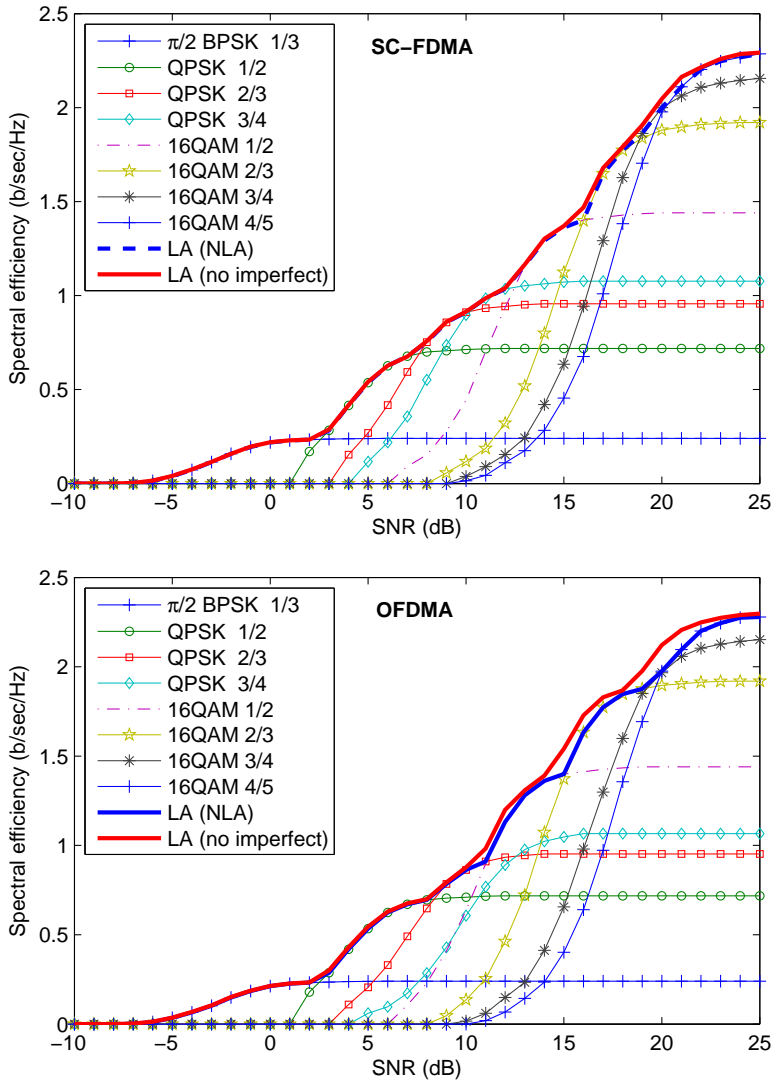
Figure 4.6: Spectral efficiency degradation for various MCS in the presence of nonlinear PA
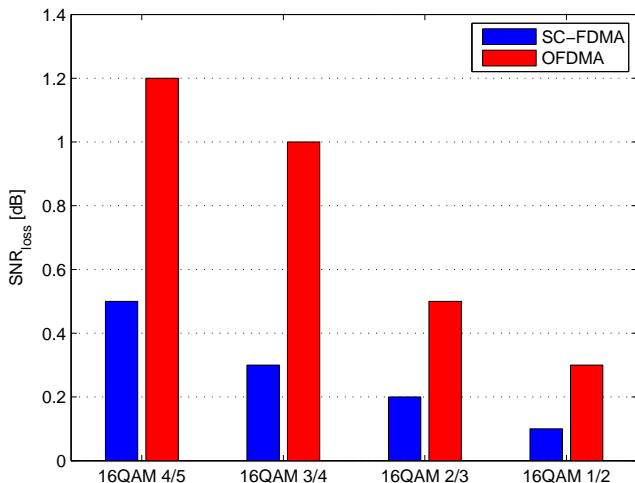
Figure 4.7: Performance loss at 10% BLER due to the nonlinear PA

The numerical calculation based on 4.18 shows a good match to the gain and phase imbalance results in Figure 4.8.

Figure 4.9 shows the spectral efficiency or throughput degradation for 16QAM rate 3/4 due to the transmitter white noise source imperfection. In this work, 16QAM rate 3/4 is considered as the highest MCS scheme in LTE uplink. If the target throughput loss due to the imperfections is 10%, the SNR loss is less than 0.4 dB for the low EVM region ($< 8\%$), whereas it significantly increases for the high EVM region. E.g. for an EVM of 16%, the SNR loss is 1.8 dB.

Figure 4.10 presents the throughput for several other uplink modulation and coding schemes (MCS) in AWGN channel together with the maximum throughput envelope curve. For the purpose of modelling, the envelope curve can be approximated from the Shannon capacity bound by accounting for an implementation margin, α:

$$C = \alpha \log_2 \left((1 + \frac{S}{N}) \right) \tag{4.19}$$

α represent the losses due to frequency guard bands, pilot overhead, cyclic prefix and imperfections. From Figure 4.10, it is observed that an $\alpha = 0.55$ reasonably approximates the maximum throughput envelope without the imperfection. Considering that the throughput loss for each MCS due to the imperfection is
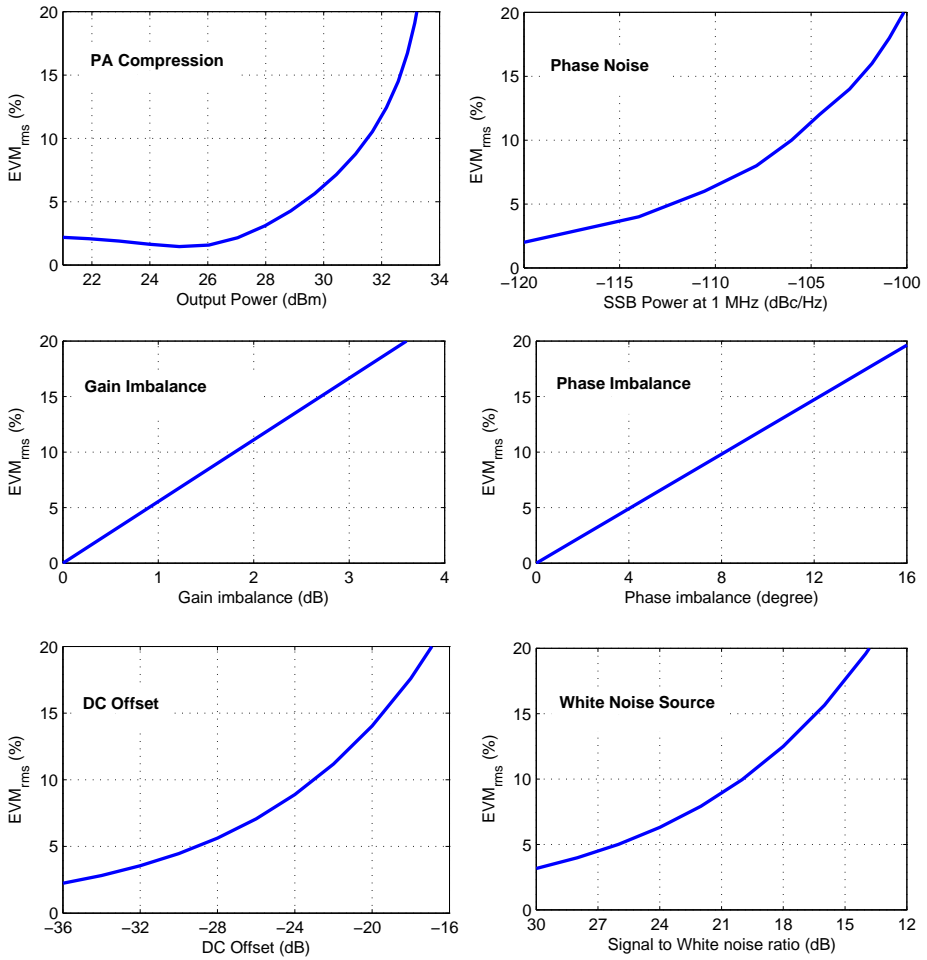
Figure 4.8: EVM results for various RF Imperfections
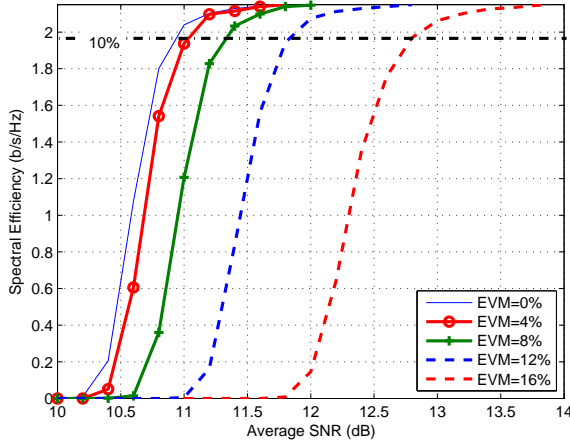
Figure 4.9: Throughput degradation for 16QAM 3/4 in AWGN channel due to the transmitter with a white noise source imperfection.

10%, the new throughput envelope curve is plotted with $\alpha= 0.52$.

If the transmitter imperfection source is a white noise source, the throughput envelope in AWGN channel is:

$$C = \alpha\log_2 \left((1 + \frac{S}{N + M}) \right) \tag{4.20}$$

where M is the white noise power at the transmitter, and N is the AWGN power at the receiver.

From (4.17) and (4.20), the SNR loss as the function of the EVM level at the transmitter is derived:

$$SNR_{loss} = \frac{1}{\left(\left(2^{\frac{C}{\alpha}} - 1\right)^{-1} - 10^{2\log(EVM)} \right)} - 2^{\frac{C}{\alpha}} + 1 \tag{4.21}$$

The degradation of the link performance by means of equivalent SNR degradation of 16QAM rate 3/4 is shown in Figure 4.11. The performance degradation is due to the RF imperfections in an AWGN channel and the result is plotted versus EVM level. From this result, the performance sensitivity to different RF imperfections are obtained. In the low EVM range (EVM $\leq$ 8%), all of the RF imperfections have almost the same corresponding SNR loss, and identical to the white noise degradation. Hence, within this range, the EVM is a good
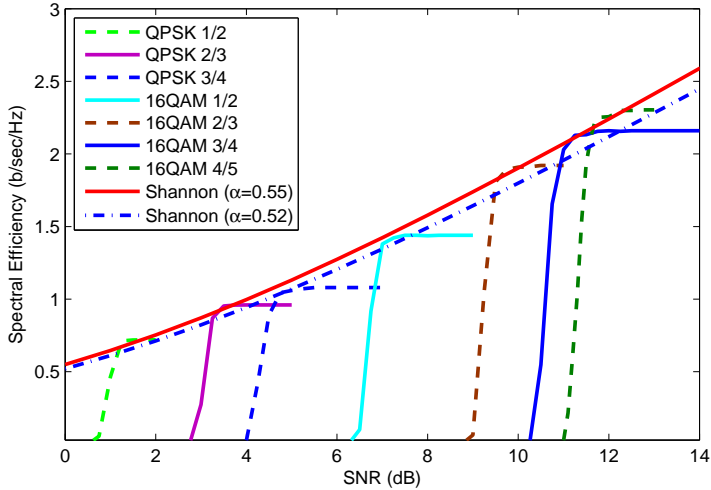
Figure 4.10: Approximating the maximum capacity of MCS envelope in AWGN Channel.

direct measure to estimate the link level performance loss. At high EVM levels, the SNR loss for each imperfection starts to deviate from the equivalent white noise source imperfection.

In Figure 4.11, phase noise has higher SNR loss compared to other imperfections. This was expected because the phase noise introduces inter-carrier interference which is more severe than additive noise. Nevertheless, practical oscillators only leads to low phase noise level, and small EVM. For example, in GSM/WCDMA applications a typical phase noise level is around -120 dBc/Hz at 1 MHz offset [54] which keeps the corresponding EVM below 2%. At the opposite end, gain imbalance introduces less performance degradation. The performance loss due to the nonlinear power amplifier is slightly higher than the loss due to the white noise source.

The result from (4.21) is also plotted in Figure 4.11. It can be observed that the derived calculation of the SNR loss due to the white noise source at the transmitter matches the simulation results. There is only a small deviation of 0.1 dB at high EVM levels (EVM=20%).

The result for higher MCS with 16QAM rate 4/5 is shown in Figure 4.12. It is shown that the higher MCS is more sensitive to the EVM. The result shows that most of the imperfections again have similar SNR loss results in the low EVM region (EVM $\leq$ 7%). The result of analytical model with the white noise
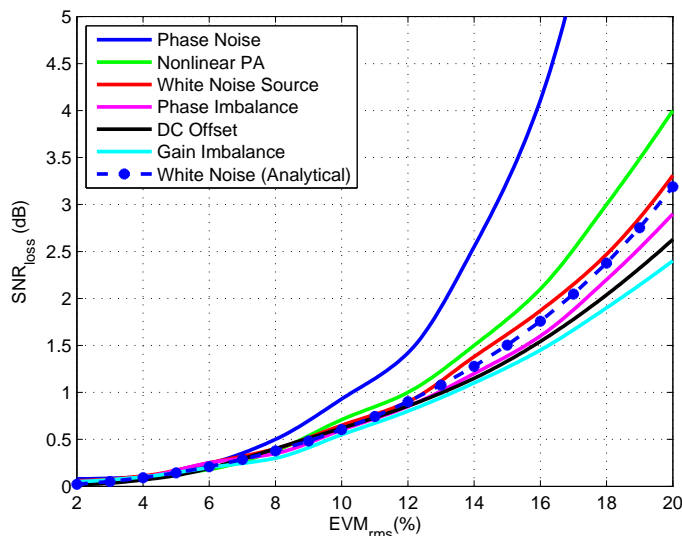
Figure 4.11: SNR loss for 16QAM 3/4 due to the RF imperfections (AWGN).

source is still in good agreement with the simulation result.

Figure 4.13 shows the relation between EVM value and equivalent SNR degradation in TU06 channel. The results follow the trend in the previous result in the AWGN channel with an SNR loss range of 5 dB. An analytical result for the effect of the equivalent white noise source in the TU06 channel is more complex than in the AWGN channel since the transmitter imperfections can appear as additional coloured noise at the receiver. Nevertheless, the white noise source imperfection model still fits well with the other imperfections, especially in the EVM < 6% region.

Figure 4.14 shows the results the impact of various imperfections to the higher MCS (16QAM rate 4/5) in TU06 channel. Higher MCS is more sensitive toward EVM values, especially at the high EVM range. However, different imperfections, including the white noise source still obtain the same SNR loss in the low EVM region. Hence, for EVM values less than 6-8%, the white noise source is useful as an equivalent transmitter imperfection source. Note that the above analysis assumes 16QAM as the maximum modulation order. The final EVM requirement will be chosen as a compromise among UE complexity and system performance. As an arbitrarily chosen reference, an EVM of 8% corresponds to a link loss of 0.5 dB for 16QAM. Recently, in e.g. [55], 64QAM has been considered for uplink which leads to increased effect of EVM.
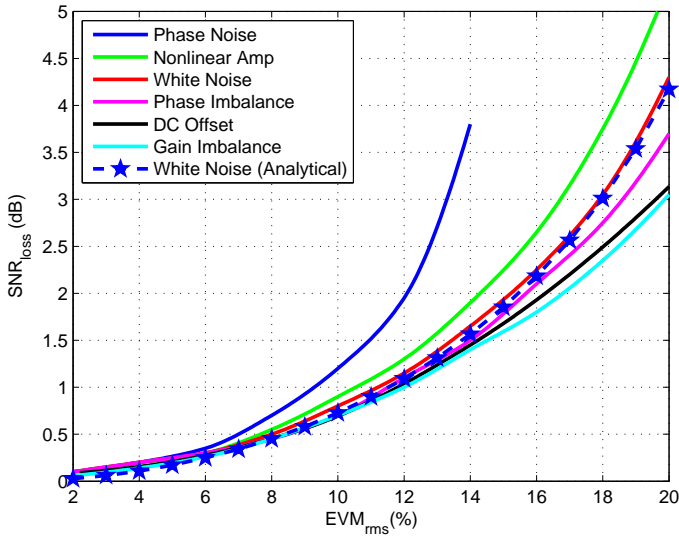
Figure 4.12: SNR loss for 16QAM 4/5 due to the RF imperfections (AWGN).
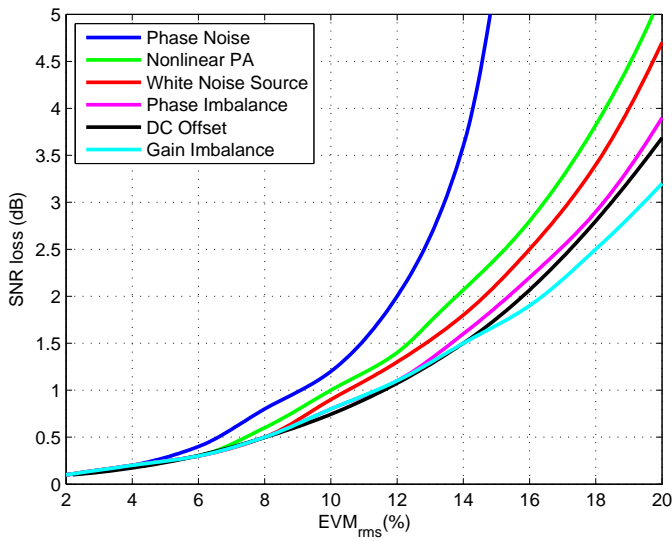
Figure 4.13: SNR loss for 16QAM 3/4 due to the RF imperfections (TU06).
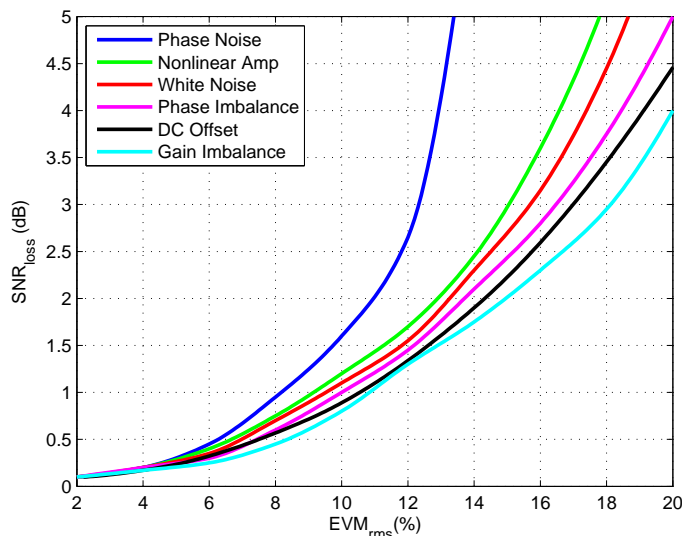
Figure 4.14: SNR loss for 16QAM 4/5 due to the RF imperfections (TU06).

4.5 Summary

The impact of the RF transmitter imperfections in LTE uplink performance is presented in this chapter. The results obtained are based on the UTRA LTE uplink parameter settings. The study is focused on the impact on the in-band channel performance, especially on EVM and link level performance loss. From this study, the EVM generated by each imperfection can be associated with the corresponding link level performance.

The most common RF imperfections in the Cartesian transmitter, including nonlinear power amplifier, gain imbalance, phase imbalance, DC offset, and phase noise are investigated. A white noise source as an equivalent RF transmitter imperfection is also investigated. SC-FDMA shows its benefit over OFDMA when a nonlinear power amplifier is taking into account. SC-FDMA with 16QAM rate 4/5 provides additional gain of 0.7 dB over OFDMA and hence leads to a better spectral efficiency. This result in favour with the selection of SC-FDMA for the access scheme in LTE.

The EVM is a good direct measure to estimate the link level performance loss in the practical EVM range (EVM < 8%) for the investigated imperfections. In our simulations, an EVM value of 8% corresponds to an SNR loss of 0.5 dB with

16QAM rate 3/4. The EVM also becomes an important parameter for higher order modulation and coding scheme, which very sensitive to the imperfections.

The main benefit from this work is to simplify the simulation effort in the study of RF imperfections, especially by including a white noise source as an equivalent model of the RF transmitter imperfections. The performance degradation in AWGN and frequency selective fading when using a white noise source as an equivalent transmitter RF imperfection model, fits well with the other imperfections in the anticipated range of EVM. With calibrated noise power settings this simple noise source may replace individual imperfection models in link level simulations.

The RF imperfections not just affect the inband performance. These imperfections can also affect the out-of-band performance lead to interfere the adjacent channel, and thus a topic for the following chapter, which cover the impact of RF imperfections on the out-of band channel.

" Does man think that he will be left uncontrolled, (without purpose)?"

<div align="center">The Resurrection 75:36</div>

CHAPTER 5

RF Hardware Imperfections Effect on Out-of-band Channel

5.1 Introduction

RF hardware imperfections are affecting both the in-band and out-of-band channel. The impact on the out-of-band channel is an increase of out-of-band emissions. Out-of-band emissions are unwanted emissions immediately outside the nominal channel resulting from the modulation process and non-linearity in the transmitter, but excluding spurious emissions [6]. The performance of a radio communication system in the out-of-band channel is measured by the parameters defined by the standard and must meet with the requirements .

SC-FDMA is the new radio access technique in beyond 3G system and offers flexibility for the user to be scheduled in both frequency and time domain to exploit the radio channel variations [8]. In LTE, the user equipment (UE) has a flexibility to transmit on 1 resource block (RB = 180 kHz) up to 100 RB depending on the bandwidth allocation from the base station leading to large dynamics in the power spectral density transmitted from the UE. Such dynamics need to be considered when analyzing LTE Radio Frequency (RF) requirements.

Each LTE channel bandwidth has its own RF requirements [56].

The spectrum emission of LTE UE must be controlled by a spectrum shaping technique in order to meet the stringent spectral mask requirements [57], [58]. The flexible UE transmission bandwidth and small guard-band size are the main issues in the area of transmit spectrum shaping for LTE. Currently, it is an open and hot topic in the 3GPP bodies [57],[59],[60],[61]. Moreover, the 3GPP has not completely addressed the effectiveness of different techniques in meeting out of band emission requirements [62]. It is not clear either the 3GPP intends to standardize the spectrum shaping techniques or leave it open to the manufactures [62].

A spectrum shaping technique implemented in the transmitter can provide a sufficient margin to the emission mask requirements towards the spectral re-growth as a result of the RF imperfections. Each RF imperfection can create different impact on the transmit signal. Combined with the flexible transmission bandwidth factor in LTE, it becomes an important issue which is addressed in this chapter. The placement of the Resource Block in the channel bandwidth is expected to create different results in terms of the out of band spectrum.

This chapter is organized as follows. The overview of LTE requirements related to the out-of band channel is given in Section 5.2. Two different spectrum shaping techniques are described in Section 5.3. Assumptions and scenarios for the assessment of the spectrum shaping techniques are given in Section 5.4. For the spectrum shaping performance results are discussed in Section 5.5. The impact of RF hardware imperfections is analyzed in Section 5.6. This section discusses the impact on different radio access techniques in LTE, and the impact on resource block allocation. Finally, a summary is presented in Section 5.7.

5.2 Out-of-band Channel Requirements

This section provides the out-of-band channel requirements of LTE, which are used as the reference for the subsequent sections. Multiple options of LTE channel bandwidth results in a complex requirement. Each channel bandwidth has a specific requirement on both Spectrum Emission Mask (SEM) and Adjacent Channel Leakage Ratio (ACLR) requirements[1] [56]. The out-of-band channel requirements are specified in terms of a SEM and ACLR [56]. ACLR and SEM serve different purposes. ACLR captures the average of signal characteristics over a carrier, while the SEM captures the variation in the spectrum emissions.

---

[1]During the work of this thesis, the requirements have not been fully standardized yet.

Table 5.1: UTRA Spectrum Emission Mask Requirement (SEM) [6].

Δf in freq.	Minimum Requirement		Meas. BW
(MHz)	Relative req.	Absolute req.	
2.5-3.5	$\left\{ -35 - 15 \cdot \left(\frac{\Delta f}{MHz} - 2.5 \right) \right\}$ dBc	-71.1 dBm	30 kHz
3.5-7.5	$\left\{ -35 - 1 \cdot \left(\frac{\Delta f}{MHz} - 3.5 \right) \right\}$ dBc	-55.8 dBm	1 MHz
7.5-8.5	$\left\{ -39 - 10 \cdot \left(\frac{\Delta f}{MHz} - 7.5 \right) \right\}$ dBc	-55.8 dBm	1 MHz
8.5-12.5	-49 dBc	-55.8 dBm	1 MHz

5.2.1 LTE Spectrum Emission Mask (SEM)

In this work the baseline spectrum emission mask is the spectrum emission mask for UTRA WCDMA, which has a fixed channel bandwidth of 5 MHz [6]. To defined the spectrum emission mask for other channel bandwidths, the scaled version of that UTRA WCDMA spectrum emission mask is assumed. The UTRA WCDMA spectrum emission mask for the UE applies to frequencies between 2.5 MHz and 12.5 MHz away from the UE center carrier frequency as described in Table 5.1.

5.2.2 LTE Adjacent Channel Leakage Ratio (ACLR)

The adjacent channel leakage ratio is defined as a ratio of the power integrated over an assigned bandwidth in the adjacent channel to the power integrated over the desired channel. Figure 5.1 illustrates the transmit spectrum for the ACLR calculation. The ACLR can be expressed as:

$$ACLR = \frac{\int_{f_1 - \Delta B_{ACP}}^{f_1 + \Delta B_{ACP}} PSD\left(f\right) \cdot df}{\int_{f_0 - BW/2}^{f_0 + BW/2} PSD\left(f\right) \cdot df} \tag{5.1}$$

Where f_0 is the center frequency, BW is the bandwidth of the desired signal, and ΔB_{ACP} is the ACLR measurement bandwidth of the adjacent channel. ΔB_{ACP} varies with the channel bandwidth settings. The measurement bandwidth of the wide channel bandwidth (≥ 5 MHz) has been specified in the standard [56]. For channel bandwidths of 5, 10, 15, and 20 MHz, the ΔB_{ACP} is 4.5, 9, 13.5,
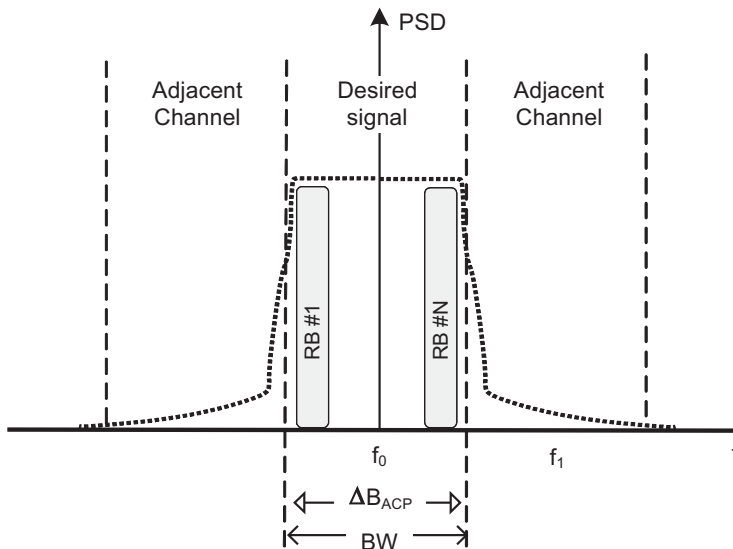
Figure 5.1: Channelization of the transmit spectrum.

18 MHz, respectively. ΔB_{ACP} for the narrow bandwidth option has not been specified yet [56].

ACLR can be classified as ACLR1, and ACLR2. ACLR1 is the ACLR measurement in the adjacent channel of the transmitted signal, and ACLR2 is the ACLR measurement in the adjacent channel of the channel where ACLR1 is measured. The ACLR requirement for LTE is below the ACLR for UTRA. UTRA has an ACLR1 requirement of 33 dB and the LTE requirement is 30 dB. The LTE ACLR1 requirement is for all the channel bandwidth options. Until this date, there is no complete agreement whether the ACLR2 is required for LTE. UTRA WCDMA has specified the ACLR2 at 43 dB [6]. In this work, the ACLR2 requirements for LTE is assumed to be 43 dB.

5.3   Spectrum Shaping Techniques

Spectrum shaping is employed at the transmitter to suppress the out-of-band emission and hence make the spectrum emission satisfy the emission mask defined in standardization. There are some design trade-off considerations in choosing the spectrum shaping technique, such as out-of band suppression ca-

SC-FDMA with Digital Filter

SC-FDMA with Time Windowing
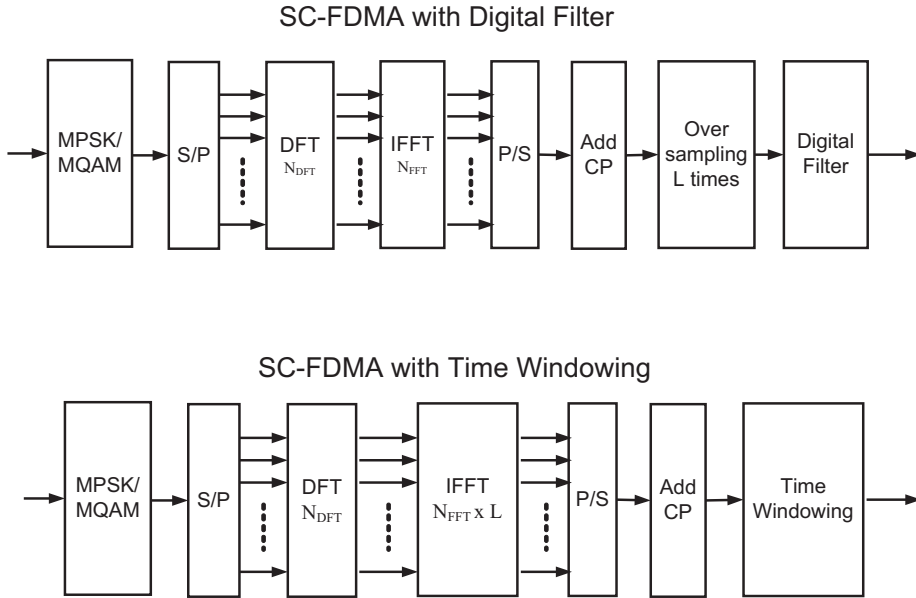
Figure 5.2: SC-FDMA transmitter structures with spectrum shaping.

pability, capacity loss, and hardware complexity.

Digital filtering and time windowing are the most commonly used spectrum shaping techniques. Time windowing offers low complexity with the cost of reduction in the cyclic prefix length due to the signal overlapping [58],[63]. In this work, a spectrum shaping technique for LTE UE using an Inverse Chebyshev Digital Infinite Impulse Response (IIR) filter is proposed and evaluated. The filter selection is based on studies in [25] where this filter type achieves minimum capacity loss. The aim of the study is to propose an IIR digital filter based spectrum shaping technique for LTE. The performance is compared with the windowing based spectrum shaping technique, so that the UE spectrum emission mask can be fulfilled for various UE allocated bandwidths with minimum capacity loss.

5.3.1 IIR Digital Filter

Spectrum shaping can be controlled by means of implementing a digital filter in the transmitter, such as a FIR filter, IIR filter and pulse-shaping. However, the SC-FDMA signal requires a sharp suppression in the transition band in

consequence of small guard band size. It requires a large FIR filter tap length. Pulse-shaping is only effective to control the sidelobes out to half sample rate [25]. Based on these limitations, an IIR digital filter is chosen to control the LTE spectral emission.

The transmitter structure is shown in Figure 5.2. Before the SC-FDMA signal passes the digital spectrum shaping filter, the signal is oversampled L times to shift the spectral images. Therefore, the filter specifications can be more relaxed.

Among the IIR digital filter classes, an Inverse Chebyshev filter is selected for its properties, maximally flat in the passband and sharp suppression in the transition band. The filter frequency response for 10 MHz system bandwidth is shown in Figure 5.3. It is a 10th order Inverse Chebyshev Filter with 20 dB stopband ripples starting at 4.8 MHz. It ensures a maximally flat region within a 4.5 MHz lowpass bandwidth. From the phase response, it can be observed that the filter introduces non-constant group delay, especially at the higher frequency part. The magnitude and phase variation within the pass-band region will be estimated and compensated by the channel estimation and frequency domain equalizer at the receiver, respectively.

5.3.2   Time Windowing

A raised cosine (RC) window function to shape the spectrum emission is selected since it provides better spectrum emission control than a rectangular window. Moreover, an RC window is also proposed for LTE [58],[63]. Fig.5.2 shows the SC-FDMA transmitter with time windowing and the window function located after the cyclic prefix insertion. The time windowing process at the transmitter is illustrated in Fig.5.4. The window function is applied at the edge of each SC-FDMA symbol with cyclic prefix, named as head and tail window, respectively. To prevent symbol distortion, samples are introduced at the end of each symbol prior to the tail window operation. The samples do not increase the symbol duration since it is overlapped with the following SC-FDMA symbol. Note that the overlapped window also shortens the effective cyclic prefix length which may affect the link level performance in the frequency selective fading channel.
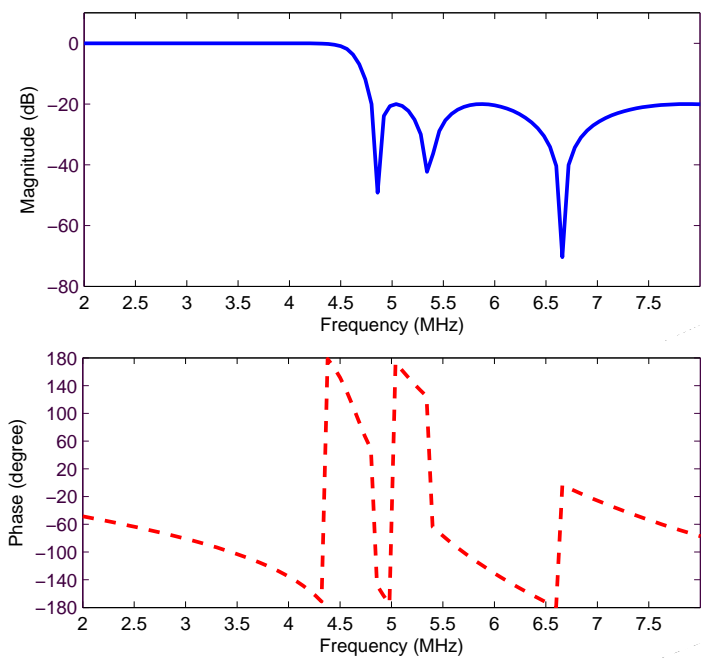
Figure 5.3: Inverse Chebyshev filter frequency response for 10 MHz system bandwidth.
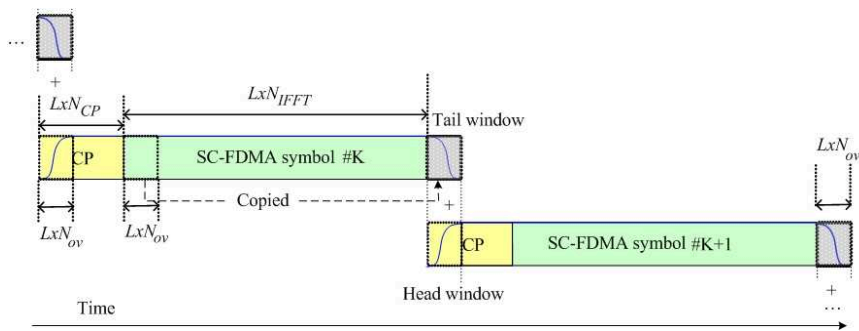
Figure 5.4: Time windowing process of the SC-FDMA symbol.

Table 5.2: LTE uplink Transmission Parameters.

Spectrum Allocation	Sampling-rate	LB size #SCs/samples	Max. RB	CP length samples
20 MHz	30.72 MHz	1200/2048	100	127
15 MHz	23.04 MHz	900/1536	75	95
10 MHz	15.36 MHz	600/1024	50	63
5 MHz	7.68 MHz	300/512	25	31
2.5 MHz	3.84 MHz	144/256	12	15
1.25 MHz	1.92 MHz	72/128	6	7

The raised cosine window function is given by:

$$
w\left[n\right] = \begin{cases} \frac{1}{2}\left(1 - \cos\left(\frac{2\pi n}{LN_{ov}-1}\right)\right) & n \leq LN_{ov} \\ 1 & LN_{ov} + 1 \leq L\left(N_{CP} + N_{FFT}\right) \\ \frac{1}{2}\left(1 + \cos\left(\frac{2\pi n}{LN_{ov}-1}\right)\right) & n \geq L\left(N_{CP} + N_{FFT}\right) + 1 \end{cases} \qquad (5.2)
$$

Where N_{ov} is the number of overlapped window samples, N_{CP} is the number of Cyclic Prefix samples, and N_{FFT} is the FFT size.

5.4   Assumptions & Scenarios on Controlling Out-of-band Emission

To compare, and eventually propose a spectrum shaping technique, the two techniques are evaluated for their ability to control out-of-band emissions. The spectrum shaping techniques are evaluated using computer based link level simulation. The simulation is performed in accordance with the parameters given in Table 5.2, and Table 5.3. Each spectrum allocation setting has specific parameters, including the sampling rate, Long Block (LB) symbol size in terms of the useful sub-carriers (SCs) and samples, maximum Resource Block (RB) size, and Cyclic Prefix (CP) length. The minimum UE transmission bandwidth is 1 RB, which contains 12 SCs in 180 kHz bandwidth. The CP duration is maintained at around 4.1 μs for different spectrum allocation settings.

Table 5.3: Simulation Parameters.

Parameter	Values
Bandwidth	1.25 MHz, 10 MHz
Modulation	16QAM
Oversampling (L)	4
Interpolation Filter	8th order FIR low pass filter
Shaping Filter	10th order Inverse Chebyshev
UE max TX Power	24 dBm
Receiver	MMSE receiver
Channel Estimation	Linear Interpolation
EVM from Gain Imbalance	4%
EVM from Phase Imbalance	4%
EVM from Nonlinear PA	4%

During the simulation, the spectral emission mask and adjacent channel leakage ratio requirements are following the assumptions defined in Section 5.2. The Error Vector Magnitude (EVM) is measured at the receiver symbol detection input as described in Section 4.2. It allows to perform amplitude/phase equalization of the unknown transmit filter response. The EVM expresses the error in the received constellation diagram and can be used as a direct measure to estimate the capacity loss as described in Chapter 4. EVM of 4 % is selected as the case study, where the typical error levels from each imperfection are created at that EVM level. The operating point of the nonlinear amplifier is at 24 dBm. It has been chosen so that it is comparable with the WCDMA transmitter operating at the maximum output power.

The sampling rate for the digital filter method is increased by 4 times using the time domain interpolation. The interpolation is done by using an 8th order FIR filter low pass filter. For the time windowing, the sampling rate is also increased by 4 times using a larger size IFFT operation. Up-conversion with a fixed local oscillator in the center of the frequency band is assumed. For the digital filter, the bandwidth setting is fixed to the system bandwidth in order not to increase the complexity. It is not practical to set the bandwidth according to the RB size since the RB size varies from 1 RB up to 1200 RB size. Moreover, The RB size can be updated in an interval of 1 TTI or 0.5 ms.
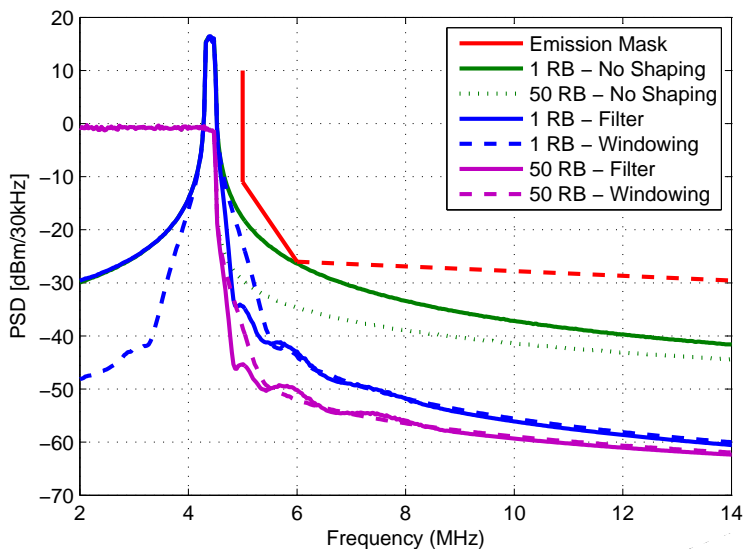
Figure 5.5: Spectrum emission with & without spectrum shaping for 10 MHz system bandwidth.

5.5   Spectrum Shaping Performance

Figure 5.5 shows the spectrum emission of 1 RB transmission at the channel edge and full 50 RBs for 10 MHz system bandwidth. It is clearly observed that spectrum emission control is required because the transmit baseband signal without the spectrum shaping provides only a small margin to the emission mask. Hence, it does not provide sufficient headroom for transmitter RF imperfections. Both digital filter and time windowing are capable of providing a satisfactory margin. It is also shown that the digital filter performs better than time windowing. In this case, the time windowing uses 20 overlapped window samples and consumes 16% of the cyclic prefix.

The time windowing still has an advantage over digital filtering to have better suppression in the in-band channel. For a smaller size RB transmission, the time windowing provides a symmetrical suppression of the transmit spectrum. Moreover, the time windowing creates a fast decaying out-of-band spectrum in comparison to the digital filter. Hence, the time windowing reduces the interference level to the other in-band RBs better than the digital filter.

Spectrum emission control for smaller channel bandwidths is getting problem-
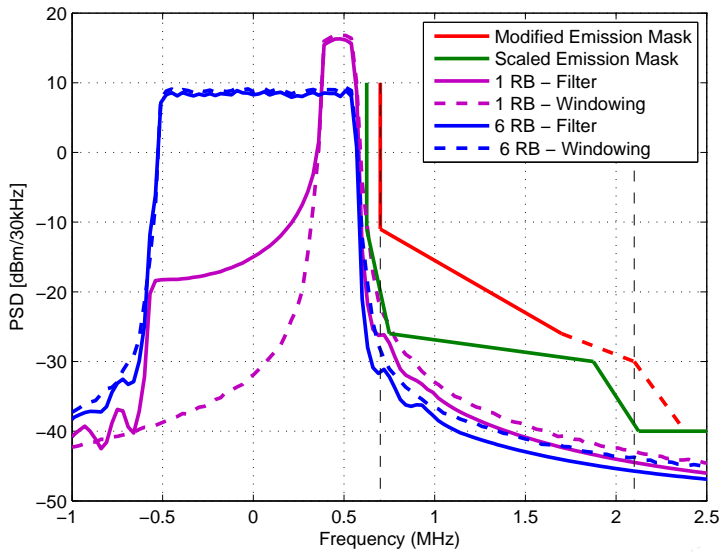
Figure 5.6: Spectrum emission of 1.25 MHz system bandwidth.

atic. Figure 5.6 shows the spectrum emission of a 1.25 MHz system bandwidth. It is shown that the transmit signal with spectrum shaping techniques is marginally below the emission mask. Moreover, the time windowing consumes 16 overlapped window samples in order to compete with digital filtering. That amount of samples exceeds the CP length (7 samples) and causes inter-symbol interference. Recently, it has been agreed to change the basic parameter/numerology for smaller bandwidth option [61]. One possibility is to change the bandwidth of 1.25 MHz to 1.4 MHz to increase the guard band size. The impact is reducing the bandwidth occupancy from 86.4% to 77.1%. The modified 1.4 MHz emission mask from [64] provides sufficient margin. For the case of smaller RB allocation, the time windowing produces less spectrum leakage in the in-band channel in comparison to digital filtering.

The EVM results for various bandwidth settings with spectrum shaping are shown in Figure 5.7. The purpose of this work is to investigate the impact on EVM when both techniques have equal performance in controlling the spectrum emission. The digital filter always applies the same filter coefficients and the time windowing uses overlapped samples at around 16-20 samples depending on the bandwidth settings. The EVM is generated as a result of the inter-symbol interference (ISI). The wider system bandwidth options result in lowered EVM value because of the higher number of CP samples. The infinite impulse response of IIR digital filter creates ISI. For the time windowing, the overlapped window

larger than the CP length creates ISI.

Both shaping techniques successfully generate very low EVM for system band-widths equal or greater than 5 MHz. However, the time windowing starts to fail for system bandwidths smaller than 5 MHz. For 2.5 MHz, the overlapped window of 16 samples is not just creating an EVM of 1.7%, but also causing the CP to become useless. It does not serve the actual purpose to absorb the ISI due to the frequency selective fading channel. The time windowing becomes significantly worse for 1.4 MHz system bandwidth option. It requires 16 over-lapped window samples to sufficiently control the spectrum emission and thus generates an unacceptable EVM of 16%. Moreover, the overlapped window is 129% longer than the CP length. The relation of the number of overlapped window samples to the EVM is also shown in Figure 5.7. It can be observed that increasing the number of overlapped samples increases the EVM. The EVM result can be improved by reducing the number of overlapped samples at the expense of unsatisfactory spectrum emission.

5.6   Impact of RF Hardware Imperfections

The capability and effectiveness of the proposed spectrum shaping techniques in LTE settings with the hardware imperfections are discussed. The impact of different channel bandwidth and RB size/placement is also studied. The results are evaluated based on the margin to the spectrum emission mask and the ACLR. The detailed descriptions on the hardware imperfections model used in this work are given in Chapter 4. To reduce the unwanted emissions, a spectrum shaping technique with IIR digital filter is included in the transmitter based on previous discussions.

Figure 5.8 shows the impact of a nonlinear amplifier on the spectrum emission of SC-FDMA and OFDMA. The power amplifier non-linearity model is according to Figure. 4.2 and including both AM/AM and AM/PM. The subsequent work also uses the same PA model. An input back off (IBO) of 4 dB is assumed so that the generated EVM value is 4%. 16QAM as the highest modulation scheme in LTE uplink is used for both SC-FDMA and OFDMA. It is shown that the spectrum emission of OFDMA is marginally below the spectrum emission mask. A better result is obtained for the SC-FDMA transmitter in agreement with PAPR results in Chapter 3.

The ACLR for SC-FDMA with a nonlinear amplifier is shown in Figure 5.9. The impact of increasing the input power of a nonlinear amplifier on both QPSK and 16QAM is illustrated. The selection of modulation scheme affects the ACLR
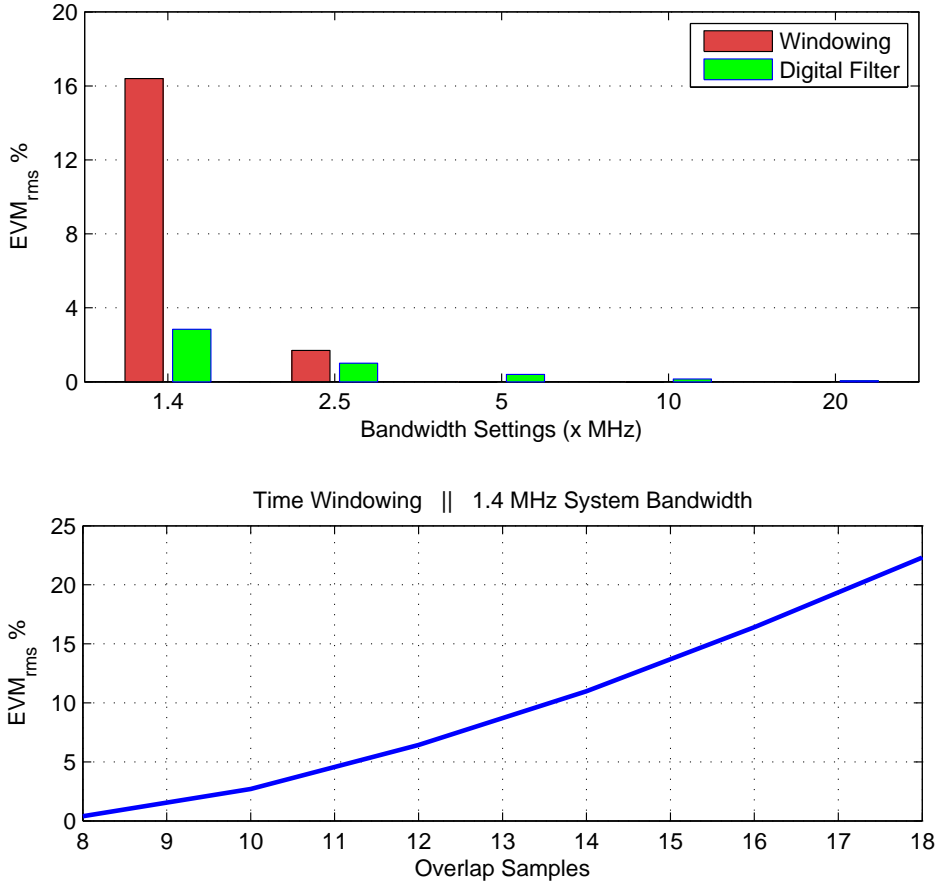
Figure 5.7: EVM results for various bandwidth settings (a) and time windowing with different overlapped window samples (b).
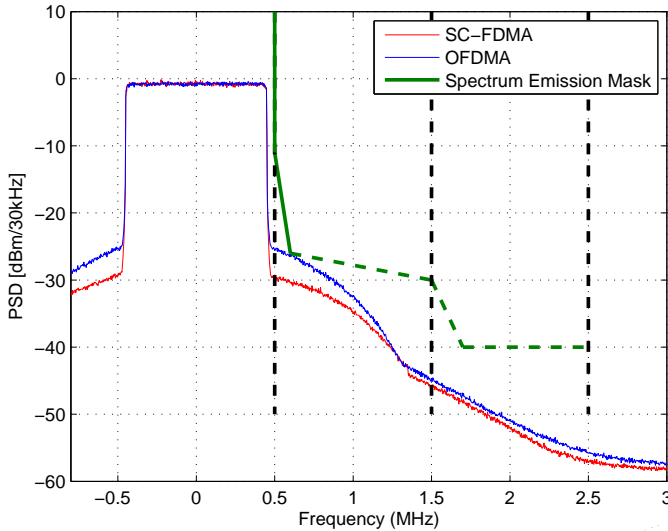
Figure 5.8: Spectrum emission of SC-FDMA & OFDMA.

result. SC-FDMA with QPSK has an ACLR result 1.5 dB lower than SC-FDMA with 16QAM. The results are related to the PAPR results of SC-FDMA in Figure 3.5, where the lower modulation scheme has a better PAPR result.

For OFDMA, the ACLR results are shown in Figure 5.10. Different from the results of SC-FDMA, the ACLR of OFDMA is not affected by the selection of modulation scheme. It is mainly due to the envelope of the OFDM signal which is not affected by the modulation scheme as shown in the PAPR result in Figure 3.5.

The above results show that SC-FDMA has better ACLR performance than OFDMA. The results for 16QAM are summarized in Figure 5.11. Assuming the input back off is 4 dB, SC-FDMA has a 3 dB better result than OFDMA for ACLR1. For ACLR2 requirement, SC-FDMA has a 1 dB better than OFDMA.

Figure 5.12 shows the spectrum emissions of a transmitter with multiple RF imperfections, such as nonlinear amplifier, gain imbalance, and phase imbalance. The EVM contribution of each RF imperfection is given in Table 5.3. The corresponding RF imperfections parameter can be obtained from Figure 4.8. To distinguish the impact of each imperfection, the nonlinear power amplifier creates spectral regrowth, and the IQ mismatch creates the additional emission peaks at the transmission of smaller RB. The impact of IQ mismatch cannot be
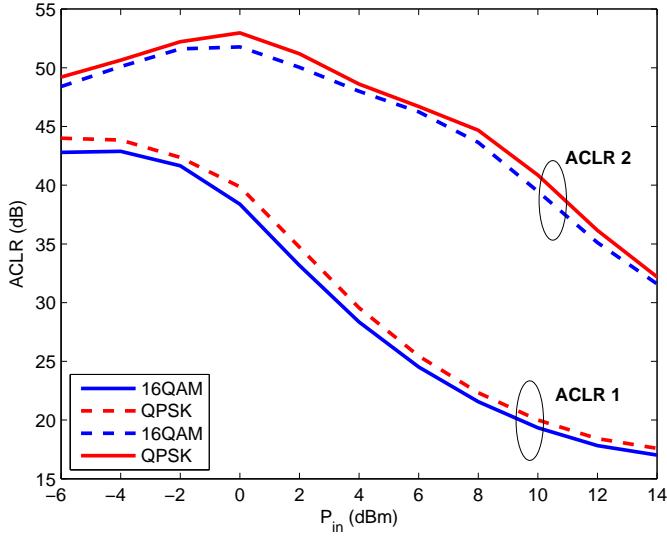
Figure 5.9: ACLR results of SC-FDMA with Nonlinear Amplifier.
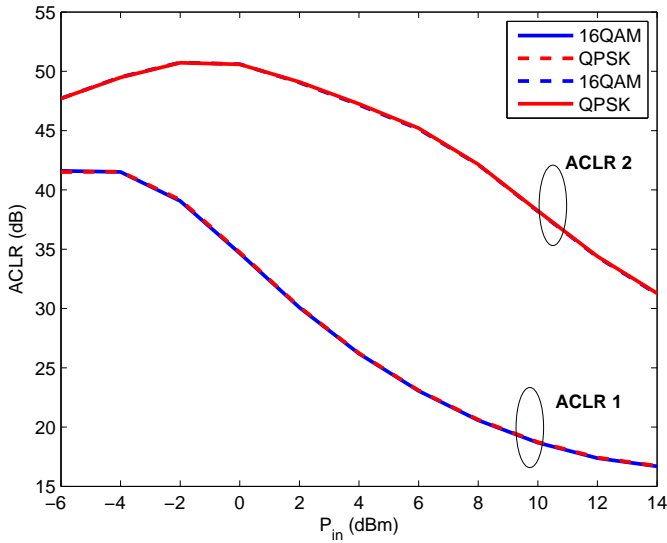
Figure 5.10: ACLR results of OFDMA with Nonlinear Amplifier.
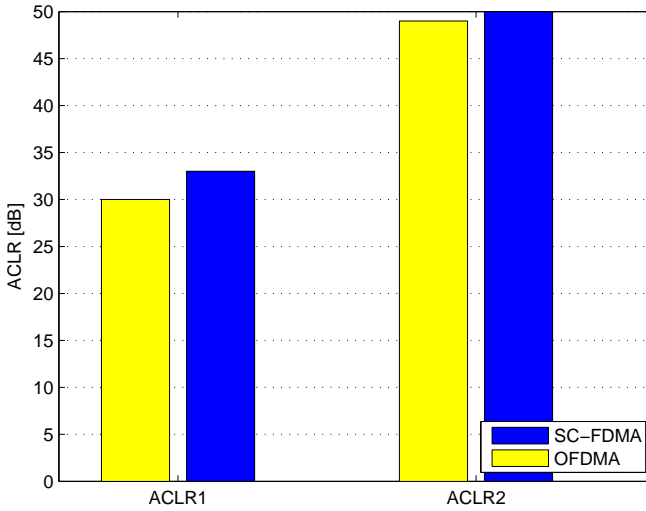
Figure 5.11: Summary of SC-FDMA and OFDMA ACLR results.

observed at the large RB allocation. These are the unwanted images which are generated by gain and phase imbalances. The IQ mismatch is created before the nonlinear PA. Therefore, the unwanted image also appears as harmonic products between the image and the wanted signal.

Based on the results in Figure 5.12, the spectral emission of both RB allocations are still below the spectral emission mask assuming that the EVM contribution from each imperfection is in the order of 4%. Beside violating the spectrum emission requirement, the hardware imperfections also reduce spectral efficiency as discussed in the previous chapter.

The ACLR results for the transmitter with the imperfections as given in Table 5.3 are illustrated in Figure 5.13. The purpose is to analyze the impact of the RB size and allocation. For the case without the imperfections, the small RB size at the channel edge has a better result than large RB size transmission. The result for small RB and large RB size is at least 19 dB higher than the LTE ACLR1 requirement. The case for the transmitter with imperfections shows the opposite. The ACLR of the transmission with large RB size is worse than the small RB size. For the RB size of 50, the ACLR1 is at 33 dB, which is 3dB above the LTE ACLR1 requirement. The ACLR2 result is also higher than the UTRA ACLR2 requirement (43 dB) by 7 dB.
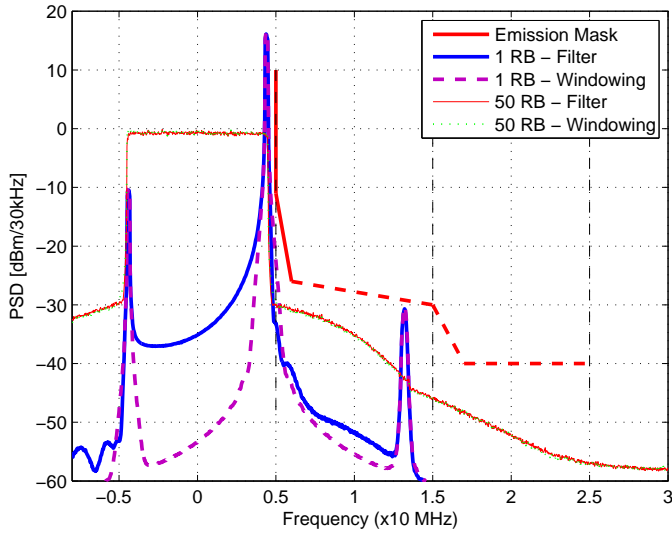
Figure 5.12: Spectrum emission of a transmitter (10 MHz) with imperfections as given in Table 5.3.
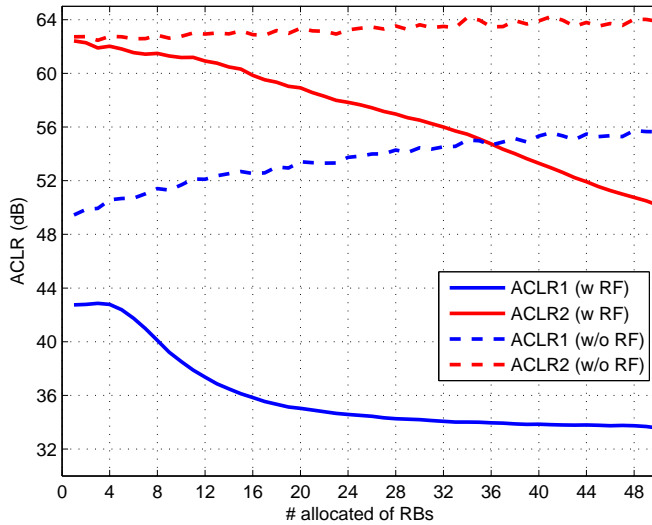
Figure 5.13: ACLR results of a transmitter (10MHz) with and without imperfections as given in Table 5.3.
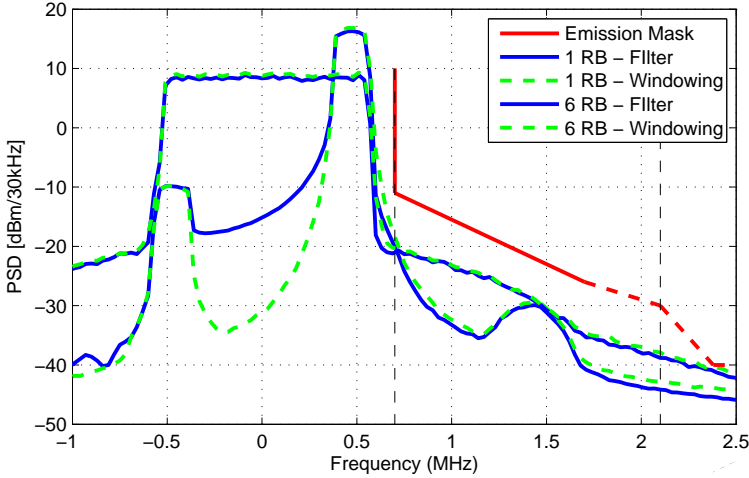
Figure 5.14: Spectrum emission of a transmitter (1.4 MHz) with imperfections as given in Table 5.3.

Figure 5.14 shows the spectrum emission of the 1.4 MHz system bandwidth with the transmitter imperfections. The results show the same trend as the results for 10 MHz channel bandwidth. Similar to Figure 5.12 one can observe the effectiveness of the two different spectrum shaping techniques. For the out-of-band spectrum, both techniques show the same performance. Without the IQ mismatch, the windowing technique shows a better performance in the in-band region. However, the presence of IQ mismatch makes an image product at the same PSD level for both digital filter and windowing. Therefore, the advantage of using time windowing is not that significant.

Figure 5.15 illustrates the ACLR results for 1.4 MHz case. The results show the same trend as the results for 10 MHz channel bandwidth, but with a higher margin. For the larger RB size, the ACLR1 is 6 dB above the LTE ACLR1 requirement.
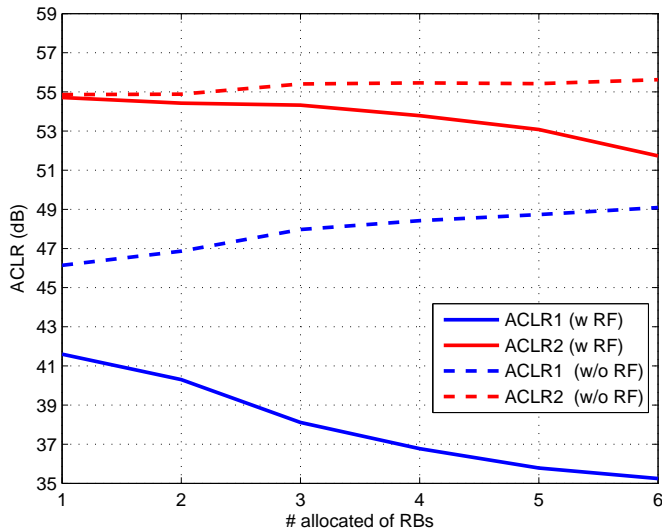
Figure 5.15: ACLR results of a transmitter (1.4 MHz) with and without imperfections.

5.7   Summary

Spectrum shaping techniques for LTE, impact of RF imperfections, and LTE RB size/placement issues have been discussed in this chapter. LTE has a stringent out-of-band requirements since the UE must be capable of controlling the spectrum emission for different bandwidth settings. On the other hand, the usage of spectrum shaping techniques must ensure sufficient margin to the spectrum emission mask, acceptable EVM level, minimize the cyclic prefix consumption, and lead to reasonable implementation complexity. The proposed spectrum shaping technique based on a 10th order Inverse Chebyshev filter is capable of controlling the spectral emission for various bandwidth settings, and provides good trade-off between spectrum emission control, capacity loss minimization, and implementation complexity.

Numerous RF imperfections have been considered in this study. A nonlinear amplifier creates spectral regrowth close to the assigned channel bandwidth, while gain and phase imbalances create unwanted image products. These RF imperfections can violate both the spectrum emission mask and ACLR requirements. Without the RF imperfections, a small RB size at the channel edge shows a potential problem to the adjacent channel. In the presence of the hard-

ware imperfections, the impact of large RB size is more severe than the small RB size. Large RB size shows to produce lower ACLR than the small RB size transmission.

Different RB size allocation makes the spectral regrowth affect both the out-of-band channel and the in-band channel. The impact on the in-band channel is the inter RB interference within the channel bandwidth. This topic is addressed in Chapter 7.

CHAPTER 6

Polar Transmitter for LTE Uplink

6.1 Introduction

In comparison with WCDMA, an LTE baseband signal has a high Peak-to Average Power Ratio (PAPR). If the RF transmitter architecture relies on a Cartesian type which typically use a class A or class AB power amplifier, this may result in a decrease of power amplifier efficiency. One of the solutions for a better efficiency is to choose a polar RF transmitter architecture for LTE uplink. A polar transmitter has been successfully implemented in existing wireless communication systems, such as GSM [65], EDGE [66], WCDMA [22], and WLAN system [39]. It can reach an efficiency up to 90% for a CDMA based system [67]. A high efficiency in the polar transmitter can be achieved by employing a switch mode class E power amplifier.

Beside the promising prospect of achieving high efficiency, the polar transmitter also suffers from numerous imperfections as described in Section 2.5. In this chapter the impact of polar transmitter imperfections on the beyond 3G system is investigated. For a case study, the LTE uplink system is considered. Beside a high PAPR, the main challenge is related to the wideband system in LTE. Similar to the previous study, the work is started and focused on the inband

performance. The aim of this work is to link the individual RF imperfection EVM characteristics to the link level performance, especially to obtain a clear insight into the sensitivity of each RF imperfection. The impact of timing delay alignment, power amplifier non-idealities, limited bandwidth on the envelope path are investigated. The PA non-idealities include the AM/AM distortion, AM/PM distortion, and signal leakage. The link level performance is evaluated for AWGN and frequency selective fading channels. Secondly, the work on LTE out-of-band performance is carried out. The polar transmitter imperfections are not just degrading the link level performance but also causing a spectral regrowth. Based on these two performance analyses, the most critical imperfections and performance aspects can be identified. Moreover, a polar transmitter can be a solution for the beyond 3G system RF front-end.

This chapter is organized as follows. Section 6.2 reviews the model of imperfections in a polar transmitter architecture for LTE uplink. Section 6.3 describes the class E PA non-idealities in a polar transmitter. In-band performance evaluation results of EVM and the impact on link level performance are discussed in Section 6.4. Section 6.5 provides the out-of-band performance results, and finally a summary is given in Section 6.6.

6.2   Modeling Assumptions

The LTE uplink transmitter with the polar transmitter imperfections model is shown in Figure 6.1. The detailed description of the SC-FDMA baseband signal generation and its performance evaluation has been described in chapter 3. The SC-FDMA signal generator output is up-sampled and filtered to further shift the image product as was done previously.

The considered polar transmitter architecture is an Envelope Elimination and Restoration (EER) type as described in Section 2.4. Prior to the RF part, the I & Q signals are converted to the envelope and phase paths in the baseband. This process is a non-linear process. The imperfections model in the EER polar transmitter consists of the timing delay between the envelope and phase paths, limited bandwidth in the envelope path, and the imperfections in the power amplifier as described in Section 2.5. These are the main polar transmitter imperfections.

The polar transmitter imperfections on LTE uplink performance are evaluated based on a link level simulation. The details on the link level processing can be found in Appendix A. The simulation is carried out in accordance with the LTE uplink main parameters given in Table 3.2. During the simulation the following

A(t)

LPF

A(t)+AM·A³(t)

e^{j(θ(t))}

Δt

PM

L

Imperfections Model of the Polar Transmitter.

SC-FDMA Signal Generator

x L

Digital Filter

x L

Digital Filter

Cartesian to Polar
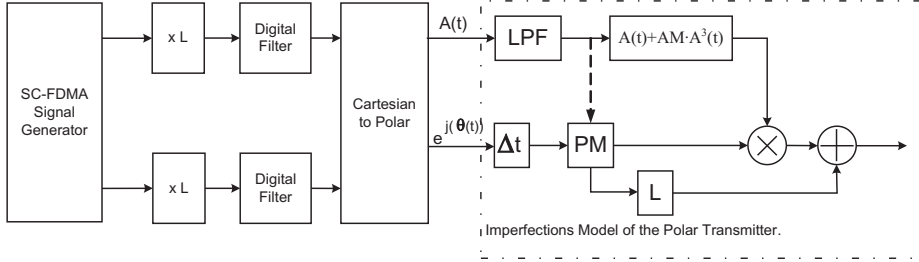
Figure 6.1: Polar transmitter imperfections model for LTE uplink.

assumptions has been used:

- Results are generated based on the baseband equivalent simulation model.

- The new frame structure as shown in Figure 3.2 is assumed in which the TTI duration is 1 ms.

- Both transmitter and receiver are perfectly synchronized in time and frequency.

- SISO antenna configuration.

- SC-FDMA transmission with 10 MHz bandwidth (50 RB).

- The maximum excess delay of the frequency selective fading channel is shorter than the cyclic prefix duration.

- The receiver performs ideal channel estimation.

- 14% pilot overhead is assumed in the spectral efficiency calculation.

- EVM measurement is performed at the receiver, and the methodology is as desribed in section 4.2.

- RF imperfections in the transmitter include the timing delay alignment, PA nonlinearities (AM/AM distortion, AM/PM distortion, and signal leakage), and limited bandwidth in the envelope path as described in Section 2.5.

- The bandwidth of the envelope signal is limited by a 4th order butterworth filter. The butterworth filter has a flat group delay and therefore the delay between envelope and phase path can easily be compensated. The 4th order butterworth filter is also commonly used for this purpose due to its practical aspects [22].
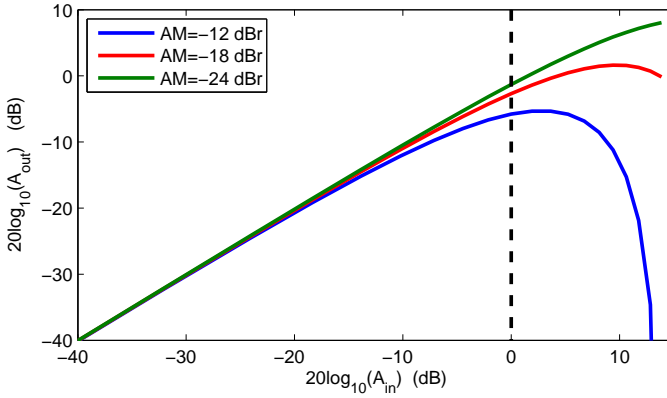
Figure 6.2: AM/AM impact on the output signal.

- Amplitude and phase distortions due to the filtering are compensated by the frequency domain equalizer at the receiver.

6.3 PA Non-idealities

A class E power amplifier is typically chosen for an EER polar transmitter. Each imperfection in a power amplifier distorts the transmit signal in a different way. The descriptions and assumptions of the PA non-idealities have been described in Section 2.5.

Figure 6.2 illustrates the impact of non-linearity on the envelope signal. The AM/AM conversion saturates the high envelope A_{in} signal. The average power level of A_{in} is assumed to be 0 dB. The AM/AM conversion with different parameters is represented in the AM factor as given in 2.23. Reducing the AM factor shifts the compression point towards the higher envelope level. Therefore, in a power amplifier which has a small AM factor, the impact of AM/AM conversion is minimized. Different from a class A/AB power amplifier, the AM/AM conversion in class E affects the drain voltage of the power amplifier. The drain voltage AM modulates the signal in a polar transmitter, and therefore the signal is a varying envelope signal.

The impact of AM/PM conversion and signal leakage are shown in Figure 6.3. AM/PM conversion shifts the output phase as a function of the drain voltage A_{in}. Several power amplifier settings with different AM/PM conversions are
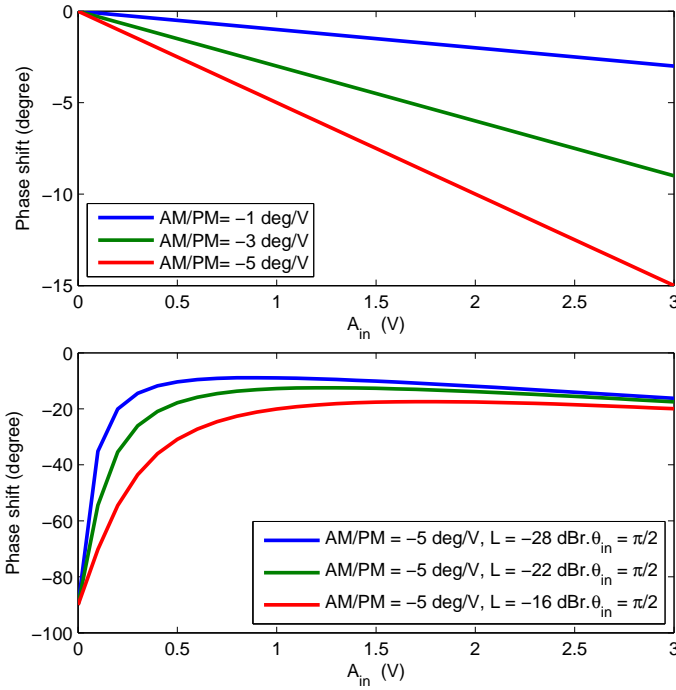
Figure 6.3: AM/PM & signal leakage impact on the output signal.

also illustrated. A power amplifier with high $|PM|$ factor has a large phase shift. The impact of both AM/PM and signal leakage can also be found. A signal leakage with initial phase shift of $\pi/2$ is assumed [20]. Hence, a low input signal provides a phase shift of $\pi/2$ corresponding to predominantly capacitive leakage through the power amplifier.

6.4 Inband Performance

The impact of the polar transmitter imperfections on the in-band channel is analyzed. In this work the analyses are based on the link level performance results on the EVM, spectral efficiency and SNR loss. The methodology is similar with the work in chapter 4.

Figure 6.4 shows the impact of timing delay imperfection on the maximum achievable spectral efficiency for different modulation and coding schemes (MCS)
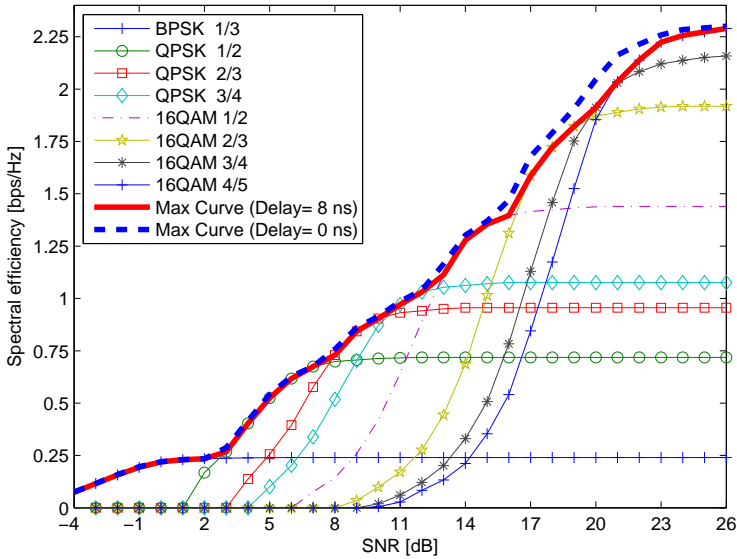
Figure 6.4: Maximum achievable spectral efficiency for various MCS.

in LTE uplink. It is observed that a timing delay of 8 ns does not affect the lower order MCS, however, it reduces the 16QAM performance. A performance loss of 1 dB is observable for 16QAM rate 4/5. In general the performance is mostly impacted for the higher order MCS, hence the analysis for the remaining works is focused on 16QAM.

The individual EVM simulation results in LTE uplink 16QAM for the different transmitter imperfections are shown in Figure 6.5. Each x-axis represents the imperfection parameters introduced in Section 2.5: the time delay (ns), AM factor (dBr), PM factor (degree/V), and leakage factor (dBr), respectively. The EVM is measured at the receiver symbol detection input as described in Section 4.2 and analyzed in an EVM range up to 20%. An EVM of 8% is generated by a timing delay of 8 ns, AM/PM slope of -4 degree/V, signal leakage of 20 dB below the average input signal, and AM/AM factor of 14 dB below the average input signal, respectively. In practice, each imperfection contributes to a small EVM since all of these are finally combined. Knowing the relation between the imperfection and the EVM, the corresponding link level performance loss can be further investigated.

The non-linear process in the Cartesian to polar conversion results in an increase of the envelope path bandwidth. In practice, the envelope path bandwidth is limited and controlled by an analog filter. The filter is inserted before feeding
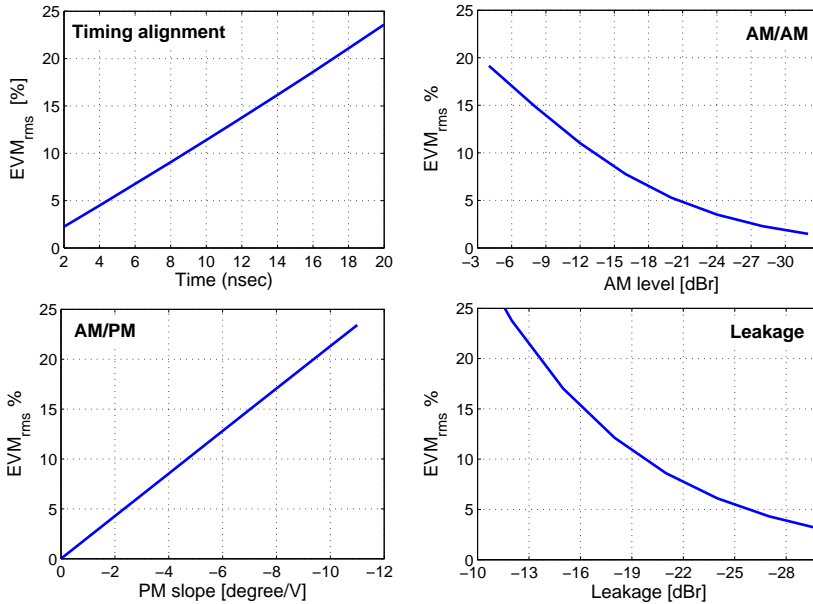
Figure 6.5: EVM results for various polar transmitter imperfections.

the signal to the class E power amplifier. However, inserting a filter also causes additional timing delay in the envelope path. The additional timing delay has to be compensated by introducing a similar timing delay in the envelope path.

Figure 6.6 illustrates the impact of limited bandwidth in the envelope path. The filter bandwidth is defined as the envelope bandwidth factor multiplied by the 3dB bandwidth of the transmitted signal. For 10 MHz channel bandwidth, the 3dB bandwidth is 9 MHz. The timing alignment issues have been compensated so that the error generated is purely as a result of the bandwidth limitation. With a bandwidth factor of 2, the EVM is around 6%. Further increase of the filter bandwidth reduces the EVM down to 2%. To maintain a low EVM, an envelope bandwidth factor of at least 3 times is required.

Figure 6.7 shows the spectral efficiency degradation for 16QAM rate 3/4 in consequence of the signal leakage. The purpose is to observe the impact of the imperfection on the spectral efficiency. The signal leakage imperfection level is defined by its EVM value. Considering the acceptable target spectral efficiency loss due to the imperfections is 10%, the corresponding SNR loss for each EVM level can be identified. For the low EVM region ($< 8\%$), the SNR loss is less than 0.4 dB. The SNR loss significantly increases at the high EVM region. For
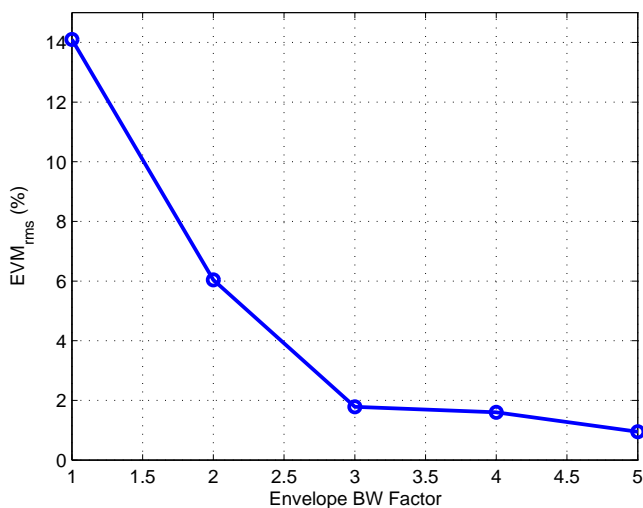
Figure 6.6: EVM results for limited bandwidth.

an EVM of 16%, the SNR loss is around 1.6 dB. In this analyzes, 16QAM rate 3/4 is assumed as the highest order modulation and coding scheme and therefore very sensitive to the imperfections. For the subsequent work, 16QAM rate 3/4 is assumed.

The results in Figure 6.8 illustrate the link level performance by means of equivalent SNR degradation of 16QAM rate 3/4 as a result of the RF imperfections in an AWGN channel. The SNR loss is plotted versus EVM level. Hence, the relation of performance sensitivity on different imperfections can be obtained. Within the low EVM region ($< 8\%$), all the imperfections have the same SNR loss of less than 0.5 dB. The results are on top of each other, and therefore the EVM is a good direct measure to estimate the link level performance loss within this range. At high EVM levels, the SNR loss for each imperfection starts to deviate. Timing delay alignment is more dominant in the SNR loss in comparison to the others. The AM/PM distortion and signal leakage show the same impact on performance, and the lowest impact is the AM/AM distortion.

Figure 6.9 further shows the relation between the EVM and equivalent SNR loss in the multipath fading channel for 16QAM rate 3/4. A typical Urban 6 paths channel model is assumed. The results follow the trend in the AWGN channel with an increase in the SNR loss range to 4 dB. For the EVM values less than 7% - 9%, the SNR loss is maintained below 0.5 dB. The results on the polar transmitter are in agreement with the previous results on the Cartesian
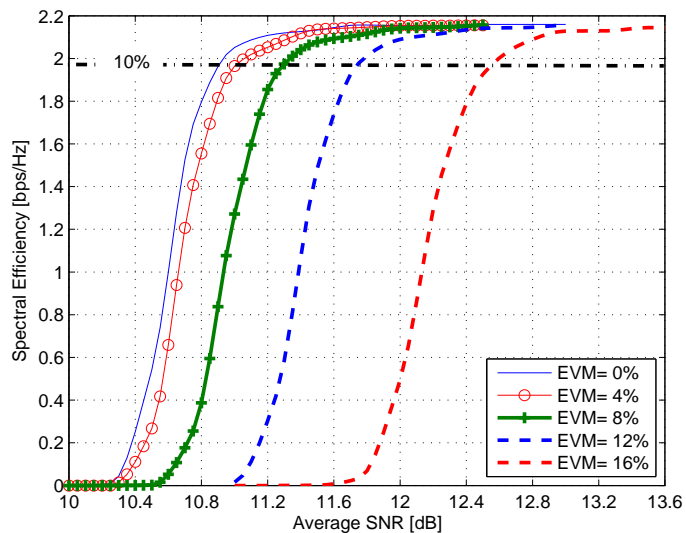
Figure 6.7: Spectral efficiency degradation for 16QAM rate 3/4 due to the signal leakage.
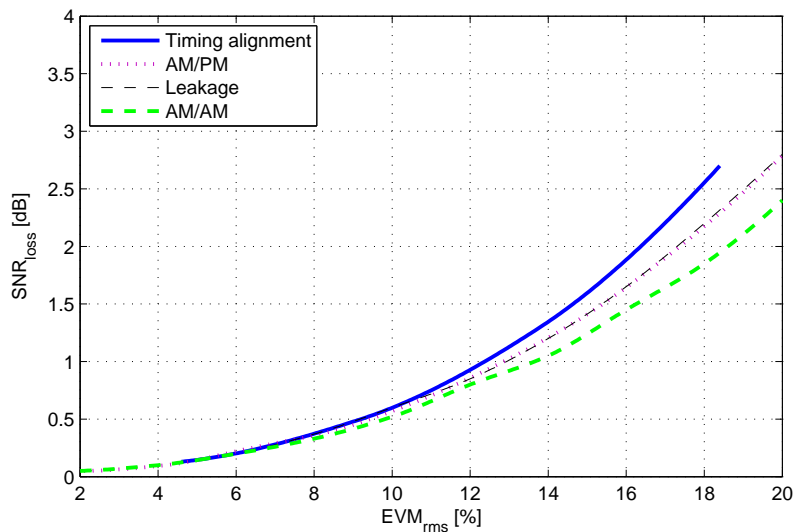
Figure 6.8: SNR loss for 16QAM rate 3/4 in AWGN channel.
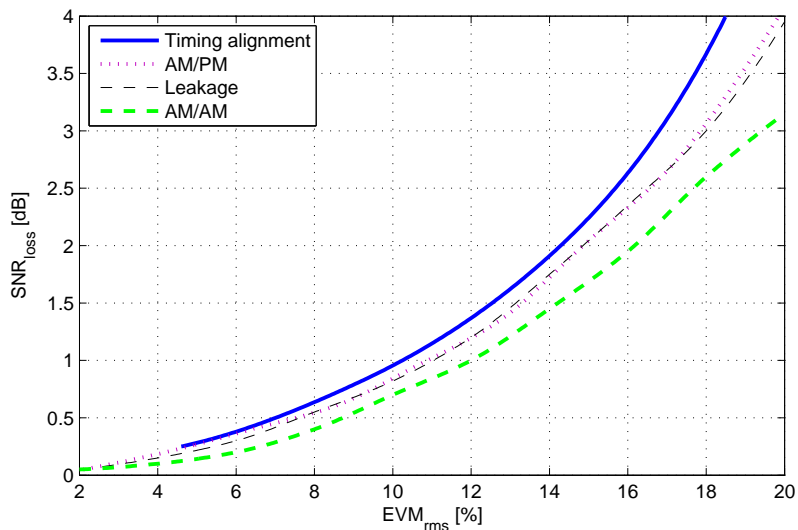
Figure 6.9: SNR loss for 16QAM rate 3/4 in TU06 channel.

transmitter in Chapter 4. For 16QAM rate 3/4, an EVM of 8% corresponds to an SNR loss of 0.5 dB. One should note that these results are MCS dependent, as a higher MCS is more sensitive to the EVM.

6.5   Out-of-band Performance

In order to obtain a complete analysis, the impact on the out-of-band spectrum is also studied. The work methodology is similar to the work on the Cartesian transmitter in Chapter 5. The transmitter structure is shown in Figure 6.1. Before the signal is converted to the polar coordinate system, the signal is oversampled by a raised cosine FIR filter to further shift the image. Afterwards, a spectrum shaping filter is applied to shape the transmit signal. The shaping filter is an IIR inverse Chebyshev filter as described in Section 5.3.

Figure 6.10 illustrates the impact of timing delay alignment on SC-FDMA spectrum emission. Timing delay alignment is the most common problem in a polar transmitter. The channel bandwidth is 10 MHz, and the modulation scheme is 16QAM. The shaped transmit signal provides a good suppression in the transition band and an excellent margin towards the spectrum emission mask requirement. A timing delay of 4 ns is required in order to meet the spectrum
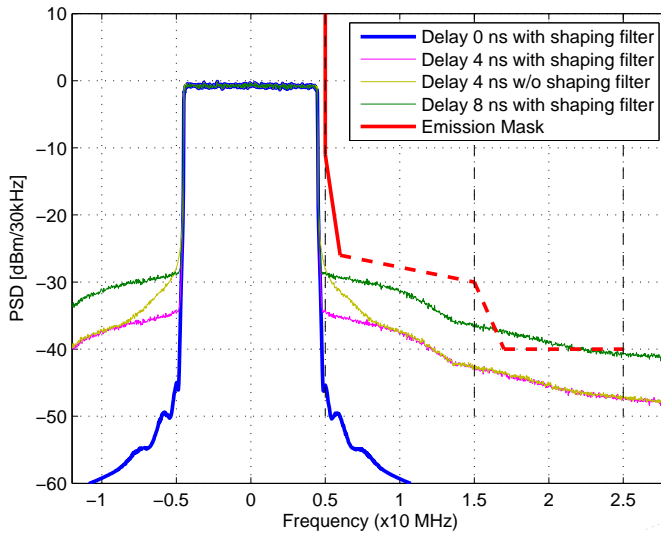
Figure 6.10: Impact of timing delay alignment on SC-FDMA spectrum emission (Channel bandwidth 10 MHz).

emission mask.

Figure 6.11 shows the ACLR results on the impact of timing delay alignment. A timing delay of 8 ns is shown to fail to meet the ACLR1 and ACLR2 requirements. A sufficient margin is shown for the timing delay of 4 ns.

The impact of limited bandwidth in the envelope path in the SC-FDMA transmission is shown in Figure 6.12. It is shown that limiting the bandwidth results in an increase of the noise level in the out-of-band spectrum. A bandwidth of at least 3 times the 3 dB transmission bandwidth is required in order to fulfil the spectrum emission mask requirement.

Fig. 6.13 illustrates the ACLR results on the impact of limited bandwidth in the envelope path. The limited bandwidth results in ACLR1 and ACLR2 at almost the same level, especially at the bandwidth factor of 4. Considering the required ACLR2 is 43 dB, the bandwidth factor of 3 results in marginally below the requirement at 42.6 dB. Therefore, the bandwidth of 3-4 times is suggested in order to obtain a good result with a realistic bandwidth limitation.

Figure 6.14 is plotted with the main purpose to compare the sensitivity of the transmit signal on different imperfections. It is assumed that each imperfection
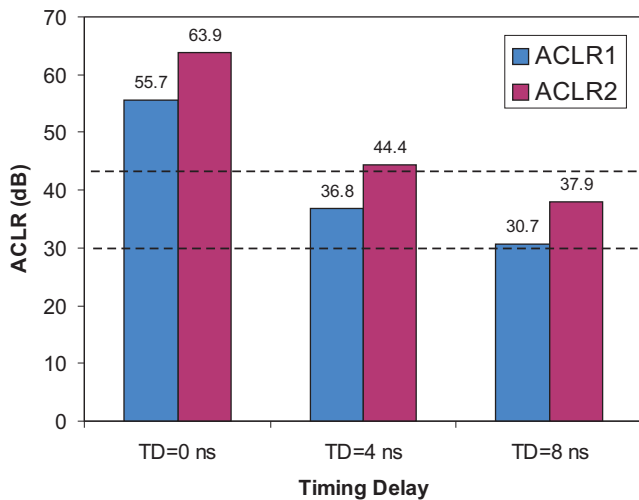
Figure 6.11: ACLR results for SC-FDMA with imperfect timing delay alignment.
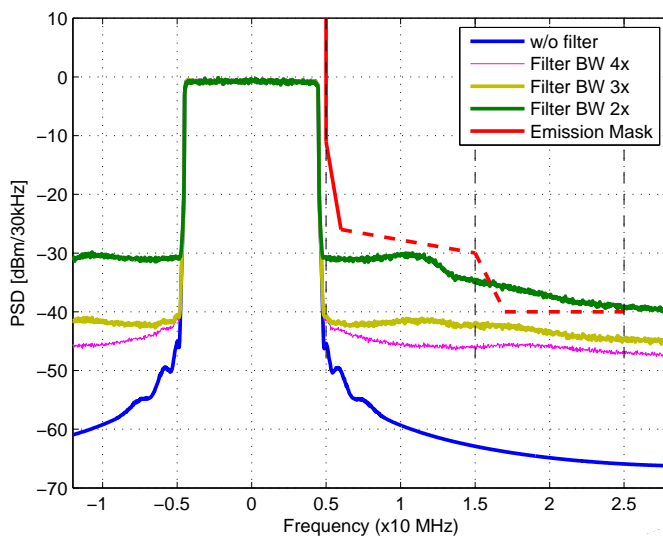
Figure 6.12: Impact of limited bandwidth in the envelope path.
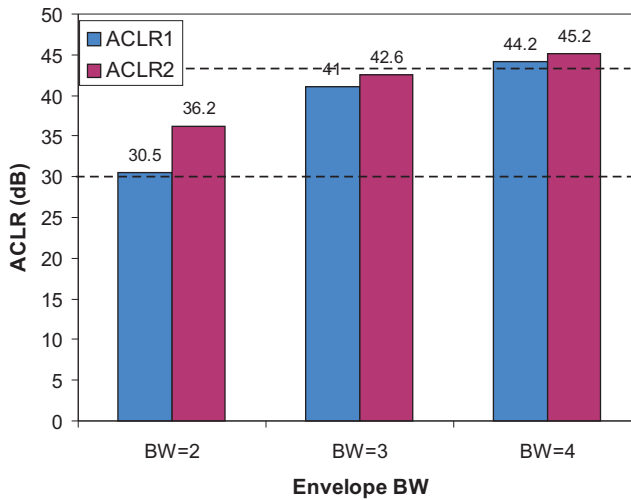
Figure 6.13: ACLR results on the limited bandwidth in the envelope path.

generates an EVM of 4%. Timing delay alignment, limited bandwidth of the envelope signal, and AM/AM conversion are the most severe imperfections. The limited bandwidth is mainly limited by the ACLR2 requirement. AM/AM conversion has a great impact on the ACLR1 result. In practice, timing delay alignment is still the most problematic imperfection because it has to maintain the delay alignment below 4 ns. Moreover, the ACLR requirement for timing delay is more stringent than the EVM requirement.
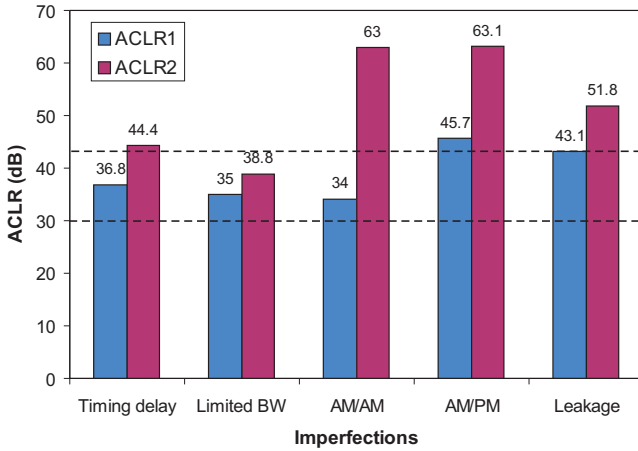
Figure 6.14: ACLR for different imperfections at EVM=4%.

6.6 Summary

The polar transmitter has a promising prospect of achieving high efficiency power amplifier. It has been successfully implemented in existing wireless communication systems. Beside the advantages, the polar transmitter also suffers from numerous imperfections.

In this work the impact of polar transmitter imperfections on LTE uplink performance is investigated. The performance of both in-band and out-of-band are studied. The considered imperfections are the timing delay alignment and non-ideal power amplifier, and limited bandwidth in the envelope path. The EVM is a good direct measure to estimate the link level performance loss for various imperfections in the practical EVM range (EVM < 8%). For 16QAM rate 3/4, an SNR loss of approximately 0.5 dB can be estimated from an EVM value of 8%. The final EVM requirement for the transmitter in LTE will be chosen as a compromise between UE complexity and system performance. The results show that the polar transmitter in the LTE uplink is very sensitive to the timing alignment between the envelope and phase paths, especially for higher order modulation and coding scheme.

Timing delay alignment, and limited bandwidth in the envelope path are the problematic imperfections. In practice, the timing delay alignment is the most difficult one because it has to control the delay alignment at below 4 ns. The other imperfections are relatively easier to control. In most cases the out-of-

band requirement are the main limiting factor.

CHAPTER 7

Inband Inter-User Interference Analysis

7.1 Introduction

UTRA Long Term Evolution has the flexibility to use existing UTRA bands
and new frequency bands [8]. The system supports scalable system bandwidth.
On top of that, the user equipment (UE) data transmission is multiplexed in
frequency domain, and it has a flexibility to transmit on 1 resource block up to
100 RB depending on the resource allocation from the base station. LTE uplink
with SC-FDMA access scheme offers flexibility for the user to be scheduled in
both frequency and time domain to exploit the radio channel variations [8].

The UE shaping filter controls the transmitted out-of-band spectrum and should
comply with the 3GPP standard [68],[69]. Hence, the transmitted signal does
not interfere with the adjacent channel. However, the in-band signal leakage for
small RB size transmission remains uncontrolled as discussed in Chapter 5. In
the ideal condition the SC-FDMA transmission maintains the user orthogonality.
However, the presence of hardware imperfections in the RF transceiver, such as
frequency offset and phase noise, destroys the subcarrier orthogonality [70], and
the UE signal leakage start to interfere with other UEs. In practice, the received
signals from different UEs experience various frequency offset/phase noise and

lead to the inter-user interference. The power spectral density of the received signals from different UEs may also vary. The different PSD level can be due to the used modulation and coding rate format, power control inaccuracy, other cell interference levels, etc [71]. The frequency offset/phase noise and signal leakage from the adjacent UEs with higher PSD can lead to a significant interference level and degrade the system performance.

The concept of in-band interference in LTE is first introduced in [72]. In a multi-user environment, the signal leakage and transmitter imperfections from the other user can additionally degrade the performance. Ref. [73] shows that the in-band unwanted emissions potentially interfere with the other resource block.

In this work the impact of the frequency offset/phase noise and different PSD of two interferers on the link level performance of a victim UE for different resource block allocation is presented. The initial performance evaluation is carried out based on the error vector magnitude (EVM) measurement. Then, the link level performance in AWGN and Typical Urban channels are performed using the approach described in [74]. The objective of the work is to relate the SNR degradation of a victim UE as the function of its resource block allocation in various interferer conditions (frequency offset, phase noise and PSD offset).

The chapter is organized as follows. The multi-user modeling scenario is given in Section 7.2. The interference source is described in Section 7.3. Simulation assumptions in the inter user interference study are discussed in Section 7.3. Finally, the impact of PSD offset and frequency offset are given in Section 7.5. The impact of PSD offset and phase noise is given in Section 7.6. The proposed solution to deal with inter-user interference is given in Section 7.7. Finally, a summary is given in Section 7.8.

7.2 Description of Multi-user Modeling

The system model of multiple simultaneous UEs transmit to the base-station is illustrated in Figure 7.1. Three active UEs occupy the whole available resouce block allocation. The two UEs are the interferer UEs, and one UE acts as the victim UE. The victim UE is allocated in between the interferer UE resource block allocation. This configuration will give the worst case scenario for the interference level to the victim UE.

The performance analysis is based on the performance measurement of the victim UE. The victim UE has an ideal transmission without any RF imperfections.
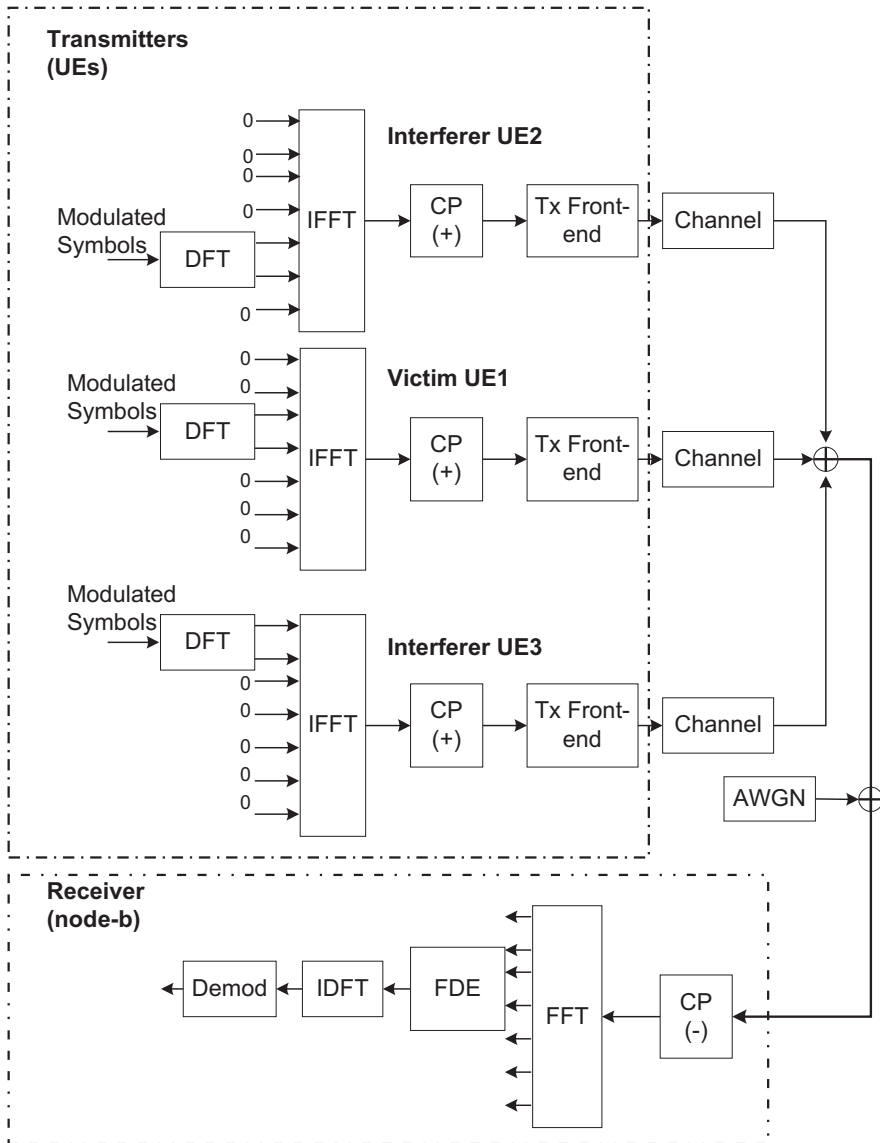
Figure 7.1: System model of the multi-user environment (3 UEs) in LTE uplink.

The transmit signal from the interferer UEs creates interference to the victim UEs. This scenario isolates the performance degradation which is caused only by the interference from other users. Only the victim UE signal is processed at the receiver, and from this the link level performance, i.e. EVM, BLER, spectral efficiency, can be evaluated. The EVM is the difference between the ideal waveform and the measured waveform for the allocated RBs and measured at the receiver symbol detection input as described in Section 4.2.

It has been concluded within 3GPP that the power control is an open-loop power control [75]. In an open-loop power control, a UE adjusts its transmit power according to the downlink pathloss calculated in the UE using the received downlink power level information. In practice, the power control is not perfect due to the power control measurement error. These conditions lead to the situation where the average received signal from different UEs has a different averaged PSD. Besides, LTE supports various modulation and coding scheme (MCS) [8]. Depending on the SNR level at the receiver, the UE with better SNR uses high-order MCS and vice-versa.

The average PSD of the simultaneously received signals from the 3 UEs is illustrated in Figure 7.2. Since the UE can transmit at different resource block size, the receiver does not just measure the power level, but also the averaged PSD [75]. Fig. 7.2 also illustrates a different resource block size among the UEs. The interferer UE has a frequency offset, f_{off}, and the average PSD is higher than the victim UE. The average PSD difference between interferer UEs and victim UE is denoted as PSD offset, P_{off}.

In ideal conditions the UE signal leakage to the adjacent resource block is the SINC responses, and the subcarrier orthogonality can still be preserved. Therefore it is not sufficient to analyze the impact of the signal leakage only from the power spectral density, which is typically obtained from a spectrum analyzer. The analysis should be based on the demodulated signal of the subcarriers within victim resource block. However, the power spectral density analysis can still be used to analyze the impact to the out-of-band spectrum or the adjacent channel [76].

7.3 Interference Sources

RF imperfections in the UE interferer can create interference to the victim UE. Frequency offset and phase noise can destroy the subcarriers orthogonality in the SC-FDMA system. Therefore, it is expected that the impact of the frequency offset and phase noise has greater impact in terms of interference on the victim
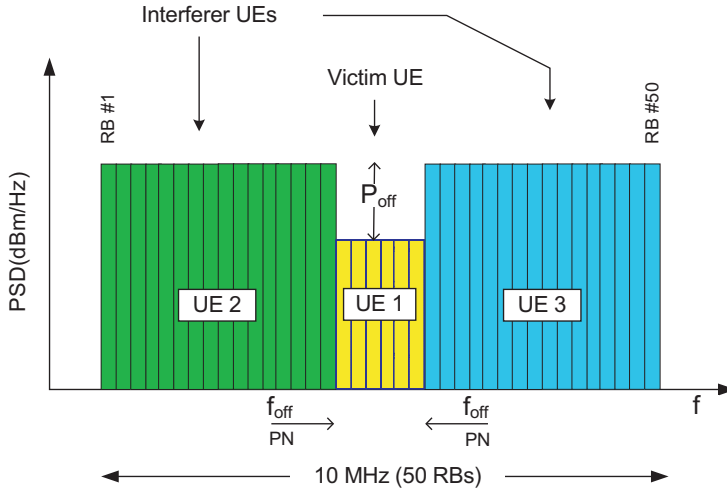
Figure 7.2: Received Power Spectral Density (PSD) of 3 UEs at the base-station.

UE, compared to the other imperfections. Beside the frequency offset and phase noise, the spectral regrowth generated by the nonlinear amplifier of the interferer UEs can also interfere to the victim UE. In this work, the impact of frequency offset and phase noise on the interferer UEs are studied.

The phase noise increases the signal leakage of the UE interferer transmit signal. This effect can destroy the orthogonality of the victim UE subcarriers, especially the subcarriers which are close to the interferer UE. A common frequency offset at the receiver can be corrected by a frequency offset compensation at the receiver. However, a specific frequency offset at the transmitter has already created interference with the other users and it should be kept at a minimum. The 3GPP release 7 specifies which the transmitter frequency accuracy should be less than 0.01 ppm, corresponds to 200 Hz of frequency offset [68]. Moreover, each UE has different mobility and results in different Doppler frequency shift. These factors lead to the situation where the received signal from different UEs has various and unequal frequency offsets.

The interferer UEs signal affected by the frequency offset and phase noise can be expressed in the following equation:

$$y(t)_{UE_n} = x(t) \cdot e^{j(2\pi f_{off} t + \phi(t))} \tag{7.1}$$

where f_{off} represents the frequency offset, and $\phi(t)$ is the phase noise.

7.4 Modeling Assumptions

A multi-user link level simulation is carried out to investigate the in-band interference. The simulation is carried out in accordance with the LTE uplink main parameters given in Table 7.2. The details on the link level processing can be found in Appendix A. The system bandwidth of 10 MHz corresponding to 50 RBs, is considered and shared among the UEs. In case the victim UE has a small RBs allocation, the remaining RBs are shared among the interferer UEs. During the simulation the following assumptions are considered:

- The victim UE transmitter is perfectly synchronized with receiver in time and frequency.

- The interferer UEs have the same PSD level.

- The interferer UEs have the same absolute frequency offset and phase noise level.

- The maximum excess delay of the frequency selective fading channel is shorter than the cyclic prefix duration.

- One sub-frame/TTI consists of 12 Long Blocks (LBs) for data and 2 LBs for reference signals (14% overhead).

The frequency offset is assumed in the worst condition between 200 Hz - 800 Hz. The frequency offset can be generated as the frequency error in the transmitter and the doppler frequency due to the fast moving UE. For simplicity in this work, these frequency offset sources are analyzed as a single frequency offset, F_{off}, generated at the interferer UE transmitter.

The phase noise follows the model described in Section 2.3. Several phase noise powers are considered based on the SSB phase noise power at 1 MHz frequency offset from the carrier. These phase noise powers can be related to the phase noise bandwidth using (2.13). The phase noise characteristics for this simulation are summarized in Table 7.1. The phase noise type A is to represent the local oscillator which is typically used in the existing GSM/WCDMA system. It may be useful to characterize the quality of an oscillator by the relation between its phase noise bandwidth and the subcarrier spacing of the LTE signal (Δf_{sc}):

$$\rho_{PN} = \frac{\Delta f_{3dB}}{\Delta f_{sc}} \tag{7.2}$$

Table 7.1: Phase Noise Characteristics.

Phase Noise (PN) Type	Bandwidth Δf_{3dB}	SSB Power at 1 MHz offset	Ratio ρ_{PN}
PN A (Good)	2 Hz	-125 dBc/Hz	0.013%
PN B (Medium)	25 Hz	-114 dBc/Hz	0.17%
PN C (Low-end)	103 Hz	-108 dBc/Hz	0.68%

Table 7.2: Multi-user link level simulation parameters.

Parameter	Value
Carrier Frequency	2 GHz
Transmission BW	10 MHz
Subframe duration	1 ms
Subcarrier spacing	15 kHz
SC-FDM symbols/TTI	14 LBs
CP duration	4.1 μs
FFT size/Useful subcarriers	1024/600
MCS settings	QPSK 3/4, 16QAM 3/4
Channel code	3GPP Rel. 6 compliant Turbo Code with basic rate 1/3
Rate Matching, Interleaver	3GPP Rel. 6 compliant
Channel Estimation	Ideal
Antenna schemes	SISO
Channel model	AWGN, Typical Urban 20 paths [5]
Speed	3 kmph
HARQ	No
RF Imperfections	Frequency offset, Phase noise
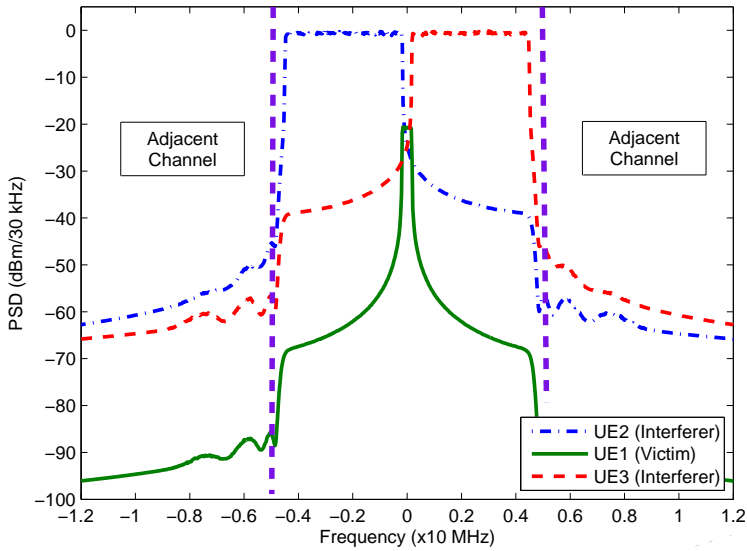
Figure 7.3: Received PSD of each UE in 10 MHz system bandwidth.

Fig.7.3 shows the power spectral density (PSD) of the received signals at the base-station. The two interferer UEs have PSD offset of 20 dB higher than the victim UE, and each of them has 24 resource blocks (RBs). The victim UE has 2 RBs allocated in-between interfering UE RBs allocations. It is shown that the signal leakage from the interferers UE is just slightly below the PSD level of the victim UE. In ideal conditions, the SC-FDMA can still maintain the orthogonality. Thus, the different PSD level and the high signal leakage does not affect the victim UE link performance. In the presence of frequency offset at the interferer UEs, the performance of the victim UE can be degraded. Fig.7.3 also shows that the signal leakage in the out-of-band spectrum is suppressed by the digital shaping filter.

7.5   Impact of Frequency Offset and PSD offset

The EVM simulation results for 16QAM and different RBs size are presented in Figure 7.4. It shows the impact of the frequency offset, and the joint impact of PSD offset and frequency offset. The EVM results are shown because the EVM results can be used to estimate the SNR degradation for a specific BLER target as suggested in Chapter 4. The results show that in case all the UEs have
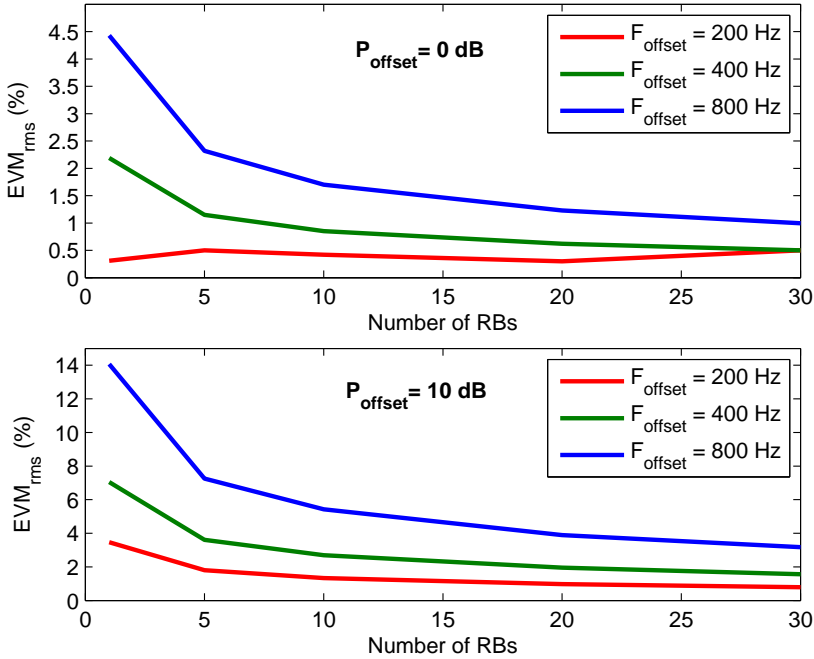
Figure 7.4: EVM results at different PSD level and frequency offset for different RB size.

the same PSD level ($P_{off} = 0$), the EVM level is very low. For the frequency offset of 800 Hz and victim UE with 1 RB, the EVM level is only 4.5%. The EVM becomes higher when the PSD offset of the UE interferer is increased. This result is expected because increasing the PSD offset will increase the non-orthogonal signal leakage power level which falls in the allocated frequency of the victim UE. The results also show that the smaller RB size obtains higher EVM than the larger RB size.

Figure 7.5 shows the BLER results for a transmission of 5 RBs in an AWGN channel. It is observed that the frequency offset in combination with the PSD offset leads to the performance degradation. Considering the target BLER is 10%, the SNR loss for the interferer UEs with a frequency offset of 200 Hz and PSD offset of 10 dB is very small, less than 0.1 dB. Increasing the PSD offset by another 10 dB results in an SNR loss of 0.3 dB.

In Figure 7.6, the degradation of the link level performance by means of equivalent SNR degradation at 10% BLER for QPSK rate 3/4 and 16QAM rate 3/4
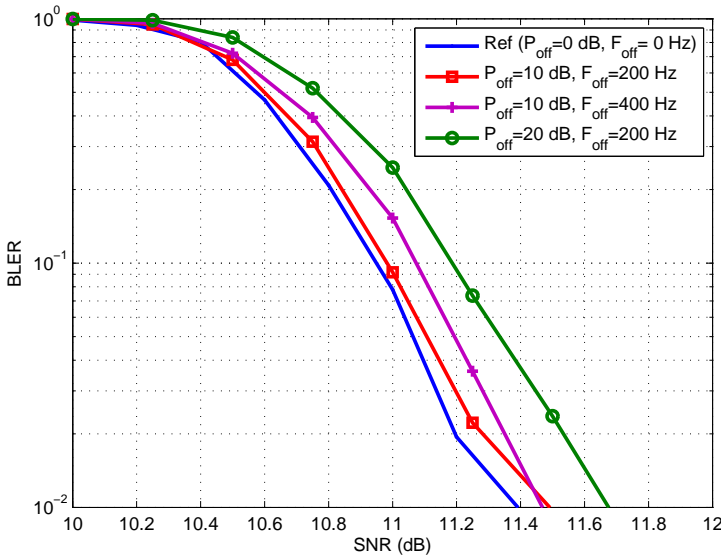
Figure 7.5: BLER results for 5 RBs transmission (Victim UE) in AWGN channel.

due to the frequency offset and power spectral density offset versus RB size in an AWGN channel is presented. The results for various PSD offset and frequency offset at the interferer UEs are also presented. Increasing the RB size of the victim UE reduces the SNR loss. This result is logical because the interferer is mainly affecting the resource block at the edge. Averaging across the available large resource block size minimizes the SNR loss.

To investigate the sensitivity of the modulation scheme, compare the results of $P_{off} = 20dB, F_{off} = 200Hz$ for both QPSK and 16QAM. 16QAM is more sensitive to the interference, as higher order modulation scheme is more sensitive than the lower order ones. For both QPSK and 16QAM, the SNR loss can be kept small for RB size more than 5 RBs. Considering $P_{off} = 30dB, F_{off} = 200Hz$ as the extreme condition, the smallest RB size allocation (less than 5 RBs) incurs an unacceptable SNR loss of more than 1 dB.

Figure 7.7 shows the relation between RB size of the victim UE and SNR degradation in Typical Urban channel which represents a realistic channel model. Also in this case results are given for both QPSK rate 3/4 and 16QAM rate 3/4. It is observed that the small RB allocation (less than 5 RBs) can experience high SNR loss. Beside the PSD offset, the fast fluctuation of the received power due to the frequency selective fading makes the SNR loss in typical urban channel
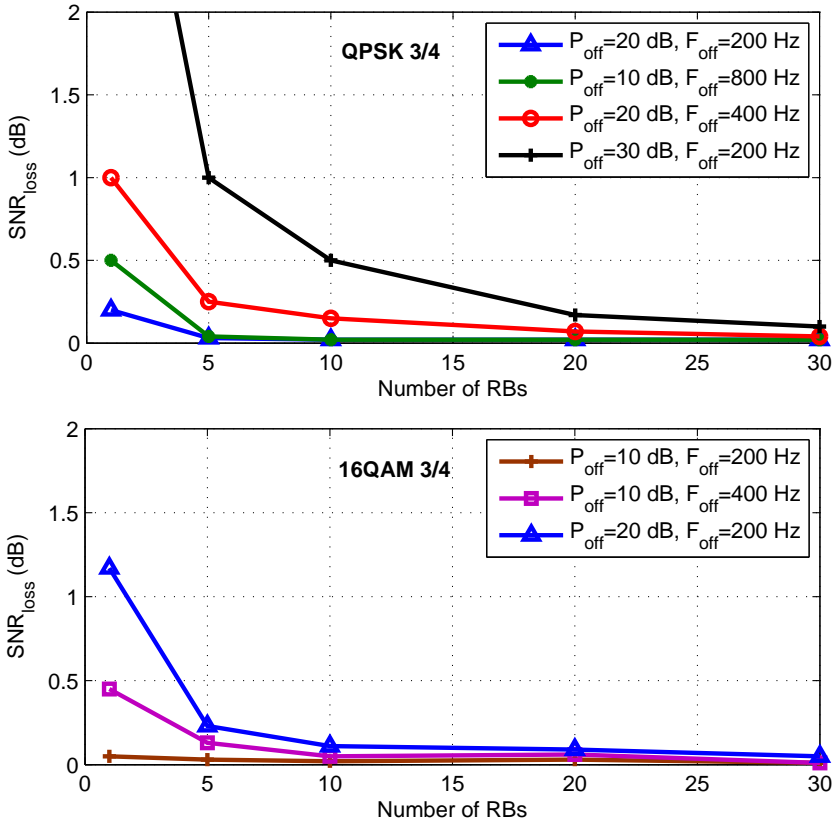
Figure 7.6: Frequency offset and PSD effects (SNR_{loss})to the in-band interference in AWGN channel for different RB size

worse than the SNR loss in AWGN channel.
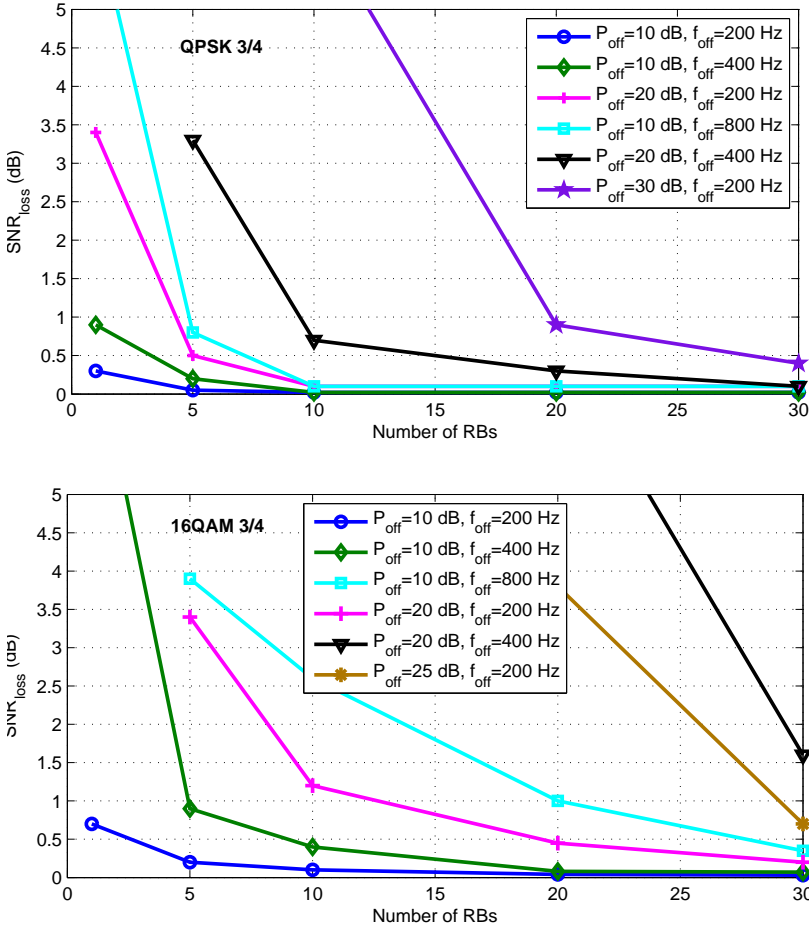
Figure 7.7: Frequency offset and PSD offset effects (SNR_{loss}) in the in-band interference in Typical Urban channel for different RB size.

Figure 7.7 also shows that for 16QAM rate 3/4 in the condition that the frequency offset is maintained below 200 Hz and the PSD offset level below 10 dB, the SNR degradation is rather small, less than 1 dB. QPSK rate 3/4 is shown to be more robust than 16QAM rate 3/4. This can be achieved by proper frequency synchronization design and resource allocation mechanism. It is expected that the PSD offset higher than 20 dB rarely occurs. In extreme condition, whereas the $P_{off} = 25 - 30 dB, F_{off} = 200 Hz$, the system is only working well (SNR

loss less than 1 dB) when a larger RB size is used by the victim UE (RB size= 30).

7.6 Impact of Phase Noise and PSD Offset

Figure 7.8 shows the impact of phase noise on the inband interference for different RB size. The results are for AWGN channel scenario so that the source of the performance degradation can be narrowed down to the AWGN noise and the interference from neighboring users. A good (PN-A) and a medium (PN-B) quality local oscillator are assumed. In most cases, the SNR loss can be kept very low for both QPSK rate 3/4 and 16QAM rate 3/4, except for a very small RB size and at the extreme condition ($P_{off} = 30dB$).

To show the results in a realistic channel, the SNR loss versus the RB size is plotted and shown in Figure 7.9. The results presented are for various PSD offsets and phase noise types. In general, the results follow the trend in the AWGN channel results. The results in a typical urban channel have a large scale of SNR loss. In most of the cases, the SNR loss can be maintained low for both QPSK rate 3/4 and 16QAM rate 3/4, especially for a large RB size (RB size $\geq$ 5). In extreme conditions in which the ($P_{off} = 30dB$, PN type A), the system can still work well for QPSK with RB size $\geq$ 5 and for 16QAM rate 3/4 is only for RB size $\geq$ 30.
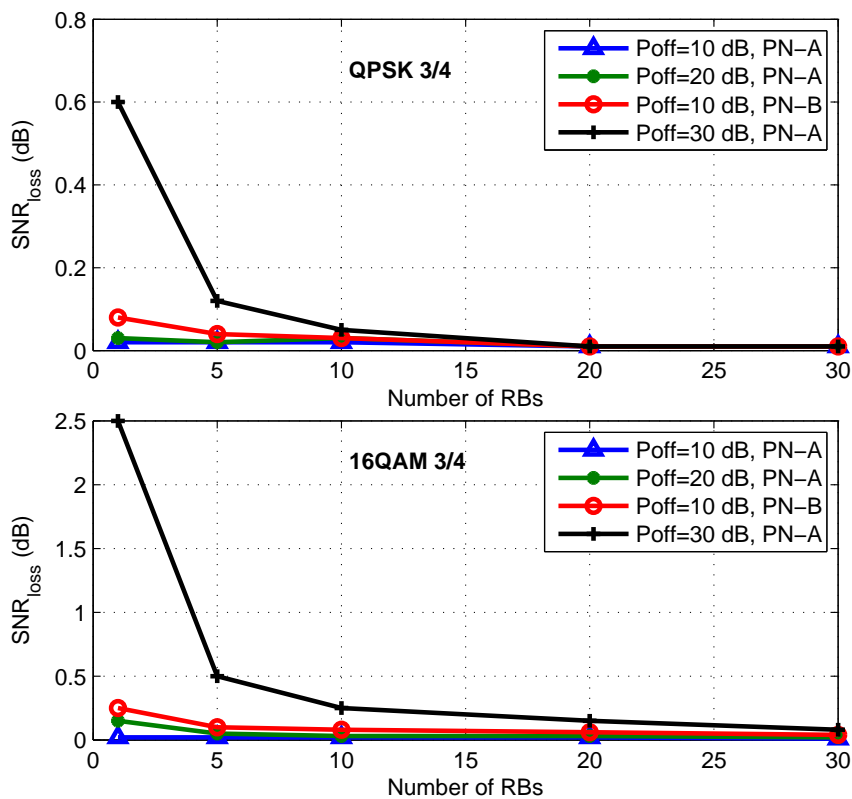
Figure 7.8: Phase noise effect (SNR_{loss}) in the in-band interference in AWGN channel for different RB size
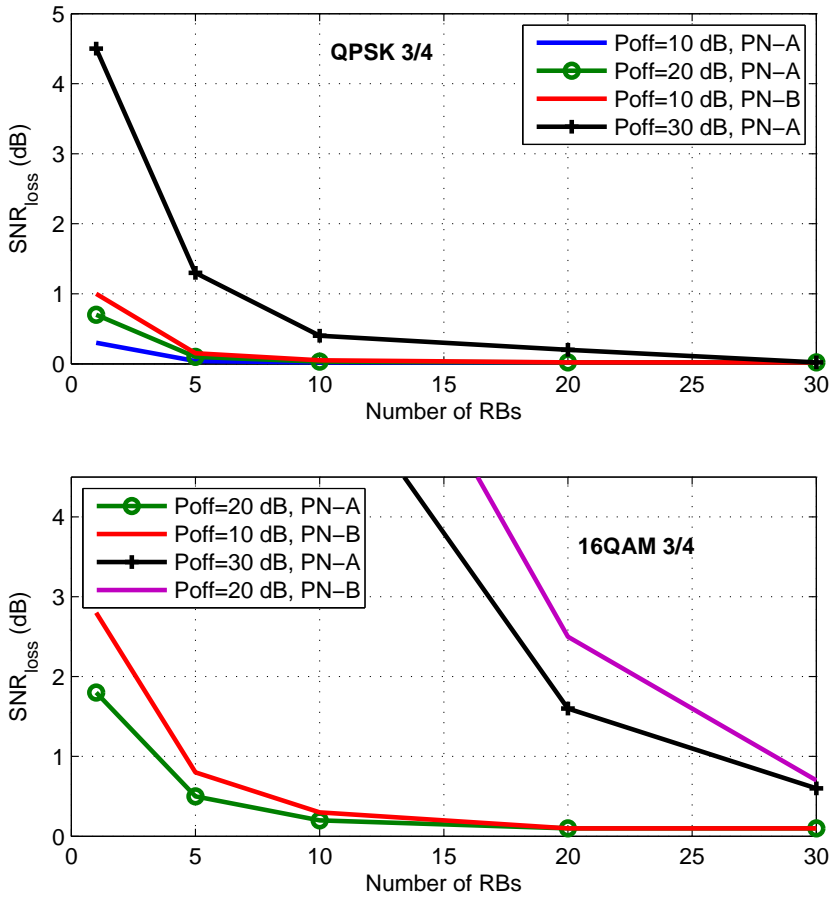
Figure 7.9: Phase noise effect (SNR_{loss}) in the in-band interference in Typical Urban channel for different RB size
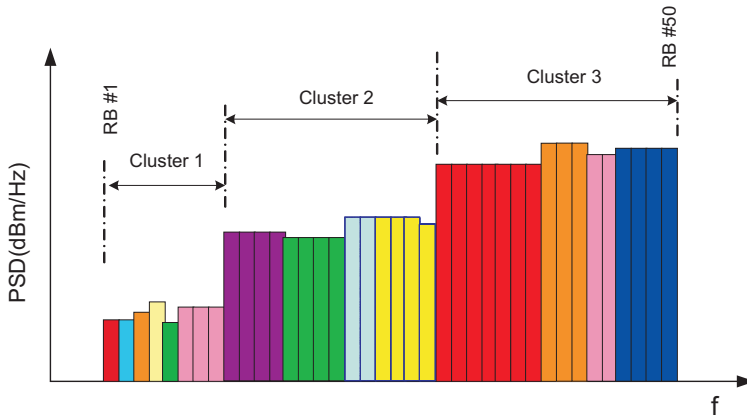
Figure 7.10: UE frequency domain scheduling solution to avoid large PSD offset

7.7   Proposed Solution

From the above analysis, the system can work well if the RF imperfections, such as the frequency offset and phase noise, can be kept low. For instance, the frequency offset below 200 Hz and a good quality local oscillator (phase noise type-A). In most cases those imperfections can be controlled by the selection of good components for the transmitter. The only remaining factor is to control the PSD offset, especially to avoid the victim UEs between the interferer UEs at larger RB size. A solution to avoid this scenario is to schedule the users in the frequency domain based on the PSD level as shown in Fig.7.10. The users are clustered based on the measured PSD at the receiver. The users with the highest PSD are allocated in a cluster and separated away from the users with the lowest PSD. Therefore, a significant PSD offset between adjacent users can be avoided. However, it will cost on the degree of freedom of the users scheduling in frequency domain.

7.8   Summary

The impact of in-band interference on the uplink multiple access of beyond 3G system has been investigated. The LTE system parameters are considered as the case study. In-band and out-of-band interference arise as a result of transmitter imperfections. Out-of-band, or adjacent channel, interference can be controlled by a spectral shaping filter. However, the shaping filter is unable to control the

leakage within the system bandwidth, and the resulting leakage can interfere with other users' transmission in the uplink multiple access. The interference from the other users is mainly due to the frequency offset and phase noise at the transmitter and potential differences in power spectral density of the received signals from multiple UEs. The effect of RF imperfections and different PSD level from the UE interferers to a victim UE are investigated.

The impact on different UE resource block size allocation is also investigated. The situation is emphasized when the resource block allocation, and hence the bandwidth of the transmitted signal, is small, and when the interfering signal is received at higher power spectral density (PSD). Results obtained from an LTE uplink link level simulation show a significant SNR degradation for the victim UE with smaller resource block allocation, especially in realistic propagation channels. Considering that the frequency offset can be maintained below 200 Hz and the PSD offset below 10 dB, the SNR loss is less than 1 dB. This can be achieved by proper frequency synchronization design and resource block allocation mechanism.

The radio resource management (RRM) mechanism should be aware of placing the UE frequency allocation to avoid significant SNR degradation, especially for the UE with small RB size. One possibility to reduce the impact of in-band interference is to allocate the UE resource blocks based on the PSD level.

" When the effective leader is finished with his work,
the people say it happened naturally. ."

Lao Tse

CHAPTER 8

Conclusion

The suitability of beyond 3G systems air interfaces with user equipment hardware imperfections has been studied in this dissertation. As a case study, the UTRA LTE uplink is assumed. The analysis is based on the results from a link level simulation. The work presented was started with the baseline performance evaluation of LTE uplink. Several prominent techniques in LTE uplink have been considered, such as radio access techniques, link adaptation, H-ARQ, and turbo equalizer. Afterwards, the impact of hardware imperfections on both in-band and out-of-band performance have been investigated. The performance and requirements aspects in consequence of the imperfections are discussed throughout the remaining dissertation.

Overall, the results and discussions in this study provide a link between system level design and RF design. System level design is mainly dealing with the spectral efficiency and the required signal to noise ratio (SNR), whereas RF design deals with Error Vector Magnitude (EVM), Adjacent Channel Leakage Ratio (ACLR), and spectrum emission mask (SEM) requirements. In this chapter, the main findings of the PhD study, recommendations, and future work are summarized.

8.1   Main Findings and Contributions

SC-FDMA and OFDMA are the salient air interface for the uplink B3G/4G systems. Baseline performance of both air interfaces combined with the key techniques in wireless communication has been analyzed. Both air interfaces have been proven to achieve high spectral efficiency. It is shown that the proposed SC-FDMA with turbo equalizer can further improve the BLER performance up to 1 dB in comparison to SC-FDMA with MMSE receiver. SC-FDMA can take advantage over OFDMA in cases where the lower order modulation schemes are selected. SC-FDMA achieves a significantly lower PAPR while OFDMA is not affected by the selection of modulation scheme. SC-FDMA with $\pi/2$ BPSK achieves PAPR 4 dB lower than OFDMA. Therefore, the UE can operate at high power and hence increase the cell coverage. Moreover, a lower PAPR results in a reduced back-off to maximize the power amplifier efficiency.

The most common RF imperfections in the Cartesian transmitter, such as nonlinear power amplifier, gain imbalance, phase imbalance, DC offset and phase noise, have been investigated. The nonlinear power amplifier is the foremost imperfection because it may affect the performance (in-band and out-of-band), the power usage, and the cell coverage. Considering the presence of nonlinear power amplifier, SC-FDMA is in favor in comparison to OFDMA as a result of the lower PAPR. For 16QAM 4/5, SC-FDMA has a better performance by 0.7 dB than OFDMA. Moreover, SC-FDMA provides a good balance between the performance loss and meeting the RF requirements (SEM & ACLR).

Similar investigations on the impact of RF imperfections for the Polar EER transmitter have been carried out. Timing delay alignment between the envelope and phase paths is shown to be the most problematic imperfection to meet the in-band and out-of band requirements. To maintain acceptable in-band requirements, the timing delay alignment must be below 8 ns, while the timing delay alignment of 4 ns is required to meet out-of-band requirements. Other imperfections, such as limited bandwidth in the envelope path and non-ideal class E power amplification are relatively easy to control.

The relation among individual RF imperfections on LTE uplink performance for both Cartesian and Polar EER RF transmitters has been presented. From this study, the EVM generated by each imperfection can be associated with the corresponding link level performance in both AWGN and realistic mobile propagation (typical urban) channel. The EVM has been shown as a good direct measure to estimate the link level performance loss in the practical EVM range. For 16 QAM, the practical EVM range is around 8 %. Furthermore, an analytical derivation relating the performance loss as result of white noise source to the EVM level shows a good match with the simulation result. The

simulation effort on the impact of RF imperfections on in-band performance can be further simplified by including a white noise source as an equivalent model of the RF transmitter imperfections.

A spectrum shaping technique based on a 10th order Inverse Chebyshev filter has been proposed to control LTE spectrum emission. The proposed technique is capable of controlling the spectral emission for various bandwidth settings and provides a good trade-off between spectrum emission control, capacity loss minimization, and implementation complexity. The spectrum shaping is only capable of controlling the out-of-band spectrum, and thus in-band inter-user interference potentially exists. Therefore, also the impact of in-band interference on the LTE uplink has been scrutinized. Considering that the RF imperfections such as frequency offset and phase noise are under control and the PSD offset below 10 dB, the SNR loss for 16QAM 3/4 is less than 1 dB.

8.2 Recommendations

In general, both SC-FDMA and OFDMA air interfaces are suitable for uplink beyond 3G systems. SC-FDMA is the preferred selection for the system deployment which requires large scale coverage. SC-FDMA in combination with a lower order modulation shows a significantly lower PAPR than OFDMA. For a small cell coverage in which the system operates at high SNR, OFDMA is preferred to SC-FDMA. At high SNR, where both air interfaces operate with high order modulation, SC-FDMA does not take a significant advantage over OFDMA in terms of PAPR.

The impact of RF transmitter imperfections must be evaluated through both in-band and out-of-band requirements. Meeting the out-of-band requirements is typically the limiting factor, but the inband performance becomes the limiting factor for higher order modulation. Higher order modulation has a small EVM requirement which is hard to achieve.

The EVM measurement results can be used to estimate the performance loss, especially in the practical EVM range. A white noise source as an equivalent model of the RF transmitter imperfections can be used to investigate the performance loss and hence simplify the investigations. However, it is strictly only for in-band performance. The impact on the out-of band should be evaluated based on each RF transmitter imperfection.

The Radio Resource Management should be aware of placing the UE resource block allocation to avoid any significant SNR loss. One possibility is to allocate

the UE resource block based on the PSD level. However, such a solution will cost on the degree of freedom of the user allocation in the frequency domain.

8.3 Future Work

There are some issues which have not been addressed in this PhD study. Thus, the work can still be extended to the following potential topics.

The impact of RF hardware imperfections on beyond 3G system is investigated based on a link level simulation. It would be interesting to assess the impact of imperfections from the real hardware measurements. There are some practical issues which can also be investigated from the hardware measurements. Investigation on the impact of power amplifier is still the most important topics. Especially, the capability of the power amplifier to deal with the LTE uplink which has a wide band bandwidth. Moreover, the actual power amplifier efficiency obtained from the measurements can be further investigated. However, this work requires at least the availability of the following parts: an LTE uplink baseband signal generation, RF transceiver, and the measurement equipments.

The study presented is mainly focused on the impact of the hardware imperfections for a single antenna configuration. Beyond 3G systems also consider to use multiple-antennas at the transmitter to further enhance the spectral efficiency. There are two scenarios: multiple antennas by combining with other user equipments antennas to form a virtual MIMO and multiple antennas in one user equipment. The Virtual MIMO scenario is suitable for a portable user equipment while the other scenario is for a larger user equipment to maintain sufficient distance among antennas. Investigating the impact of hardware imperfections on a multiple-antenna configuration is also a prominent topic. The hardware imperfections are not just affecting the single antenna stream. It is expected to create in-band interference between antennas.

The other potential topic is to investigate a method to overcome the hardware imperfections. Linearization and pre-distortion of the power amplifier, DC offset compensation, IQ imbalance minimization are some example in this topic. During this PhD work, the anticipated hardware imperfections have been discussed to provide the baseline for this future work.

APPENDIX A

LTE Uplink Link Level Simulator: Descriptions & Validation

The LTE link level simulator for both uplink and downlink direction has been developed together with other colleagues in Aalborg University[1] and Nokia Siemens Networks[2]. The LTE uplink part is carried out in this PhD project. The modeling of link level simulator is based on Matlab script and C language. In this Appendix general descriptions and validation of the simulator are provided.

A.1   Descriptions

The model of LTE uplink is shown in Figure A.1. The left side is the transmitter, corresponding to the user equipment (UE), and the right side is the receiver, corresponding to the base station (BS). The transmission from the UE

---

[1]PhD students at Department of Electronic Systems, Aalborg University: Akhilesh Pokhariyal, Wei Na, and Christian Rom

[2]Researcher at Nokia Siemens Networks Aalborg: Frank Frederiksen, Claudio Rosa

starts with the Transport Format and Resource Combination (TRFC) information from the Link Adaptation (LA) module to the transport block generator. Transport block generator generates the packet based of the requested size. Then, the Cyclic Redundancy Check (CRC) based error-detecting code is performed to the corresponding packet. According to the packet size and the maximum code block size, the packet is segmented into several blocks. Each block is coded and the coding used for this study is the turbo coding defined in the UTRA Release 6. The rate matching block adjusts the output bit rate according to the requirements by puncturing or repeating the coded bits. The rate matching implementation is following the description in the UTRA Release 6 [12]. Afterwards, the output coded bits are interleaved and are passed to the modulator. The modulator is implemented based on the supported modulation schemes defined in [5], such as $\pi/2$ BPSK, QPSK, 8PSK and 16QAM. For QAM modulation, a QAM remapping is performed to set the systematic bits at more reliable constellation points as this improves the decoder performance.

Single carrier transmission is formed by the DFT spreading. The DFT spreading block pre-coded the PSK / QAM data symbols. Thus, all of data symbols are mixed together to form an SC-FDMA symbol. Afterwards, several SC-FDMA symbols are combined with pilot symbols in a time division multiplex (TDM) and mapped to the proper subcarriers. 3GG study item report [5] specified both localized and distributed allocation mapping. Finally, the basic OFDM processing is performed. The data symbols are placed on orthogonal subcarriers by the IFFT and the addition of cyclic prefix.

At the receiver side, the base station basically performs the reverse operations with respect to the process in the transmitter. The amplitude and phase variation due to the transmission in a frequency selective fading are compensated by an equalizer. The equalizer is basically a one tap frequency domain equalizer located at the output of the FFT in the receiver. The equalizer coefficients in (3.10) can be generated based on either Zero Forcing (ZF) or Minimum Mean Square Error (MMSE). The Zero forcing applies channel inversion and the equalization coefficient is given by:

$$\mathbf{C_{m,k}} = \frac{\mathbf{H^*_{m,k}}}{|\mathbf{H_{m,k}}|^2} \tag{A.1}$$

The zero forcing has a disadvantage in terms of noise enhancement for small amplitudes of $H_{m,k}$ [77]. To overcome the noise enhancement problem in the zero forcing technique, the FDE complex coefficient, $C_{m,k}$ can also be obtained
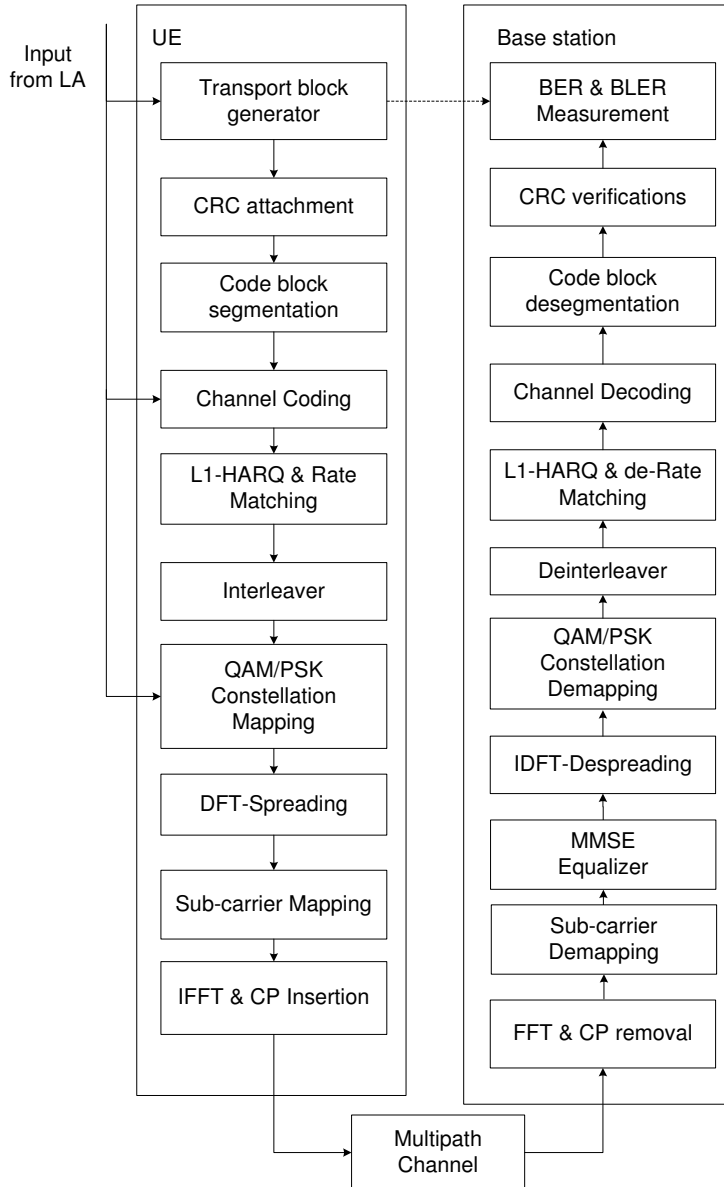
Figure A.1: Layer 1 UTRA LTE uplink Link Level Simulator

under the minimum mean-square error (MMSE) criterion. This is given by [78]:

$$\mathbf{C_{m,k}} = \frac{\mathbf{H^*_{m,k}}}{|\mathbf{H_{m,k}}|^2 + \frac{\sigma_n^2}{\sigma_s^2}} \tag{A.2}$$

where k denotes the subcarrier index, σ_n^2 the variance of the additive noise, and σ_s^2 is the variance of the transmitted pilot symbol.

A.1.1   Channel Estimation Algorithms

The channel estimation problematic will be solved in a two step strategy. Firstly the channel transfer function (CTF) is estimated from the received short blocks. Secondly, time domain channel interpolation is considered. For the simplicity of derivation of the channel estimation algorithm, the channel impulse response is considered constant over the duration of an OFDM symbol.

Frequency-Domain Channel Estimation

An estimate of the channel transfer function at the pilot subcarriers is obtained. Then, the full channel transfer function is calculated using an interpolation method.

1. Estimate at Pilot Position: Let p_i $i = 0, ..., N_p - 1$ be a set of indexes containing the subcarrier indexes that carry pilot symbols, where N_p is the number of pilot symbols in the short block. A Least-Squares (LS) estimate of the channel transfer function at these pilot positions can be calculated as:

$$\tilde{\mathbf{h}}_p[i] = \frac{\mathbf{z}[\mathbf{p_i}]}{\mathbf{d}[\mathbf{p_i}]} \tag{A.3}$$

Where $\mathbf{z}[\mathbf{p_i}]$ and $\mathbf{d}[\mathbf{p_i}]$ are respectively the received short block after the FFT and the transmitted short block in the ith pilot subcarrier. $\mathbf{h_p}$ is a N_p long column vector containing the LS estimates of the channel at pilot subcarriers.

2. Wiener filtering Interpolation: Wiener Filtering is the optimum interpolation method in terms of MSE. Using the statistics of the channel and noise, it performs a minimum mean square error (MMSE) interpolation of the estimates at pilot subcarriers, optimally reducing the effects of noise and channel distortion.

The full CTF is obtained by:

$$\tilde{\mathbf{h}} = \mathbf{R_{hh_p}} \cdot \left(\mathbf{R_{h_p h_p}} + \sigma_\mathbf{w}^2 \mathbf{I_{N_p}}\right)^{-1} \tilde{\mathbf{h}}_\mathbf{p} \qquad (A.4)$$

where $\mathbf{R_{hh_p}}$ is the cross correlation matrix of the true CTF and the true CTF at pilot subcarriers, $\mathbf{R_{h_p h_p}}$ is the autocorrelation matrix of the true CTF at pilot subcarriers, σ_w^2 is the noise power and $\mathbf{I_{N_p}}$ is the $N_p \times N_p$ identity matrix. Note that the channel transfer function coefficients are assumed to be uncorrelated to the noise process.

Time-Domain Channel Estimation

A simple time-domain channel estimation based on linear interpolation is assumed. In a sub-frame, the short block are transmitted. The channel estimation for each sub-frame is a linear interpolation between these two short blocks.

A.1.2 Enhancement Mechanisms

Several throughput enhancement mechanisms are implemented in the simulator, including adaptive modulation coding (AMC) based on link adaptation (LA) and Hybrid ARQ (HARQ) based on fast L1 retransmissions. The HARQ is based on chase combining (CC) and incremental redundancy (IR). LA with various modulations and channel coding sets (MCS) is applied to the shared data channel. Here, a simple LA is assumed in which the MCS selection is based on averaged SNR. No errors are assumed in the transmission of ACK/NACK messages. As a result of the short retransmission delays, it is possible to operate at a 1st transmission block error rate (BLER) values of around 10-30%. A retransmission scheme based on the stop and wait (SAW) principle with several independent HARQ processes per user is assumed [43].

A.2 Validation

This section provides the validation of the link level simulator. The validation starts with the examining the performance of both QPSK and 16QAM in AWGN channel. The results for uncoded BER of QPSK in AWGN channel is shown in Figure A.2. The simulated results is perfectly matched with the theoretical calculation as described in [79].
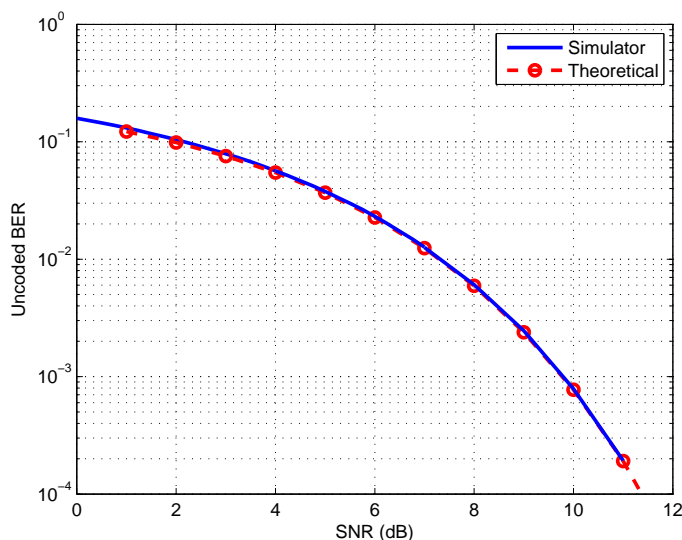
Figure A.2: Uncoded BER results of QPSK in AWGN.

Figure A.3 shows the results for 16QAM and both simulated and theoretical calculation are obtained the same results.

Figure A.4 depicts the BLER performance in AWGN channel for several MCS settings. The results are compared with the results presented in [2]. The turbo decoder used for both link-level simulations used a log-MAP decoding algorithm. Results show that the simulated results has a good agreement with the reference results. It is noted a small deviation of 0.3 dB for 16QAM rate 2/3.

Figure A.5 shows the BLER performance in typical urban channel. The result
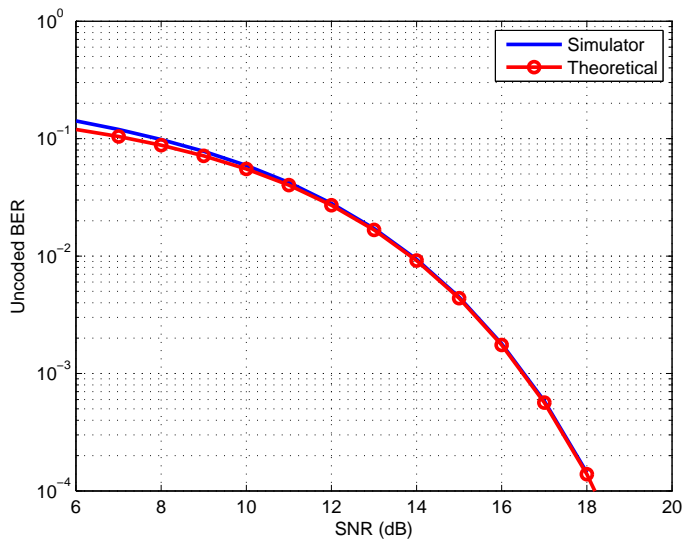
Figure A.3: Uncoded BER results of 16QAM in AWGN.
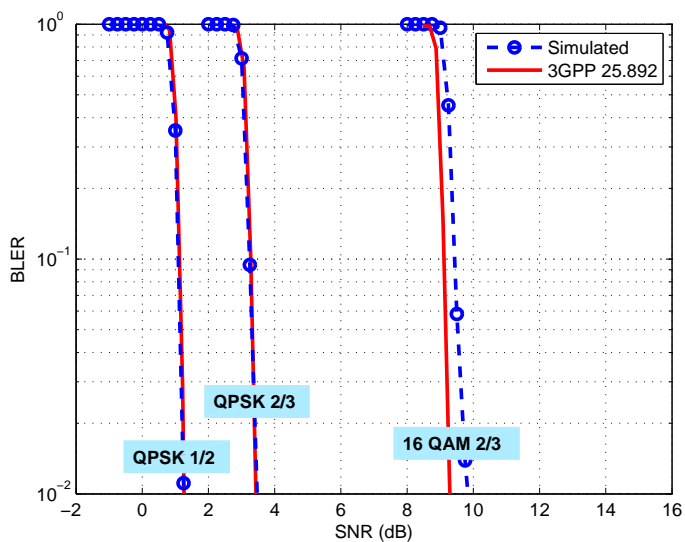
Figure A.4: Comparison of BLER results in AWGN channel.
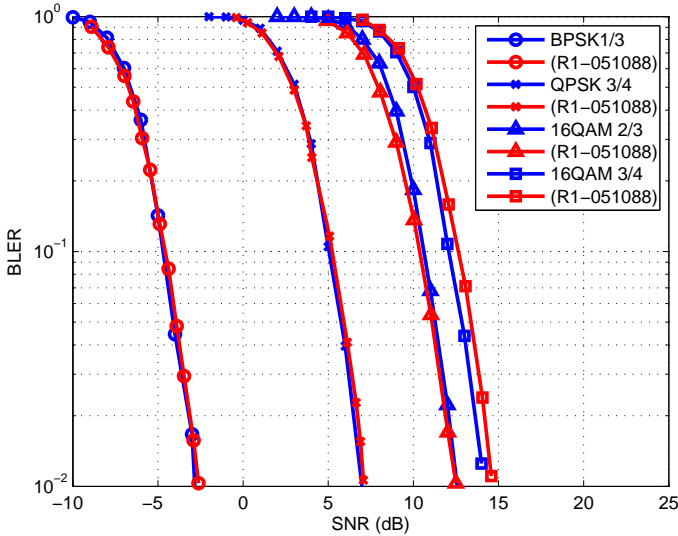
Figure A.5: Comparison of BLER results in Typical Urban Channel.

is compared with Nokia result [80]. The simulation scenario is for 1x2 SIMO configuration with MMSE receiver. The channel profile is typical urban channel and UE speed of 3 kmph. It is observed that both results have considerably the same performance.

The results of QPSK rate 3/4 with Chase combining and incremental redundancy HARQ in AWGN channel are shown in Figure A.6. Chase combining always send an identical copy for each retransmission. The total combining gain is 3 dB, 4.7 dB and 6 dB for retransmission 1, 2 and 3 respectively. Incremental redundancy shows better performance than chase combining. Beside the combining gain, incremental renudancy has additional coding gain.

Spectral efficiency results from different companies are shown in Figure A.7. The result shown is for 16QAM rate 3/4 with 50 RB. The simulation scenario is described in [81]. The results from NTT DoCoMo [82], LG Electronic [83], and Qualcomm Europe [84] are compared with the link level simulator result. The results show that the simulated result is in good agreement with other results.
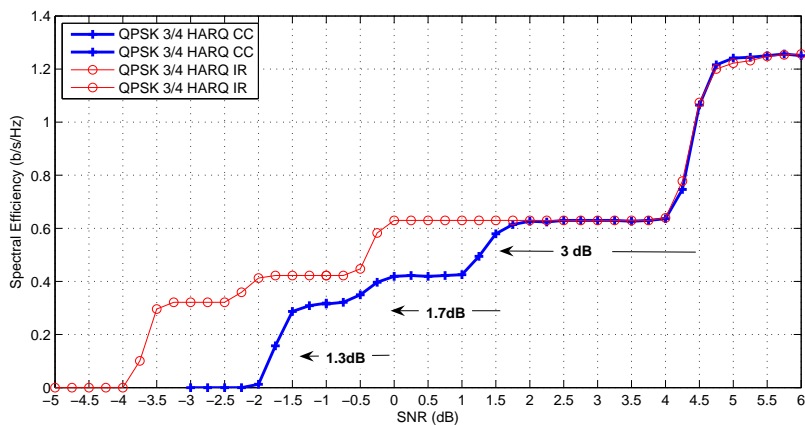
Figure A.6: HARQ Chase Combining and Incremental Redundancy.
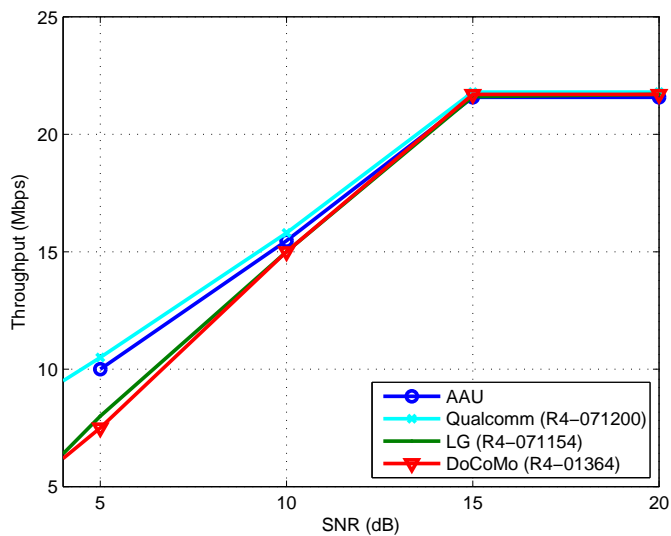
Figure A.7: Spectral Efficiency for 16QAM 3/4 in Typical Urban Channel.

APPENDIX B

Channel Model

The multipath channel model realization is based on the implementation in [85]. Several channel model have been implemented, including ITU Vehicular & Pedestrian channel, and Typical Urban channel. This channel model has also been used in previous PhD project [86] in which the detailed channel model verification is provided.

The channel model uses the correlation-based stochastic MIMO model. To ensure that the correlation properties in the frequency domain are realistic, the typical urban with power delay profile (PDP) 6 paths and 20 paths are assumed. The path loss, shadowing, and other cell noise is modeled as AWGN noise. The PDP of the typical urban is shown in Table B.1. These PDP have been used as the tapped delay line coefficients to represent the multipath channel.

The frequency correlation property of both channels is shown in Figure B.1. It is shown that the coherent bandwidth for both channels are equal at around 375 kHz. Therefore, for a wideband transmission, i.e. 10 MHz, the channel profile is highly frequency selective fading channel.

Table B.1: Typical Urban Channel Power Delay Profile.

Number of	TU 06		TU 20	
path	Delay (ns)	Power (dB)	Delay (ns)	Power (dB)
1	0	-7.22	0	-5.7
2	195	-4.22	217	-7.6
3	488	-6.22	512	-10.1
4	1595	-10.22	514	-10.2
5	2311	-12.22	517	-10.2
6	5013	-14.22	674	-11.5
7	-	-	882	-13.4
8	-	-	1230	-16.3
9	-	-	1287	-16.9
10	-	-	1311	-17.1
11	-	-	1349	-17.4
12	-	-	1533	-19.0
13	-	-	1535	-19.0
14	-	-	1622	-19.8
15	-	-	1818	-21.5
16	-	-	1836	-21.6
17	-	-	1884	-22.1
18	-	-	1943	-22.6
19	-	-	2048	-23.5
20	-	-	2140	-24.3
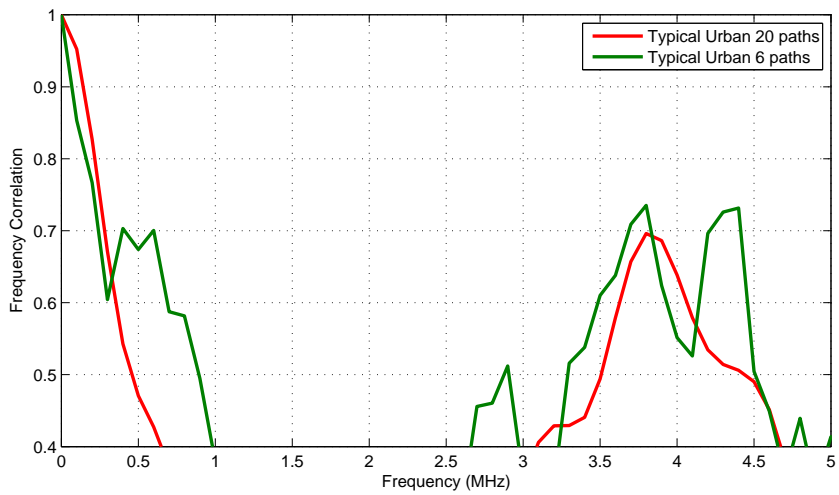
Figure B.1: Frequency correlation property of Typical Urban Channel Model.

Appendix C

Turbo Equalizer

C.1 System Model

The transmission scheme is presented in fig.C.1. A frame of information bits b_i is encoded by a turbo encoder. The resulting b_l bits are interleaved using a random permutation function. The interleaving coded bits b_m are grouped in N q-length blocks $\{[b_{1,1}, ..., b_{1,q}], ..., [b_{N,1}, ..., b_{N,q}]\}$, and each block of bits is mapped to a complex symbol s^i, i=1,...,M, where $M = 2^q$ is the number of symbols of the considered constellation. The SC-FDMA processing part of the transmitter is identical to the OFDM one [5], except for the Discrete Fourier Transform (DFT) spreading operation performed on the source symbol sequence s_n, n=1,...,N before the subcarrier mapping operation

$$\mathbf{S[k]} = \frac{\mathbf{1}}{\mathbf{N}} \sum_{\mathbf{n=0}}^{\mathbf{N-1}} \mathbf{s_n e}^{\frac{\mathbf{j2\pi kn}}{\mathbf{N}}} \quad \mathbf{k = 0, ..., N-1} \tag{C.1}$$

where N is the number of active subcarriers.

This operation spreads the source symbol sequence over all the subcarriers, so
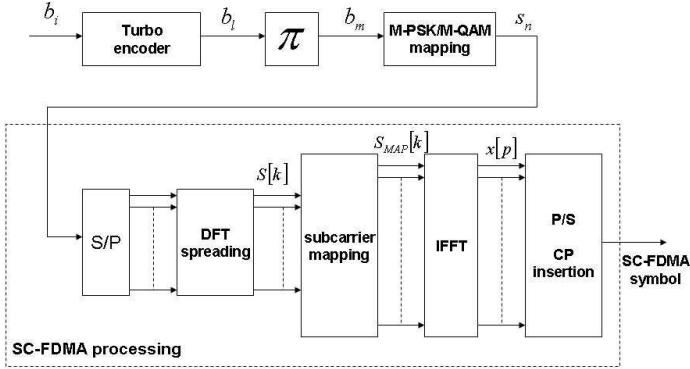
Figure C.1: SC-FDMA transmitter

that each subcarrier takes information of the entire symbol sequence. Since the data vector is processed by a DFT operation, the data generation is done in time-domain. The different samples are mapped to their definitive subcarrier (S_{MAP}) for the transmission [74].

Finally, the data is OFDM-processed by an IFFT block

$$\mathbf{x}[p] = \sum_{\mathbf{k=0}}^{\mathbf{N_{FFT}-1}} \mathbf{S_{MAP}[k]e}^{-\frac{\mathbf{j2\pi kl}}{\mathbf{N}}} \quad p = 0, ..., \mathbf{N_{FFT}} - 1 \qquad (C.2)$$

where N_{FFT} is the FFT size, and a cyclic prefix (CP) is added [9], at the purpose of eliminating the intersymbol interference caused by time dispersive channel. SC-FDMA is expected to reduce the PAPR [87]; this characteristic is very important for uplink since the UE has to be power-efficient due to battery limitations. Nevertheless, in SC-FDMA the symbol transmission is performed in time domain; therefore it shows a noise enhancement compared with OFDM given that each received symbol contains the noise over all the frequencies.

In this work we assume that the maximum excess delay of the channel is shorter than the ciclic prefix, and, therefore, the ISI can be completely removed.
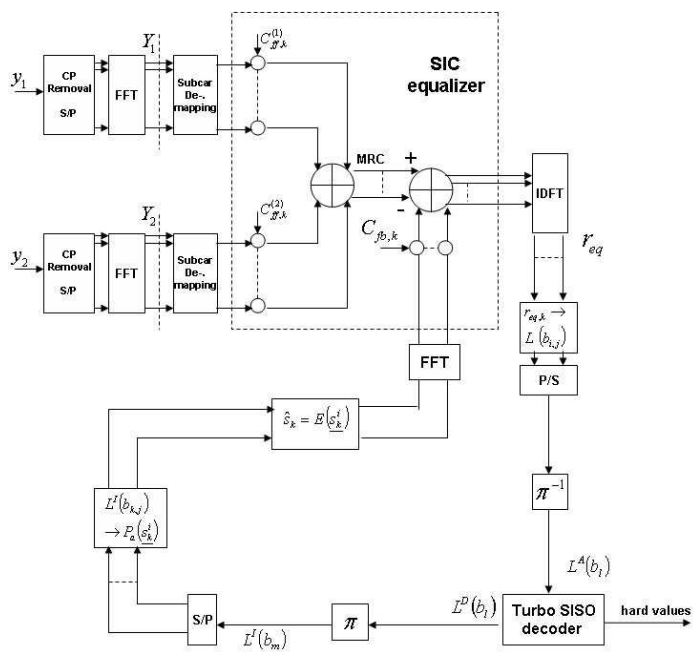
Figure C.2: Turbo equalizer structure

C.2 Turbo Equalization

Considering that the frequency selective channel can be regarded as an encoder serially concatenated with the channel encoder of the transmitter, the main idea of the turbo equalization is to perform jointly equalization/demodulation and decoding operation at the receiver [88]. In this case, equalizer and decoder are considered as SISO (Soft Input Soft Output) blocks, separated by bit-deinterleavers and bit-interleavers: the information produced by one of these blocks can be viewed as apriori information for the other one. The purpose of this system is to produce a more reliable estimation of the transmitted symbol sequence in each iteration. It is obtained through the progressive cancellation of the noise (interference) component and the knowledge of the structure of the coded words given by the decoder.

The block diagram of our turbo equalizer is shown in Fig. C.2.

It uses soft interference cancellation (SIC) equalizer as described in [89] and the equalization is performed in frequency domain. It results in more efficient operation than traditional time domain equalization [90], since equalization is performed on a block of data at a time, and the operations on this block involve an efficient FFT operation and a simple channel inversion operation.
For the two receive antennas cases (1x2 SIMO), the received signals at each antenna can be written as:

$$\mathbf{y_1} = \mathbf{X} \cdot \mathbf{H_1} + \mathbf{w_1} \tag{C.3}$$

$$\mathbf{y_2} = \mathbf{X} \cdot \mathbf{H_2} + \mathbf{w_2} \tag{C.4}$$

where X is diagonal matrix of the transmitted sub-carrier symbols, H_1 and H_2 are the channel frequency responses for the two antennas and w is the noise component.

After the CP removal, the received signal is converted to frequency domain through a FFT operation. Frequency domain equalization is then performed, with a simple one tap equalizer. The equalizer coefficients are indicated as forward coefficients $(C_{ff}^{(1)}, C_{ff}^{(2)})$, and these will be discussed in the next section.

After the maximal ratio combining (MRC) operation in SIMO case, the equalized signal is converted in time domain through an IDFT operation. The output

is an estimation of the transmitted M-PSK or M-QAM symbols.

Remembering that at each symbol s^i of the constellation is associated a known sequence of bits of length q, the log-likelihood ratio of all the coded bits is computed by using the max log MAP (Maximum A Posteriori) technique, as following:

$$\mathbf{L^E(b_{i,j})} = \left(\min_{\epsilon_\mathbf{k}^\mathbf{i}:\mathbf{b_{i,j}}=-\mathbf{1}} \epsilon_\mathbf{k}^\mathbf{i} - \min_{\epsilon_\mathbf{k}^\mathbf{i}:\mathbf{b_{i,j}}=\mathbf{1}} \epsilon_\mathbf{k}^\mathbf{i} \right) \tag{C.5}$$

where $b_{i,j}$ is the jth bit associated at the constellation point s^i, k is the frequency bin, and ϵ_k^i denotes the squared euclidean distance of the equalizer output to s^i, defined as:

$$\epsilon_\mathbf{k}^\mathbf{i} = \left| \mathbf{r_{eq,k}} - \mathbf{s^i} \right|^\mathbf{2} \tag{C.6}$$

where $r_{eq,k}$ is the SIC equalizer output after the IFFT operation. The log-likelihood ratios of all the coded bits ($L_a^D(b_l)$, obtained from (5) after the parallel-to-serial and the deinterleaving operations) are submitted to the turbo decoder, that should compute an improved log-likelihood ratio of all of them ($L^D(b_l)$), that takes into account of the knowledge of the encoder scheme. This soft output has been obtained modifying the structure of each MAP (Maximum A Posteriori) decoder inside the turbo decoder structure [91], applying the BCJR algorithm [92] at both the systematic and the parity bits [93]. At this information is then subtracted the *apriori* information of the coded bits as follows:

$$\mathbf{L_e^D(b_l)} = \mathbf{L^D(b_l)} - \mathbf{L_a^D(b_l)}, \tag{C.7}$$

at the purpose of extracting the so called *extrinsic* information [88] introduced by the channel encoder from $L^D(b_l)$. Hence $L_e^D(b_l)$ does not include any channel information.

After the symmetrical interleaving operation, the resulting $L_a^E(\cdot)s$ are grouped in q-length blocks $\left\{ \left[L_e^E(b_{1,1}), ..., L_a^E(b_{1,q}) \right], ..., \left[L_a^E(b_{N,1}), ..., L_a^E(b_{N,q}) \right] \right\}$ at the purpose of constructing a matrix having in each row the log-likelihood ratios of the bits related to each transmitted symbol. The probability of each bit is computed as follows:

$$\mathbf{P_e(b_{k,j} = 0)} = \frac{1}{1 + \exp(\mathbf{L_a^E(b_{k,j})})}; \tag{C.8}$$

$$\mathbf{P_e(b_{k,j} = 1)} = 1 - \mathbf{P_e(b_{k,j} = 0)}. \tag{C.9}$$

Thus, it is possible to compute the *(NxM)* apriori symbol probability matrix $\left\lfloor P_a(s_k^i) \right\rfloor$, that has in each row the probability of each symbol of the constellation at frequency step *k*. Assuming independence between the interleaved coded bits, each element of this matrix is given by:

$$\mathbf{P_a(s_{\underline{k}}^i)} = \prod_{j=1}^{q} \mathbf{P_e(b_{k,j} = b_{i,j})} \tag{C.10}$$

for *k=1,...N* and *i=1,...M*.
From each row of this matrix the estimation of the transmitted symbol vector can be computed:

$$\widehat{\mathbf{s_k}} = \mathbf{E}\left(\mathbf{s_{\underline{k}}^i}\right) = \sum_{i=1}^{M} \mathbf{s^i P_a(s_{\underline{k}}^i)} \tag{C.11}$$

So the estimated sequence is converted in frequency domain through a FFT operation, multiplied with the feedback coefficients (C_{fb}), in order to extract from it the noise component, and then subtracted from the equalized vector.
Note that, for the next iterations of the algorithm, before passing the information generated by the equalizer to the decoder, the *apriori* information accruing from the previous iteration must be removed as follows:

$$\mathbf{L_e(b_l)} = \mathbf{L_D(b_l)} - \mathbf{L_a(b_l)} \tag{C.12}$$

in order to prevent the decoder from "reprocessing" its own information and having the so called "positive feedback"[88].
The computational complexity of the turbo equalizer processing is mostly related to the computation of the *(NxM)* apriori symbol probability matrix, that should be recomputed at each iteration of the algorithm. Nevertheless, the complexity could be reduced through the Cyclic Redundancy Check (CRC) verification after the decoding operation: if the checking result is 0, no other iterations are necessary.

C.3   SIC Equalizer Coefficients

The main problem affecting the performances of the turbo equalizer is the proper derivation of the forward and feedback coefficients of the SIC equalizer working in frequency domain. The forward coefficient C_{ff} should be computed at the purpose of increasing the signal to noise ratio and obtaining a good estimation of the transmitted symbols. The feedback coefficients C_{fb} should be computed at the purpose of evidencing the residual noise component in the estimated symbol vector.

Instead of using the traditional fixed frequency domain SIC coefficients as defined in [90], we opt for an adaptive solution where the coefficients are updated at each iteration of the algorithm. The main idea is updating the coefficients depending on the variance of the estimated symbol vector. The considered forward coefficients are as follows:

$$\mathbf{C}_{\mathbf{ff,k}}^{(1)} = \frac{\sigma_\mathbf{s}^\mathbf{2}}{1 + \beta\sigma_\mathbf{\hat{s}}^\mathbf{2}} \frac{\mathbf{H}_{\mathbf{1,k}}^*}{\left(\sigma_\mathbf{s}^\mathbf{2} - \sigma_\mathbf{\hat{s}}^\mathbf{2}\right)\left(\left|\mathbf{H}_{\mathbf{1,k}}\right|^\mathbf{2} + \left|\mathbf{H}_{\mathbf{2,k}}\right|^\mathbf{2}\right) + \frac{\sigma_\mathbf{w}^\mathbf{2}}{\sigma_\mathbf{s}^\mathbf{2}}} \tag{C.13}$$

$$\mathbf{C}_{\mathbf{ff,k}}^{(2)} = \frac{\sigma_\mathbf{s}^\mathbf{2}}{1 + \beta\sigma_\mathbf{\hat{s}}^\mathbf{2}} \frac{\mathbf{H}_{\mathbf{2,k}}^*}{\left(\sigma_\mathbf{s}^\mathbf{2} - \sigma_\mathbf{\hat{s}}^\mathbf{2}\right)\left(\left|\mathbf{H}_{\mathbf{1,k}}\right|^\mathbf{2} + \left|\mathbf{H}_{\mathbf{2,k}}\right|^\mathbf{2}\right) + \frac{\sigma_\mathbf{w}^\mathbf{2}}{\sigma_\mathbf{s}^\mathbf{2}}} \tag{C.14}$$

where σ_w^2 is the noise variance, σ_s^2 is the variance of the transmitted symbols, $\sigma_{\hat{s}}^2$ is the variance of the estimated symbols, and β is defined as:

$$\beta = \frac{\mathbf{1}}{\mathbf{N}} \sum_{\mathbf{k=1}}^{\mathbf{N}} \frac{\left|\mathbf{H}_{\mathbf{1,k}}\right|^\mathbf{2} + \left|\mathbf{H}_{\mathbf{2,k}}\right|^\mathbf{2}}{\left(\sigma_\mathbf{s}^\mathbf{2} - \sigma_\mathbf{\hat{s}}^\mathbf{2}\right)\left(\left|\mathbf{H}_{\mathbf{1,k}}\right|^\mathbf{2} + \left|\mathbf{H}_{\mathbf{2,k}}\right|^\mathbf{2}\right) + \frac{\sigma_\mathbf{w}^\mathbf{2}}{\sigma_\mathbf{s}^\mathbf{2}}} \tag{C.15}$$

where N is the length of the channel frequency response vector. For analytical derivation of (13) and (14) we recall at [94], where a similar approach has been used in time domain equalization.
At the first iteration, when no apriori information is available, we assume $\sigma_{\hat{s}}^2 = 0$, and the forward coefficients perform as the traditional MMSE coefficients [78]. For the next iterations, the estimation of the transmitted symbols becomes more accurate, we have $\sigma_{\hat{s}}^2 \approx \sigma_s^2$.

The feedback coefficients are given by:

$$\mathbf{C_{fb,k}} = \mathbf{H_{1,k}C_{ff,k}^{(1)}} + \mathbf{H_{2,k}C_{ff,k}^{(2)}} - \mathbf{1}. \qquad (C.16)$$

It can be shown that feedback coefficients are defined in condition where the estimated symbol sequence is very accurate ($\sigma_{\hat{s}}^2 \approx \sigma_s^2$), the resultant noise component becomes very small. Using these adaptive coefficients the vector obtained after the multiplication with the forward coefficients changes at each iteration, and becomes closer to the trasmitted vector as the noise component decreases.

Bibliography

[1] P. Rysavy, "Mobile broadband: EDGE, HSPA, & LTE," *Online Material URL: http://www.itu.int/ITU-D/imt-2000/index.html*, September 2006.

[2] 3GPP, "Feasibility study for orthogonal frequency division multiplexing (OFDM) for UTRAN enhancement," *Tech. Spec. TR 25.892 V6.0.0*, June 2004.

[3] J. Garcia, S. L. Jeunesse, and D. Bartow, "Measuring spurious free dynamic range in a D/A converter," Intersil, Tech. Rep. TB326, January 1995.

[4] J. Staudinger, "An overview of efficiency enhancements with application to linear handset power amplifier," in *Proc. IEEE Radio Freq. Integrated Circuits Symposium.*, 2002.

[5] 3GPP, "Physical layer aspects for evolved universal terrestrial radio access (UTRA) (release 8)," *Tech. Spec. TR 25.814 V7.1.0*, September 2006.

[6] ——, "User Equipment (UE) radio transmission and reception (FDD) (release 8)," *TS 25.101 V8.1.0*, December 2007.

[7] ——, "Requirements for Evolved UTRA (E-UTRA) and Evolved UTRAN (E-UTRAN)," *TR 25.913*, March 2006.

[8] 3GPP, "Physical channels & modulation," *TS 36.211 V0.2.2*, December 2006.

[9] D. Falconer, S. Ariyavisitakul, A. Benyamin-Seeyar, and B. Edison, "Frequency domain equalization for single-carrier broadband wireless systems," *IEEE Commun. Mag.*, vol. 40, no. 4, pp. 58–66, April 2002.

[10] H. Sari, G. Karam, and I. Jeanclaude, "Transmission techniques for digital terrestrial TV broadcasting," *IEEE Commun. Mag.*, vol. 33, no. 2, pp. 100–109, February 1995.

[11] A. Czylwik, "Comparison between adaptive OFDM and single carrier modulation with frequency domain equalization," in *Proc. Veh. Technology Conf'97.*, vol. 2, Phoenix, AZ, May 1997, pp. 865–869.

[12] 3GPP, "Multiplexing and channel coding," *TS 25.212 V6.5.0(2005-06))*, June 2005.

[13] E. Costa and S. Pupolin, "M-QAM-OFDM system performance in the presence of a nonlinear amplifier and phase noise," *IEEE Trans. on Communications*, vol. 50, no. 3, pp. 462–472, March 2002.

[14] A. Georgiadis, "Gain, Phase Imbalance, and Phase Noise Effects on Error Vector Magnitude," *IEEE Trans. on Vehicular Technology*, vol. 53, no. 2, March 2004.

[15] Q. Gu, *RF System Design of Transceivers for Wireless Communications.* New York, USA: Springer, 2006.

[16] B. Razavi, *RF Microelectronics*, 1st ed. New Jersey, USA: Prentice Hall PTR, 1998.

[17] B. Priyanto, T. Sørensen, and O. Jensen, "On investigation of nonlinear amplifier distortion in OFDM transmission," in *Proc. Wireless Personal Multimedia Communications 2005.*, September 2005.

[18] S. Han and J. Lee, "An overview of peak-to-average power ratio reduction techniques for multicarrier transmission," *IEEE Wireless Communications*, vol. 12, no. 2, pp. 56–65, April 2005.

[19] B. Priyanto, C. Rom, C. Navarro, T. Sørensen, , P. Mogensen, and O. Jensen, "Effect of phase noise on spectral efficiency for UTRA Long Term Evolution," in *Proc. IEEE PIMRC 2006.*, September 2006.

[20] A. Diet, C. Berland, M. Villegas, and G. Baudoin, "EER architecture specifications for OFDM transmitter using a class E amplifier," *IEEE Microwave and Wireless Comp. Letters*, vol. 14, no. 8, August 2004.

[21] M. Talonen and S. Lindfors, "System requirements for OFDM polar transmitter," in *Proc. Euro Conf. on Circuit Theory and Design*, vol. 3, August 2005.

[22] Y. Huang and T. Larsen, "Investigation of polar transmitter for WCDMA handset applications," in *Proc. IEEE NORCHIP 2006.*, November 2006.

[23] F. Raab, "Power amplifiers and transmitters for RF and microwave," *IEEE Trans.on Microwave Theory and Tech.*, vol. 50, no. 3, March 2002.

[24] D. Rudolph, "Out-of-band emissions of digital transmissions using kahn EER technique," *IEEE Trans.on Microwave Theory and Tech.*, vol. 50, no. 8, August 2002.

[25] M. Faulkner, "The effect of filtering on the performance of OFDM systems," *IEEE Trans. On Veh. Tech*, vol. 49, no. 5, September 2000.

[26] B. Razavi, "RF transmitter architectures and circuits," in *Proc. IEEE Custom Integrated Circuits.*, vol. 12, San Diego, CA, May 1999, pp. 197–204.

[27] M. Feulner, "Direct up-conversion lowers base-station costs," *Wireless Europe Mag.*, vol. 38, pp. 27–28, April 2005.

[28] A. Loke and F. Ali, "Direct conversion radio for digital mobile phone-design issues, status, and trends," *IEEE Trans. Microwave Theory and Techniques*, vol. 50, no. 11, pp. 2422–2435, November 2002.

[29] J. MacLeod, M. Beach, P. Warr, and T. Nesimoglu, "Filter considerations in the design of a software-defined radio," in *Proc. IST Mobile Communication Summit.*, vol. 1, Barcelona, Spain, September 2001, pp. 363–368.

[30] S. C. Cripps, *RF Power Amplifiers for Wireless Communications*, 2nd ed. Norwood, MA: Artech House, 2006.

[31] S. Mann, M. Beach, and J. McGeehan, "Increasing the talk-time of mobile radios with efficient linear transmitter architectures," *Elec and Commun Engineering Journal*, vol. 13, no. 2, pp. 65–76, April 2001.

[32] X. Huang, "On transmitter gain/phase imbalance compensation at receiver," *IEEE Communications on Letters*, vol. 4, no. 11, November 2000.

[33] W. Songping and Y. Bar-Ness, "OFDM systems in the presence of phase noise: Consequences and solutions," *IEEE Trans. Communications*, vol. 52, no. 5, pp. 855–865, May 2004.

[34] A. Armada, "Understanding the effects of phase noise in orthogonal frequency division multiplexing (OFDM)," *IEEE Trans. Broadcasting*, vol. 47, no. 2, pp. 153–159, June 2001.

[35] Ericsson, "Impact of EVM on data throughput for different transmitter impairments," 3GPP, Gyeongju, Korea, Tech. Rep. R4-020779, May 2002.

[36] C. Masse, "A direct-conversion transmitter for WIMAX and WiBro applications," *RF design Mag.*, vol. 1, pp. 42–46, January 2006.

[37] L. Kahn, "Single-sideband transmission by envelope elimination and restoration," *Proc. of IRE*, pp. 803–806, July 1952.

[38] Y. Huang, Y. Wang, and T. Larsen, "Filter considerations in polar transmitters for multi-mode wireless applications," in *Proc. IEEE Wireless Microwave Tech. 2005.*, November 2005, pp. 133–136.

[39] F. Wang, D. F. Kimball, J. D. Popp, A. H. Yang, D. Y. Lie, P. M. Asbeck, and L. E. Larson, "An improved power-added efficiency 19-dBm hybrid envelope elimination and restoration power amplifier for 802.11g WLAN applications," *IEEE Trans. Microwave Theory and Techniques*, vol. 52, no. 12, pp. 4086–4099, December 2006.

[40] J. Bingham, "Multicarrier modulation for data transmission: An idea whoce time has come," *IEEE Commun Mag.*, pp. 5–14, May 1990.

[41] K. Kansanen, "Wireless broadband single-carrier systems with MMSE Turbo Equalization Receivers," Ph.D. dissertation, University of Oulu, Oulu, Finland, 2005.

[42] L. Electronics, "PAPR comparison of uplink MA schemes," 3GPP, Athens, Greece, Tech. Rep. R1-050475, May 2005.

[43] T. Kolding, F. Frederiksen, and P. Mogensen, "Performance aspects of WCDMA systems with High Speed Downlink Packet Access (HSDPA)," in *Proc. IEEE VTC Fall 2002.*, Vancouver, Canada, July 2002, pp. 477–481.

[44] H. Holma and A. Toskala, *WCDMA for UMTS, HSPA evolution and LTE*, 4th ed. Chichester, UK: Wiley, 2007.

[45] P. Hoher, "TCM on frequency-selective land-mobile fading channels," in *Proc. Intl. Workshop on Digital Communications.*, vol. 1, Tirrena, Italy, September 1991.

[46] 3GPP, "Deployment aspects," *TR 25.943 V7.0.0*, June 2006.

[47] Ericsson, "Impact of EVM on data throughput for different transmitter impairments," 3GPP, Tech. Rep. R4-020779, May 2002.

[48] Motorola, "Effect of modulation accuracy on HSDPA radio link performance," 3GPP, Tech. Rep. R4-011439, November 2001.

[49] Nokia, "Definition of E-UTRA EVM for the BS," 3GPP, Tallinn, Estonia, Tech. Rep. R4-060737, September 2006.

[50] ——, "Methodology for deriving E-UTRA EVM BS requirements," 3GPP, Tallinn, Estonia, Tech. Rep. R4-060738, September 2006.

[51] Siemens, "EVM Measure for LTE," 3GPP, Riga, Latvia, Tech. Rep. R4-061227, November 2006.

[52] 3GPP, "Base station (BS) conformance testing (FDD)," *Tech. Spec. TS 25.141 V7.6.0*, December 2006.

[53] T. Larsen, O. Jensen, and J. Mikkelsen, "Power amplifier modeling for varying envelope modulation," in *Proc. IEEE NORCHIP Conf.*, November 2004.

[54] A. Koukab, Y. Lei, and M. Declercq, "Multi-standard carrier generation system for quad-band GSM/WCDMA (FDD-TDD)/WLAN (802.11 a-b-g) radio," in *Proc. IEEE ESSCIRC.*, 2005.

[55] Motorola, "64 QAM for UL LTE," 3GPP, St.Louis, Missouri, USA, Tech. Rep. R1-070759, February 2007.

[56] 3GPP, "Evolved UTRA (E-UTRA) user equipment (UE) radio transmission and reception," *TR 36.803 V1.0.0*, December 2007.

[57] Nokia, "Analysis of LTE UL spectrum shaping requirements," 3GPP, Riga, Latvia, Tech. Rep. R4-061314, November 2006.

[58] Huawei, "Analysis of out-of-band spectrum emission of uplink transmission under current numerology," 3GPP, Cannes, France, Tech. Rep. R1-061857, June 2006.

[59] Freescale, "Spectral mask issues for the LTE Uplink," 3GPP, Tallin, Estonia, Tech. Rep. R4-061004, August 2006.

[60] Ericsson, "UE ACLR and spectrum emission requirements," 3GPP, Sophia Antipolis, France, Tech. Rep. R4-070388, April 2007.

[61] N. S. Networks, Nokia, V. Wireless, Vodafone, and Ericsson, "Recommendations on lower E-UTRA bandwidth options," 3GPP, Orlando, USA, Tech. Rep. R4-070918, June 2007.

[62] Nokia, "Considerations regarding specification of E-UTRA BS spectrum shaping," 3GPP, Tallin, Estonia, Tech. Rep. R4-060746, August 2006.

[63] L. Technologies, "Windowing and spectral containment for OFDM downlink," 3GPP, London, UK, Tech. Rep. R1-050919, August 2005.

[64] Nokia, "UE ACLR and SEM," 3GPP, Sophia Antipolis, France, Tech. Rep. R4-070348, April 2007.

[65] M. Elliott, T. Montalvo, B. Jeffries, F. Murden, J. Strange, A. Hill, S. Nandipaku, and J. Harrebek, "A polar modulator transmitter for GSM/EDGE," *IEEE Trans. on Solid-State Circuits*, vol. 39, no. 12, pp. 2190–2199, December 2004.

[66] N. D. Lopez, J. Xufeng, D. Maksimovic, and Z. Popovic, "Class-E power amplifier in a polar EDGE transmitter," in *Int. IEEE Microwave Symposium Digest*, vol. 1, June 2006, pp. 785–788.

[67] J. Staudinger, B. Gilsdorf, D. Newman, G. Norris, G. Sadowniczak, R. Sherman, and T. Quach, "High efficiency CDMA RF power amplifier using dynamic envelope tracking technique," in *Int. IEEE Microwave Symposium Digest.*, vol. 2, June 2000, pp. 873–876.

[68] 3GPP, "User Equipment (UE) radio transmission and reception (FDD) (release 7)," *TS 25.101 V7.7.0*, March 2007.

[69] B. Priyanto, T. Sørensen, O. Jensen, T. Kolding, T. Larsen, and P. Mogensen, "A spectrum shaping technique to control spectrum emission of UTRA LTE User Equipment," in *Proc. IEEE NORCHIP 2007.*, November 2007.

[70] W. Zhengdao, M. Xiaoli, and G. Giannakis, "OFDM or single-carrier block transmissions?" *IEEE Trans. Communications*, vol. 52, no. 3, pp. 380–394, March 2004.

[71] N. S. Networks, "On in-band adjacent RB selectivity requirements," 3GPP, Athens, Greece, Tech. Rep. R4-071402, August 2006.

[72] Ericsson, "Initiation of modulation quality discussions for LTE," 3GPP, Denver, USA, Tech. Rep. R4-060071, February 2006.

[73] ——, "On UE in-band unwanted emissions," 3GPP, Tallinn, Estonia, Tech. Rep. R4-060881, September 2006.

[74] B. Priyanto, H. Codina, S. Rene, T. Sørensen, and P. Mogensen, "Initial Performance Evaluation of DFT-Spread OFDM based SC-FDMA for UTRA LTE Uplink," in *Proc. IEEE VTC Spring 2007.*, April 2007.

[75] CATT, Ericsson, LGE, Motorola, Nokia, Nokia-Siemens, Nortel, N. DoCoMo, Orange, Panasonic, Philips, Qualcomm, S. Samsung, TI, and Vodafone, "Way forward on power control of pusch," 3GPP, Orlando, USA, Tech. Rep. R1-073224, June 2007.

[76] Nokia, "LTE UL coexistence with LTE and other radio technologies," 3GPP, Tallinn, Estonia, Tech. Rep. R4-060764, September 2006.

[77] K. Fazel and S. Kaiser, *Multi-Carrier and Spread Spectrum Systems.* Chichester, UK: Wiley, 2003.

[78] H. Sari, G. Karam, , and I. Jeanclaude, "Frequency-domain equalization of mobile radio and terrestrial broadcast channels," in *Proc. IEEE Global Telecommun. Conf.*, vol. 1, November 1994.

[79] J. G. Proakis, *Digital Communications*, 4th ed. New York, USA: McGraw-Hill, 2001.

[80] Nokia, "Coverage comparison between UL OFDMA and SC-FDMA," 3GPP, San Diego, USA, Tech. Rep. R1-051088, October 2005.

[81] Ericsson, "Common simulation assumptions for eNodeB demodulation requirements," 3GPP, Orlando, US, Tech. Rep. R4-070983, June 2007.

[82] N. DoCoMo, "Initial simulation results for LTE UL Demodulation," 3GPP, Athens, Greece, Tech. Rep. R4-071364, August 2007.

[83] L. Electronics, "Simulation results for LTE eNodeB demodulation performance with rel-6 Turbo codec," 3GPP, Athens, Greece, Tech. Rep. R4-071154, August 2007.

[84] Q. Europe, "LTE eNB demodulation link performance," 3GPP, Athens, Greece, Tech. Rep. R4-0701200, August 2007.

[85] L. Schumacher, J. Kermoal, F. Frederiksen, K. Pedersen, A. Algans, and P. Mogensen, "MIMO Channel Characterisation," IST Project, Tech. Rep. IST-1999-11729, February 2001, METRA Deliverable.

[86] L. Berger, "Performance of Multi-Antenna Enhanced HSDPA," Ph.D. dissertation, Aalborg University, Aalborg, Denmark, 2005.

[87] J. Tubbax, B. Come, L. Perre, L. Deneire, and M. Engels, "OFDM versus single carrier with cyclic prefix: A system-based comparison," in *Proc. 54th Veh. Technology Conf'2001.*, vol. 2, Atlantic City, NJ, October 2001, pp. 1115–1119.

[88] R. Koetter, A. Singer, and M. Tuchler, "Turbo equalization," *IEEE Signal Processing Mag.*, vol. 21, no. 1, pp. 67–80, January 2004.

[89] C. Laot, A. Glavieux, and J. Labat, "Turbo equalization: adaptive equalization and channel decoding jointly optimized," *IEEE Journal on Sel. Areas in Commun.*, vol. 19, no. 9, pp. 1744–1752, September 2001.

[90] M. Tuchler and J. Hagenauer, "Turbo equalization using frequency domain equalizers," in *Proc. Allerton Conference.*, vol. 1, Monticello, AR, October 2000, pp. 144–153.

[91] W. Ryan, "A turbo code tutorial," *Online Material URL: http://www.ece.arizona.edu/ ryan/publications/turbo2c.pdf*, pp. 1–9, 1997.

[92] C. Berrou, A. Glavieux, and P. Thitimajshima, "Near shannon limit error-correcting coding and decoding: Turbo codes," in *Proc. 1993 Int.Conf. Comm.*, Geneva, Switzerland, May 1993, pp. 1064–1070.

[93] D. Raphaeli and Y. Zarai, "Combined turbo equalization and turbo decoding," *IEEE Communications Letters*, vol. 2, no. 4, pp. 107–109, April 1998.

[94] C. Laot and R. Bidan, "Low-complexity MMSE turbo equalization: A possible solution for EDGE," *IEEE Transactions on Wireless Communications*, vol. 4, no. 3, pp. 965–974, May 2005.